INFLUENCE OF SYNOPTIC SCALE CIRCULATION ON TEMPERATURE AND EQUIVALENT TEMPERATURE EXTREMES IN CHICAGO, IL (1948-2014)

by

Brooke Haldeman
B.S., Indiana State University, 2012

A Thesis
Submitted in Partial Fulfillment of the Requirements for the
Masters of Science

Department of Geography and Environmental Resources
in the Graduate School
Southern Illinois University Carbondale
December 2015

THESIS APPROVAL

INFLUENCE OF SYNOPTIC SCALE CIRCULATION ON TEMPERATURE AND EQUIVALENT TEMPERATURE EXTREMES IN CHICAGO, IL (1948-2014)

By

Brooke Haldeman

A Thesis Submitted in Partial

Fulfillment of the Requirements

for the Degree of

Masters of Science

in the field of Geography and Environmental Resources

Approved by:

Dr. Justin Schoof, Chair

Dr. Trent Ford

Dr. Jonathan Remo

Graduate School
Southern Illinois University Carbondale
October 28, 2015

AN ABSTRACT OF THE THESIS OF

BROOKE LARAE HALDEMAN, for the Master of Science degree in GEOGRAPHY & ENVIRONMENTAL RESOURCES, presented on October 23, 2015, at Southern Illinois University Carbondale.

TITLE: INFLUENCE OF SYNOPTIC SCALE CIRCULATION ON EQUIVALENT TEMPERATURE EXTREMES IN CHICAGO, IL (1948-2014)

MAJOR PROFESSOR: Dr. Justin Schoof

Heat waves are responsible for significant economic impacts and loss of life each year in the United States with humidity often playing an important role. This study examined synoptic patterns associated with extreme temperature and equivalent temperature events in Chicago, IL over the period of 1948-2014 using summertime (June 1st- September 15th) values. Temperature and equivalent temperature-based heat waves were defined as periods with at least eight consecutive six-hour observations exceeding the historical 95th percentile values of temperature and equivalent temperature, respectively, using data from O'Hare International Airport. Self-organizing maps (SOMs) were then applied to 500 mb geopotential height and 850 mb specific humidity from the NCEP/NCAR reanalysis dataset to identify synoptic states associated with extreme temperature and equivalent temperature events. SOM nodes associated with heat waves were identified and assessed for trends using median of pairwise slopes regression. While mean summertime temperature and equivalent temperature in Chicago did not exhibit significant

trends, yearly summertime minimum temperatures were found to be increasing with a significant trend. Additionally, several synoptic patterns favorable for the development of high temperature and high humidity heat waves were increasing significantly.

ACKNOWLEDGEMENTS

I would like to thank everyone involved in the collection of data for my research including Keah Schunneman for her assistance and with self-organizing maps data usage and implementation. A special thank you my committee members Dr. Trent Ford and Dr. Jonathan Remo; I appreciate your direction and assistance. Most of all, I would like to thank Dr. Justin Schoof for his expertise, continuous support, and guidance.

TABLE OF CONTENTS

LIST OF TABLES

LIST OF FIGURES

CHAPTER 1

INTRODUCTION

During the historic 1995 heat wave in Chicago an estimated 739 excess deaths were reported with over 500 identified as being directly heat related (Hayhoe et al. 2010a). Emergency department visits and hospital admissions increased drastically and the electric grid was stressed resulting in outages. During peak intensity temperatures reached 40°C with dew points of 25°C and minimum temperatures exceeding 26.6°C for two consecutive nights. The absence of nighttime cooling prolonged oppressive conditions and provided little relief from extreme temperatures (Livezey and Tinker, 1996). Future projections indicate that by the end of the century events similar in magnitude to the 1995 heat wave can occur as frequently as every other year; this increase in frequency is accompanied by an estimated near double increase in mortality (Hayhoe et al. 2010a). Predicted increases in heat wave frequency are validated by the successive Chicago 1999 event (Palecki et al. 2001). During this event dew points exceeded 26°C with heat index values of 38°C. These extreme temperatures caused roads to buckle while power outages stalled passenger trains leaving individuals stranded without cooling mechanisms (Palecki et al. 2001). Overall, the Midwest suffered 258 deaths with 110 occurring in Chicago and surrounding suburbs. The lower mortality rate for this event is attributed to Chicago's improved planning, response, and awareness to extreme events. Identifying large-scale systems associated with heat wave development will enhance the prediction of extreme events and contribute to current knowledge of heat wave development and formation. With future knowledge and advanced information, city officials can mitigate impacts by creating relief areas for at risk individuals. Better understanding of heat wave formation and progression can reduce the mortality associated with extreme events.

The events described above reflect the importance of both temperature and humidity for human heat stress during extreme heat events. Commonly, the combined effects of both variables are quantified using the heat index, or apparent temperature (Steadman, 1984). However, the heat index can be elevated under high temperatures, even if the humidity is low. Therefore, several authors (Pielke et al. 2004; Davey et al. 2006; Rogers et al. 2007; Fall et al. 2010; Schoof et al. 2014) have recommended the use of equivalent temperature, defined as the temperature that an air parcel would achieve if all of the associated water vapor were condensed and the resulting latent heat used to heat the parcel. This study uses temperature and equivalent temperature data to focus on extreme events in Chicago, Illinois. To identify large-scale circulation patterns responsible for development of extreme heat events, self-organizing maps (SOMs) are used to extract the associated mid-tropospheric conditions. These synoptic patterns were analyzed to determine if a relationship exists between temperature and equivalent temperature extremes and atmospheric circulation; features responsible for high temperature and equivalent temperature were evaluated further.

Chicago's heat wave history combined with heightened temperature and equivalent temperature projections establish the need for a synoptic heat wave analysis. As global temperatures continue to rise, heat waves in the Chicago region are expected to increase in duration and frequency with an extension in their seasonality (Varvus and Van Dorn, 2009). Since heat extremes are the leading cause of weather related deaths in the United States (Hayhoe et al. 2010a) projecting these high temperature, high equivalent temperature heat waves is imperative. By determining synoptic conditions favorable for equivalent temperature extremes, forecasting for events will improve; enhanced prediction methods can result in advanced warnings and potentially decrease overall mortality.

1.1 Study Area

Chicago is located in northern Illinois on the coast of Lake Michigan. Hot, humid temperatures with elevated precipitation characterize Chicago summers with 33% of total annual rainfall occurring in the summer months (Hayhoe et al. 2010a). Chicago's characteristic warm summer temperatures are attributed to a semi-permanent high that resides over the sub-tropical Atlantic prompting the flow of warm, humid oceanic air into the area. However, other additional factors impact Chicago's climate. The polar jet stream, which often located over Illinois, drives low-pressure systems and contributes to the formation of clouds and transient weather systems. These passing systems can impact Chicago's short-term weather resulting in a variety of conditions (Hayhoe et al. 2010b). Additionally, because of Chicago's size, urban heat island effects can lead to further warming; this is the increase in temperatures that occurs from anthropogenic sources resulting in warmer urban environments when compared to rural counterparts. Large buildings and structures can inhibit wind flow resulting in stagnant air and degraded air quality from pollution accumulation (Vanos et al. 2014). Urban heat island effects were analyzed in Vanos et al. (2014) where larger cities were paired with a smaller city within the same synoptic classification to determine the impact of large urban areas. For example, Chicago was paired with Peoria, Illinois to determine if, relative to a smaller city, Chicago experienced heat island impacts. After analyzing trends in warming in both cities, results indicate the same level of warming has been occurring at both locations. Therefore, increasing temperatures in the Chicago region are not caused by urban heat island impacts (Vanos et al. 2014). However, areas located near Lake Michigan coastline receive a lake cooling breeze that can diminish the effects of urban heat. The presence of Lake Michigan also moderates maximum

and minimum temperatures and lessens the impact of extreme conditions (Varvus and Van Dorn, 2009).

Associating surface conditions with upper atmospheric circulation is imperative to accurately analyze climate dynamics. Perkins (2015) identified several large scale features associated with heat wave development and Greene and Kalkstein (1996) found extreme synoptic patterns produced a statistically significant impact on mortality rates for Chicago, IL (Greene and Kalkstein, 1996). Historical heat wave events in Chicago have been associated with large-scale features that drive surface climate and generate hot, humid, and stagnant conditions (Livezey and Tinker 1996; Palecki et al. 2001). Identifying synoptic states associated with extreme events can improve the understanding of heat wave formation and provide a greater understanding of development of extreme events. In this study large-scale circulation features are analyzed by developing self-organizing maps to determine prevalent heat wave synoptic patterns.

1.2 Research Questions

To determine if temperature or equivalent temperature heat waves are impacting Chicago several analyses were necessary. Temperature and equivalent temperature values were assessed to determine if a significant trend was present. Large scale patterns of heat wave formation for temperature and equivalent temperature were identified; once distinguished, these patterns were examined to determine heat wave characteristics for extreme temperature and equivalent temperature heat wave development. Additionally, equivalent temperature values depend upon temperature fluctuations and available moisture content; the potential large-scale changes in these variables were studied. To complete this analysis the following questions were answered:

Q1: How have temperature and equivalent temperature in Chicago changed over time?

Q2: What synoptic drivers are responsible for extreme equivalent temperature events? Are these features different from extreme temperature events?

Q3: Are synoptic patterns associated with extreme temperature and extreme equivalent temperature events becoming more or less prevalent?

CHAPTER 2

LITERATURE REVIEW

2.1 Temperature Extremes

Global average maximum temperature increases were 0.14°C per decade from 1950-2004. As greenhouse gasses continue to drive climate change heat waves are projected to increase in duration and severity (Perkins, 2015). Temperature intensification will be accompanied by higher dew points resulting in greater heat stress during heat waves (Gaffen and Ross, 1999). Elevated temperatures will increase mortality rates and cause further stress on at risk populations who may be less able to cope with temperature extremes. Therefore, increasing temperature projections could imply a higher mortality rate for extreme events (Hayhoe et al. 2010a).

With an increase in average annual temperatures intense rainfall becomes more frequent and severe, long-lasting heat waves are imminent (Perkins, 2015). Hayhoe et al. (2010b) and Vavrus and VanDorn (2009) completed several climate change scenarios for Chicago and the Great Lakes region using IPCC's defined emission scenarios. Hayhoe et al. (2010b) determined by the end of the century a low emission scenario generated a 3±1°C temperature increase while a high emission scenario produced an increase of 5±1.2°C (Hayhoe et al. 2010b). Vavrus and VanDorn, (2009) analyzed temperature extremes and determined 'very hot days', the historical warmest 5% of all days considered, increased to include 22 additional days for a low emission scenario and 58 for a high emissions scenario (Vavrus and VanDorn, 2009). For the low scenario, the number of days where daily temperature maximum exceeded 32°C increased from 15 per year mid-century to 36 with high estimates exceeding 70 days per year by 2100 (Vavrus and VanDorn, 2009). As temperatures rise, heat wave duration is projected to increase. For high

emissions, consecutive days exceeding 32°C reached 9.8 by the end of the century with consecutive days exceeding 38°C reaching 5.3 days. These values are a considerable increase from the established late 20th century values of 2.9 and 0.7 respectively (Vavrus and VanDorn, 2009). Hayhoe et al. (2010b) used hourly temperature and precipitation data to develop a migrating climate analysis. Projected increasing temperatures indicate Illinois summer temperature characteristics resemble east Texas by 2100. When temperature is combined with humidity, average heat index for a typical June, July, August summer reaches 40.5°C by 2100. (Hayhoe et al. 2010b).

Upon analyzing the 2003 heat wave occurrence in France, Hayhoe et al. (2010a) completed a heat wave study for an event of similar magnitude in Chicago. Three global coupled atmosphere-ocean general circulation models were used to predict heat wave intensity and mortality for several extreme scenarios. Heat waves for this study were defined as at least seven consecutive days where maximum daily temperatures exceeded 32°C, nighttime minimum temperature exceeded 21°C, and at least two days where maximum daytime temperatures were in excess of 38°C and nighttime temperatures were greater than 27°C (Hayhoe et al. 2010a). For the European heat wave total excess death rates range between estimates of 40,000 to 70,000 for 16 European countries. Although a heat wave of this magnitude has not affected the United States, Chicago is predicted to experience an event of similar intensity before 2050. Hayhoe et al. (2010a) determined under a low emissions scenario five events equivalent to the European heat wave will occur in Chicago by 2100. For a high emission scenario, 25 events are predicted with increasing frequency as the end of the century is approached (Hayhoe et al. 2010a). With all demographics and infrastructure factors remaining constant for Chicago, the European heat wave atmospheric characteristics were introduced. Models predict significant impacts with four days

of maximum temperatures exceeding any recorded temperature values since 1926; in addition, minimum temperatures would surpass record temperature values for eight days. Decreases in diurnal temperature range provide little relief from heat stress, especially for residence without air conditioning units. The number of excess deaths was estimated at 13.4 per 100,000 for this event compared to 11.5 per 100,000 for the 1995 heat wave. By 2050 Chicago is projected to experience at least one summer where extreme heat results in a mortality rate exceeding 1,000 individuals (Hayhoe et al. 2010a).

2.2 Equivalent Temperature

Temperatures in the Chicago region are projected to increase (Vavrus and VanDorn 2009) and Davey et al. (2006) notes that high temperature values in Chicago are often accompanied by elevated humidity. Although temperature extremes are predicted, analysis of air temperature alone is not a complete measure of surface heat (Pielke et al. 2004). Metrics that also consider the moisture contribution are considered a more comprehensive assessment of heat impacts and human heat stress. This analysis employs equivalent temperature to accurately assess temperature and humidity values for Chicago, IL.

Equivalent temperature calculations are described in length in (Bolton, 1980); however, computations similar to Schoof et al. (2014) will be used in this study. Rogers et al. (2007) uses moist static energy as a measure of total energy content to determine temperature. Moist static energy accounts for air temperature fluctuations as well as moisture content variations and provides an accurate representation of the perceived ambient temperature. The formula for moist static energy is:

$$H = C_P T + L_V q \qquad (1)$$

Where C_p is the specific heat of air at constant pressure, T is temperature, L is latent heat of vaporization and q is specific humidity. Division of the equation by C_p yields the formula for equivalent temperature given above.

$$T_E = \frac{H}{C_P} \tag{2}$$

Fall et al. explains the calculation for equivalent temperature:

$$T_E = \frac{H}{C_P} = T + \frac{qL_V}{C_P} \tag{3}$$

where C_p is the specific heat of air at constant pressure, T is the air temperature (°C), L_v is the latent heat of vaporization (J/kg), and q is the specific humidity (kg/kg).

Increasing temperatures are likely to be accompanied by higher humidity and several studies have identified trends in humidity in the eastern United States. Gaffen and Ross (1999) found that stations in the eastern United States have specific humidity values q, twice as high as western stations. As previously stated, T increases are accompanied by q increases and thus T_a, or apparent temperature also known as the heat index, rises as well (Gaffen and Ross 1999). Increases in T_a indicate a rise in human heat stress and associated mortality (Perkins and Alexander, 2013). Robinson (1999) determined that dew point temperatures have been increasing in spring, summer and fall over the Ohio region. During a study period of 1951-1990 dew temperatures had an overall increase of 0.5 °C/ 100 years over the United States; when the shortened period of 1961-1990 is examined overall trends increase 2.0 °C/ 100 years (Robinson,

1999). Rising dew point temperatures reflect increasing atmospheric moisture and can contribute to higher equivalent temperatures.

Analysis of moisture is imperative for understanding changes in equivalent temperature. Since T_E is calculated by determining the moisture content from an air parcel, changes in available moisture are essential to humidity and T_E values. Fall et al. (2010) concluded that maximum moisture content occurs during summer months with contributions being most significant in eastern United States (Fall et al. 2010). Dominguez and Kumar (2004) used 6 hour NCEP-NCAR data spanning from 1979-2001 to determine principal factors of moisture flux for the United States. The principal feature controlling spring moisture values was a high pressure region persisting over the west coast preventing moisture flow into the U.S. Primary summer month moisture for the Great Lakes Region is determined by three factors: moisture flow from the Gulf of Mexico, anticyclonic circulation over the western Atlantic Ocean, and cyclonic circulation in the Pacific Ocean. Another influence, the Great Plains Low Level Jet, is responsible for moisture advection into central regions of the states (Dominguez and Kumar, 2004).

2.3 Soil Moisture

Davey et al. (2006) examined the relationship between temperature, equivalent temperature and the microclimate of an area. Urban locations and areas within close proximity to water bodies had larger T_E trends significant over 99%. Fall et al. (2010) also evaluated land cover influence on T_E and identified locations with large evaporation and transpiration rates as areas with inflated T_E values. Moisture flux was mostly attributed to transpiration from vegetation and soil evaporation rates (Fall et al. 2010). Saturated soils increased overall moisture

availability and excessive moisture was identified by Kunkel et al. (1996) as a contributing factor to increased humidity. According to this study an increase in precipitation will saturate soils and increase equivalent temperature values through evapotranspiration (Kunkel et al. 1996). Pan et al. (2004) attributes summer cooling temperatures to the moisture flux and available soil moisture. Increased precipitation replenishes the soil moisture and allows for late-summer evapotranspiration which can decrease maximum daily temperatures. Overall, late season precipitation changes for Chicago's can result in a warming hole effect where moisture is more abundant but temperatures are suppressed (Pan et al. 2004). However, a rise in the available moisture can result in higher humidity values; therefore, an increase in equivalent temperature. For the 1995 event, soil moisture met or exceeded average values throughout the Midwest; this resulted from an exceptionally wet spring and early summer. Consequently, moisture levels were found to be almost at capacity during the event (Kunkel et al. 1996). With Chicago's yearly precipitation projected to increase by 30% (Hayhoe et al. 2010a) soils could become saturated indirectly resulting in higher equivalent temperatures.

2.4 Warming Hole

From 1975-2000 eastern United States summer temperatures have cooled by 0.2-0.8°C. Pan et al. (2004) determined summer is characterized by convergence of low-level moisture over the central United States that results in greater values of evaporation, soil moisture, and cooler temperatures from increased cloud cover (Pan et al. 2004). Increase in moisture availability coupled with high summer temperatures results in high evaporation rates. With higher dew points projected for the Chicago region, more moisture will be retained in the atmosphere. Chicago will experience an initial temperature decrease from evaporative cooling; however,

moisture and humidity values will increase subsequently elevating equivalent temperature values. Schoof, et al. (2014) analyzed several locations in the eastern united states and determined that, despite cooling temperatures, equivalent temperature values increased at some locations (Schoof et al. 2014). Therefore, it is imperative to complete a combined analysis for this region to determine the influences of both temperature and humidity.

2.5 Heat wave Characteristics

Heat wave definitions vary broadly with no established criteria. Gershunov et al. (2009) determined heat wave definitions necessitate nighttime minimum as well as daytime temperature extremes. Cool nights provide relief from excessive daytime temperatures and their absence intensifies heat stress and impacts (Miralles et al. 2014). Additionally, duration of extreme temperatures should also be considered when developing heat wave definitions (Gershunov et al. 2009). Grotjahn et al. (2009) reviewed existing heat wave literature reporting a spectrum of definitions. Robinson (2001) defined a heat wave as a minimum of 48 hours where the daytime heat index and overnight low exceed National Weather Service heat stress thresholds. If more than 1% of data met the established criteria, 1% values were used as a threshold. Lyon (2009) defined a heat wave as a consecutive three day period where temperatures exceeded the 90th percentile; the percentiles were determined by June, July and August values. Several definitions require the exceeding of a percentile for a minimum duration with others employing methods such as: standard deviations, moving averages, and even simply established temperature thresholds.

Although heat wave definitions vary, atmospheric features necessary for heat wave development are consistent. Upper atmospheric ridging, available moisture, and positive height

anomalies are characteristics necessary for heat wave development and formation (Palecki et al. 2001). Gershunov et al. (2009) analyzed historical heat wave synoptic conditions and determined significant heat waves are associated with surface highs, available moisture, and positive geopotential height anomalies. The July 2006 California heat wave was accompanied by ridging aloft and moisture advection. Five days prior to the onset of heat wave conditions southwesterly flow caused moisture accumulation; available moisture increased humidity and produced elevated nighttime temperatures that suppressed diurnal temperature range (Gershunov et al. 2009). For the 1995 Chicago event, excessive moisture and a ridge originating over the Rocky Mountains led to the development of high values of equivalent temperature. In addition, decreasing mixing layer height attributed to extreme temperatures. This event also had above average amounts of moisture available from a wet spring and early summer (Kunkel et al. 1996). Other notable heat waves that were characterized by anticyclonic flow and upper atmospheric ridging are the European 2003 event and the Great Plains drought and heat wave of 1980 (Black et al. 2004; Namias, 1982).

Another common feature of extreme heat waves is the presence of a high-pressure or a blocking high; this is a system that resides in an area for an extended period. Blocking highs form when upper level winds separate from a jet stream blocking the upper atmospheric flow generating stagnant conditions (Perkins, 2015). Cooler air from the northern latitudes is prevented from southerly movement causing warm temperatures to persist and intensify. These weather features tend to prolong heat wave events by allowing for stagnation and temperature intensification. Blocking highs were responsible for the Russian 2010 event, the European 2003 heat wave and the Chicago 1995 extreme temperatures. Low pressure systems may accompany the stagnant highs contributing to pattern continuation (Black et al. 2004; Namias, 1982; Kunkle

et al. 1996). For example, an omega block system contains a high pressure system flanked on either side by low pressure which promotes persistence; the longevity of Russia's 2010 heat wave was attributed to a lasting omega block (Perkins, 2015). Future analysis projects an increase in persistent highs (Perkins, 2015), which, coupled with rising temperatures, indicates an increase heat wave frequency.

2.6 Chicago Historic Events

During the 1995 heat wave temperatures climbed to extraordinary levels with record setting dew points resulting in over 700 deaths (Hayhoe et al. b, 2010). The combination of extreme temperatures and elevated humidity values created significant human heat stress that persisted from July 7th- July 15th 1995 (Livezey and Tinker, 1996). Heat wave formation began with the development of an upper level ridge over the southern United States leading to elevated temperatures on July 7th (Figure 2.1). As the ridge migrated east the heat wave expanded and temperatures intensified. The ridge encompassed the eastern coast with a closed lobe over Illinois on July 12th. The slow progression of the system allowed for moisture accumulation and daily temperature intensification generating dew points that exceeded 25°C (Figure 2.2) (Livezey and Tinker 1996; Kunkel et al 1996). However, by July 15th the ridge moved off the eastern coast and was replaced by a weak cold front that offered cool temperatures (Kunkel et al. 1996). High equivalent temperature was a critical factor for producing the oppressive conditions with unprecedented humidity values recorded at several stations. Kunkel et al. (1996) stated root zone moisture was approaching capacity on July 12th indicating the potential for extreme humidity values. In addition to high equivalent temperature, mixing depths were suppressed during the event creating stagnant near surface moisture.

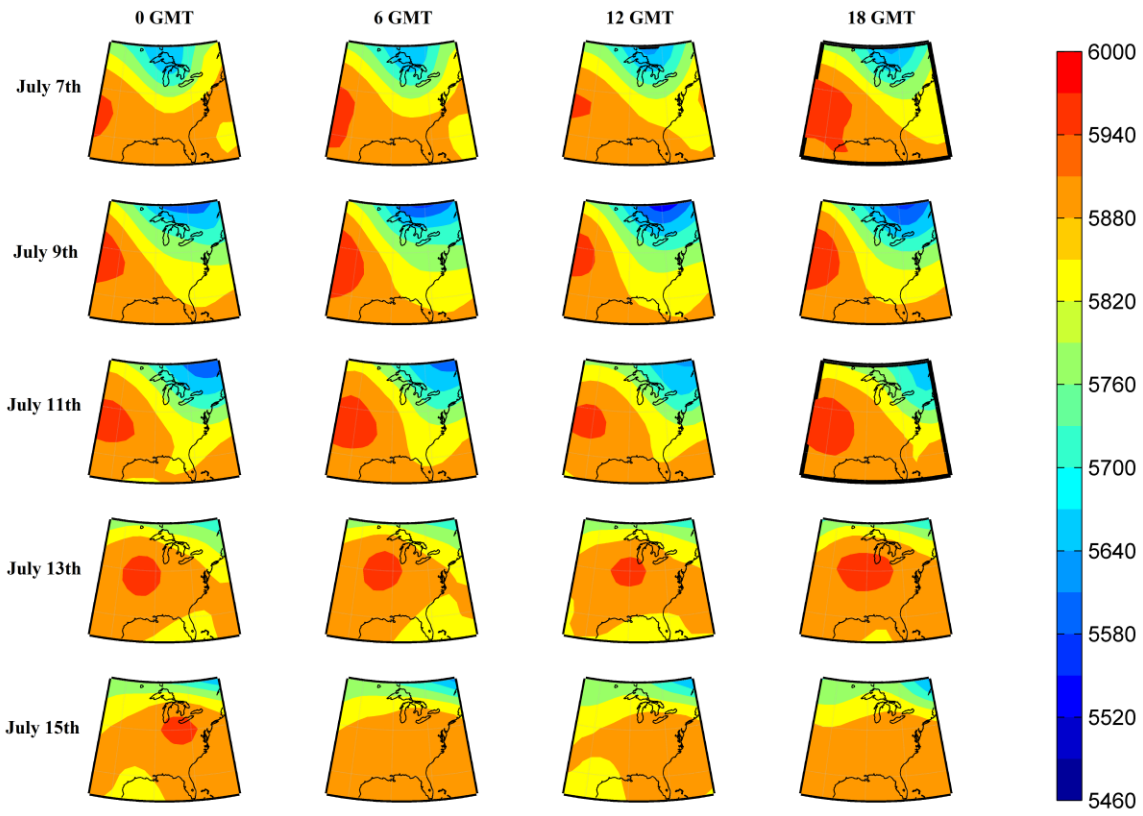

Figure 2.1: Chicago 1995 heat wave synoptic patterns for 500 mb geopotential height. Starting July 7th every other day is plotted with 4 six-hourly patterns per day to display heat wave development. Units are in meters

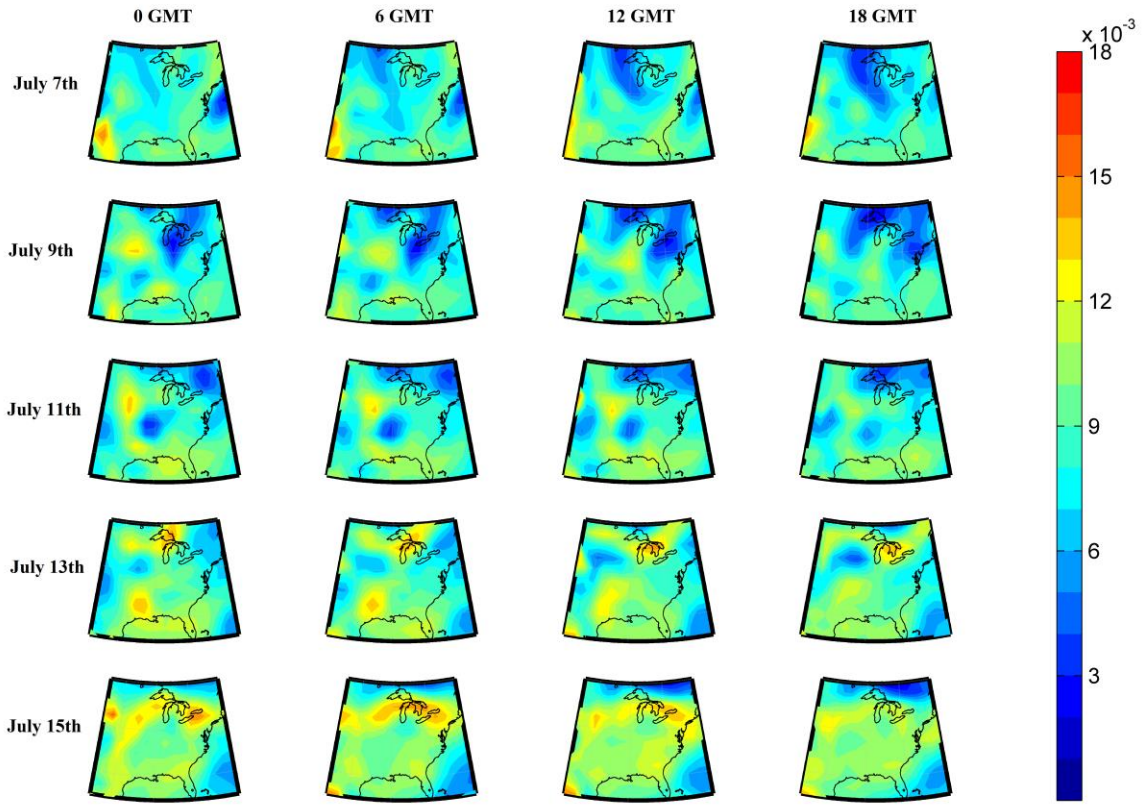

Figure 2.2: Chicago 1995 heat wave synoptic patterns for 850 mb specific humidity. Starting July 7th every other day is plotted with 4 six-hourly patterns per day to display heat wave development. Units are in kg/kg.

Minimum mixing depth was achieved on July 13th with a value of 500 meters in Davenport, Iowa; this prevented moist, hot air in the lower troposphere from mixing with cooler air above. Lastly, urban heat island effect increased the temperatures experienced during the event. Due to urban heat island effects nighttime urban temperatures were increased by up to 2°C (Kunkel et al. 1996). Maximum daily temperatures for the event reached or exceeded 32°C for seven days with peak intensity reaching 38°C for two days (Hayhoe et al. 2010b). Karl and Knight (1997) completed a return analysis for the Chicago 1995 heat wave. With IPCC's

projections of a 3°C temperature increase by 2100 return periods significantly decline. Apparent temperatures reaching 47.8°C would decrease from a current return period of 1 in every 23 years to 1 in every 6 years. Return periods for a two-day event with maximum temperatures of reaching 47.8°C decreases from 1 in 150 years to 1 in 25 years indicating higher temperatures and more frequent heat waves are likely for Chicago (Karl and Knight, 1997).

Chicago also experienced elevated temperatures during July of 1999. From July 22nd -26th maximum temperatures were 4°C above average. July 26th marked the passage of a cold front with accompanying rain to the south providing slight relief (Palecki et al., 2001). July 29th and 30th were characterized by a significant increase in temperatures when an upper level ridge and surface high progressed over Chicago (Figure 2.3). Although Chicago received minimal amounts of rainfall, wet areas to the southwest advected moisture north elevating dew point temperatures (Figure 2.4); the southwesterly flow also effectively suppressed cooling from the lake breeze effect (Palecki et al. 2001). Alleviation from extreme temperatures occurred when dry air aloft began mixing with the underlying moisture and a cold front passed on July 31st.

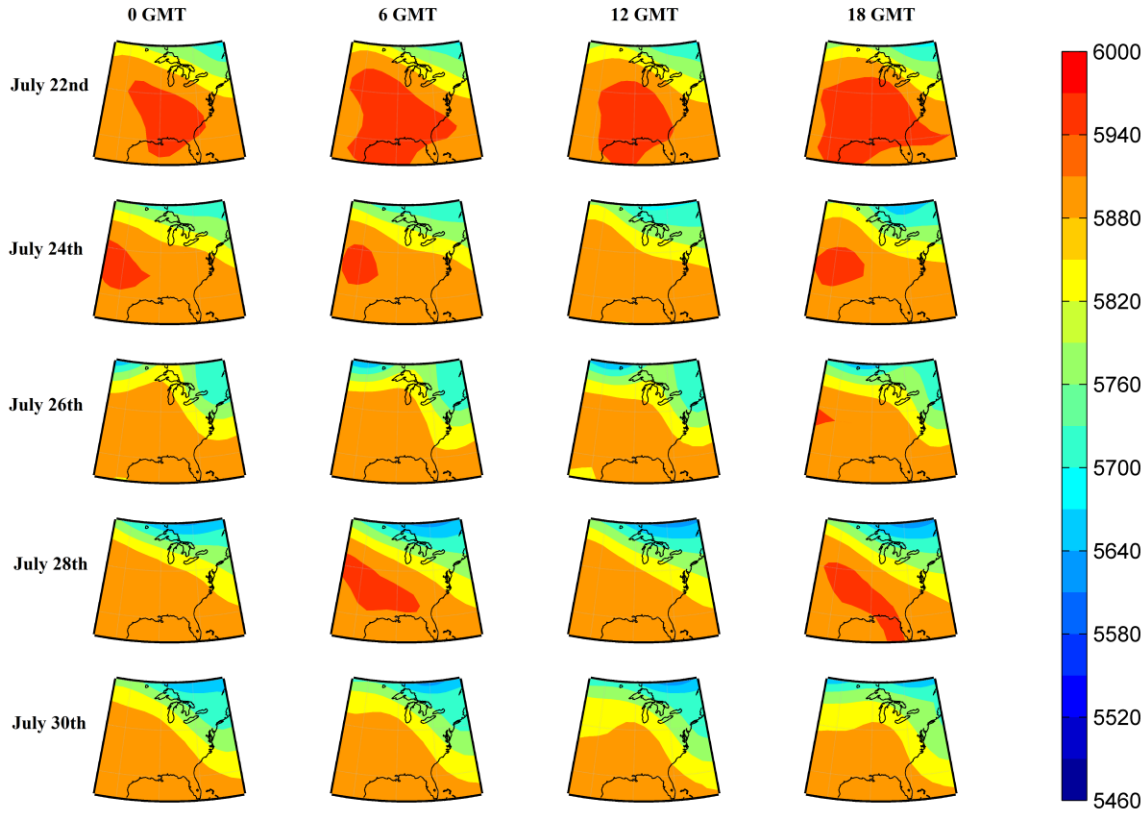

Figure 2.3: Chicago 1999 heat wave synoptic patterns for 500 mb geopotential height. Starting July 22nd every other day is plotted with 4 six-hourly patterns per day to display heat wave development. Units are in meters.

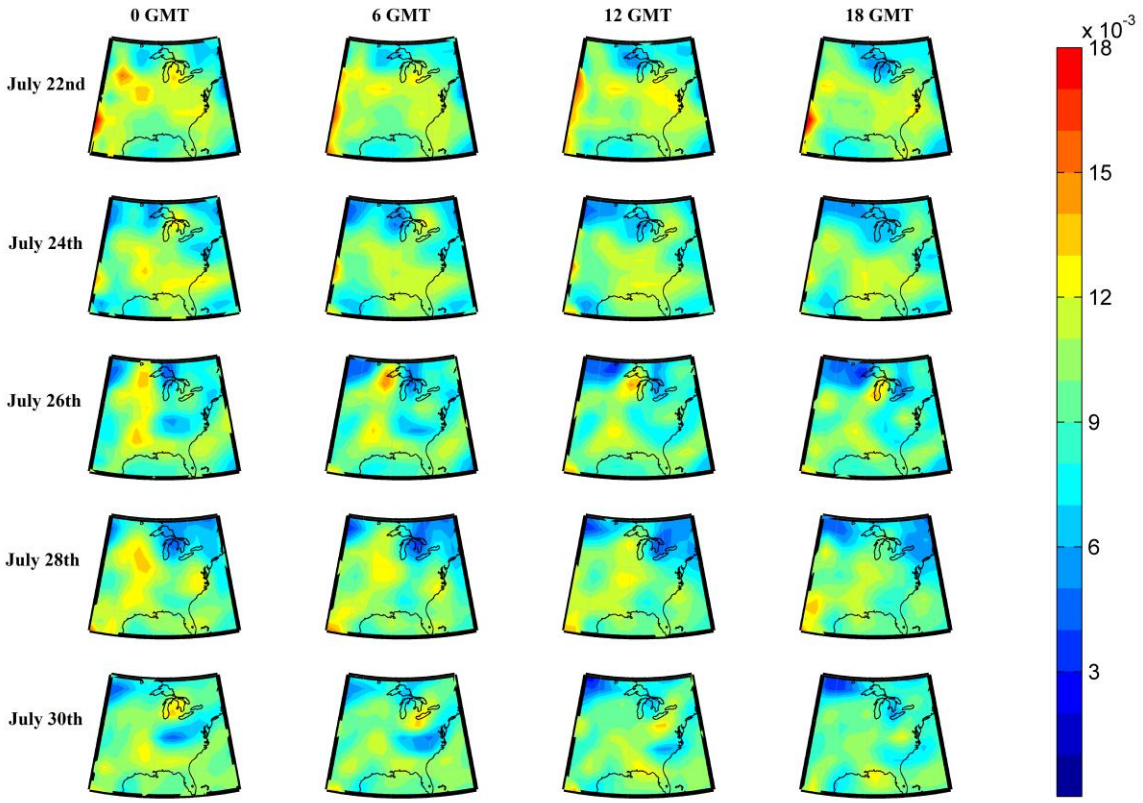

Figure 2.4: Chicago 1995 heat wave synoptic patterns for 850 mb specific humidity. Starting July 22nd every other day is plotted with 4 six-hourly patterns per day to display heat wave development. Units are in kg/kg.

The extremes of the July 1999 heat wave led to increased electric demand and strained Chicago's energy providers. Outages occurred from lines overheating or sagging and contacting surfaces that caused shortages. During the peak of the heat wave, a major power outage left several communities without power for up to three days; these electricity outages left individuals without cooling mechanisms and caused several economic disruptions as businesses were closed and refrigerated products spoiled. Intense heating of the highway surface caused buckling which left commuters trapped in vehicles for extended periods of time. To minimize deaths, Chicago

officials opened several cooling centers and provided free bus services to these facilities however, during this event there were 110 heat related fatalities in Chicago with 93 occurring within the city, 17 in suburbs and 4 located in distant suburbs (Palecki et al. 2001).

Despite an expansive amount of research on heat waves, development of extreme events with association to equivalent temperature has been neglected. Although heat wave characteristics have been determined for several locations, existing literature lacks an analysis of temperature and associated moisture heat events for Chicago. Completion of this analysis will provide a detailed study on specific temperature and equivalent temperature values in Chicago and identify large-scale atmospheric conditions associated with extreme temperature and equivalent temperature events. Additionally, analysis will be completed to determine if temperature or equivalent temperature values possess a significantly increasing trend, and determine if extreme events are becoming more prevalent in Chicago.

2.7 Self-Organizing Maps

Synoptic climatology is defined as "obtaining insight to local or regional climates by examining the relationship of weather elements, individually or collectively, to atmospheric circulation processes" (Hewitson and Crane, 2002). Synoptic climatology often focuses on identifying atmospheric patterns. For climate research, the self-organizing map has become a prevalent method of data analysis. The self-organizing map (SOM) is a neural network that organizes input variables to cluster synoptic patterns as well as present transitional stages. The introduction of the SOM to climatology research has led to better representation of atmospheric patterns and improved visualization (Sheridan and Lee 2011). Implementation of SOM's spans several sub-disciplines of climatology and include: cloud classification, monsoon variability,

precipitation, and atmospheric circulation as a few examples. SOMs have become widespread in climate science because of their ability to represent multidimensional data in two dimensions while clustering, which preserves data relationships. Additionally, SOMs can analyze multiple variables making them valuable tools for climate analysis. Wind, temperature, humidity and other variables have been included in SOMs to determine co-variability (Liu and Weisberg, 2011). For example, Cavazos (2000) employed a SOM to examine humidity and circulation anomalies to better understand precipitation extremes (Cavazos, 2000). Furthermore, the ability to visualize the synoptic states and transitions allows for better understanding of patterns (Sheridan and Lee, 2011). The output map of a SOM has similar synoptic patterns clustered with those most dissimilar farther away; often the most extreme synoptic states reside on the farthest corners of the map. Therefore, the SOM improves data comprehension and visibility by creating a simplistic and easily understood output of high dimensional data (Hewitson and Crane, 2002).

The mathematics behind the SOM are described by Kohonen (2013). The input data in the time sequence is represented by {x(t)} for any Euclidean vector x with n-dimensions where an integer t, represents a step in the sequence; $\{m_i(t)\}$ is another sequence of real vectors of n-dimensions that represents the computed output approximations of model m_i. In this formula, i represents the spatial index of the node that m_i is associated with. The SOM algorithm is then given by:

$$m_i(t+1) = m_i(t) + h_{ci}(t)[x(t) - m_i(t)] \qquad (4)$$

$h_{ci}(t)$ represents the neighborhood function. The subscript of c represents the winning node; this node is the most similar to x(t). The modification of neighboring nodes is given by the below equation where argmin is a function determining the minimum distance (Kohonen, 2013).

$$c = argmin\{\|x(t) - m_i(t)\|\} \quad (5)$$

Steps to producing a SOM are outlined by Sheridan and Lee (2011) where a SOM's application to climatology data is evaluated. First, a SOM creates an array composed of a two dimensional matrix of nodes (Sheridan and Lee 2011). These nodes incorporate the entire data set and contain no prior assumptions of potential relationships or data distribution. A user-defined number of nodes are selected with node density determining the detail of the output map. Too few nodes will lead to underrepresentation of patterns and excessive amounts of data points residing on each node. Too many nodes result in areas with no correlation to the data and generate wasted space on the map. Determining the correct number of nodes usually involves a trial and error method and the creation of several maps (Schuenemann et al. 2009). Establishing the correct number of nodes is imperative because each node is a visual representation of a neuron, the data object in the neural network. Neurons contain weights which are the variables being analyzed. In synoptic climatology these variables are often pressure, height, and precipitation among many possible attributes. Once the SOM is initiated, each neuron is assigned a random attribute value then data points are presented to every neuron repeatedly. This processed continues through a user defined number of iterations and again, the appropriate number is identified through several trials. After analyzing the current data point, the neuron's weights are adjusted (Hewitson and Crane, 2002). The learning parameters determine how much influence data points exert on neurons. Heavy influence can result in data points being pulled great distances with minimal influence not moving neurons enough (Sheridan and Lee, 2011). The neuron that most resembles the data point presented is the winning neuron and is adjusted the most; surrounding neurons are adjusted slightly through a neighborhood distance decay

function. The decay function decreases in size with each iteration until the radius becomes zero; once the radius is zero, competitive learning takes over and neighboring values are not influenced. This means, the closest neuron "wins" and is the only one adjusted, neighbors are not influenced. When the final iteration has completed, each data point should have a neuron associated with it. This neuron is most representative of the data point's attributes. If there are neurons that do not have data points associated with them then the number of nodes chosen at the beginning is too large and the data is not accurately represented. Furthermore, clustering of neurons signifies a pattern; if no clustering is apparent the data may have outliers or other factors influencing the neurons (Sheridan and Lee, 2011).

The user-defined variables can greatly influence the interpretation of the data and the recognition of patterns within the information presented. Number of nodes, learning rate, and neighborhood distance decay rate are all information that is determined by the SOM creator. Creating several SOM's with varying intensities and combinations of these values usually discovers the optimal number. The quantity where further addition fails to add significant amount of information was established as a reasonable estimate. The appropriate amount varies depended upon trends analyzed and number of transitional states. Wise and Dannenberg (2014) initiated a SOM with 15 nodes to evaluate the occurrence and duration of pressure patterns. This study used a K+1 method where the exact number of nodes is chosen by the determining when the addition of nodes does not result in a distinguishable difference in the SOM pattern at a 95% confidence level (Wise and Dannenberg, 2014). However, even when using the exact same dataset, each time the SOM is initiated, different maps can be produced based on the random input of the data values. Sheridan and Lee (2011) suggest simply testing various size arrays and determining what number accounts for the data variability. Once the node density has been

determined the SOM is initiated several times with different learning parameters and neighborhood radius values to determine the SOM with the smallest distance between nodes or the smallest quantization error. A method mentioned in Sheridan and Lee (2011) was the creation of a small, 3×3, SOM to determine principal nodes of circulation then use the information to create a larger, more representative map (Sheridan and Lee, 2011). Kohonen (2013) explains that the correct number of nodes cannot be initially determined; several SOMs must be created. As suggested by Sheridan and Lee (2011) a smaller map may be implemented to determine the principal nodes then nodes can be added until a comprehensive map is obtained. Nigro and Cassano (2014) analyzed wind patterns across the Ross Ice Shelf and used several various arrays to determine which amount of nodes captured the appropriate amount of atmospheric patterns. SOM map sizes of 4×3, 5×4, and 7×5 among several others were tried before a 6×4 array was chosen for a total of 24 nodes (Nigro and Cassano, 2014). Determining the appropriate SOM depends on the desired characteristics. Nodes should not be too sparse or dense. As previously mentioned, a data set with too few nodes will lead to underrepresentation of patterns and excessive amounts of data points on each node. Too many results in nodes with too few data points mapped to them and patterns of little significance or variance on the SOM.

To demonstrate the diversity of SOM parameters, two studies are compared below. For their research, Schuenemann et al. (2009) used training parameters of a neighborhood radius of 2, learning rate of .01, and 1,000,000 iterations (Schuenemann et al. 2009). While Richardson et al. (2003) employed a neighborhood radius of 5, learning rate of .2, and 1000 iterations for a 6×4 array of wind analysis on the first training run; for their second training, the learning rate was decreased to .02, neighborhood radius was decreased to 0 and iterations were increased to 50,000. Similar values were also chosen for their analysis of sea surface temperatures from

satellite images using SOM techniques on a 5×3 array (Richardson et al. 2003). Another method is a two-phase approach where the SOM creation process is created in two steps: initial run and network optimization. The first step includes reducing in the learning rate from a high value such as .9 to a low value such as .1 with a neighborhood radius that reduces from half of the network to the surrounding neurons. Phase two uses a neighborhood radius of approximately one with a decreasing the learning rate from .1 to 0. The total number of iterations in the second phase should be at least twice as many as phase one (Tozuka et al. 2008).

Several methods for examining the effectiveness of SOMs are available. Schuenemann et al. (2009) mentions several tests to determine the accuracy of SOMs in climatology. Once the SOM has been trained the frequency, or number of times a node is representative of a data point is calculated. Schuenemann et al. (2009) used a 7×5 SOM, which includes 35 neurons. The probability of any data point mapping to any neuron was then calculated; this value is the node frequency of occurrence. Areas with high frequency reveal data clusters and prevalent synoptic states (Schuenemann et al. 2009). Frequency maps resemble the original SOM because all nodes retain their position but the percentage of occurrence is displayed on each node (Hewitson and Crane, 2002). A frequency map shows the prevalence of each node as a percentage of overall data points. Another SOM benefit is the analysis for the migration atmospheric states. For each node on the SOM the percentage of recurrence can be determined along with the chance of the next point mapping to a neighboring or any other node. Because extreme events require pattern persistence or specific antecedent synoptic conditions, the transition between atmospheric states is a beneficial analysis tool.

Other emerging fields of SOM application are the extraction of features from satellite images and the coupling with general circulation model data. Sheridan and Lee (2011) reference

several papers that use SOMs to classify cloud characteristics from satellite imagery. Richardson et al. (2003) applied SOM techniques to satellite imagery to determine prevalent wind patterns in the southeast Atlantic. The initial input was separated into *u* and *v* wind components then analyzed by the SOM to determine major patterns of wind for the region. In addition, the SOM was also used to depict events of known cyclones and extreme wind events. By creating SOMs of historical events, a comparison of main features is possible. Richardson et al. (2003) also displayed the SOMs satellite interpretation ability by mapping sea surface temperatures from satellite imagery. First, clouds were removed and treated as missing values because SOM's have exceptional ability to interpolate missing data points; next, land surfaces were removed. Warming and cooling sea surface temperatures, in addition to transitional states, were successfully represented by the SOM (Richardson et al. 2003). For future climate scenarios, general circulation models (GCMs) are used to predict climate change. SOMs have also been successfully employed to discover bias in GCMs and determine how well they represent circulation patterns. The under or over-emphasis of synoptic patterns can be determined by SOM output as well as identify areas of model inaccuracy (Sheridan and Lee, 2011). Additionally, future projections from GCM have been couple with historical data to create SOMs predictions of synoptic states for a region. Using projected data combined with known trends, future synoptic states for a region can be determined by SOM analysis (Sheridan and Lee, 2011).

For synoptic climatology research the incorporation of the SOM has several advantages. SOMs can provide accurate representations of data sets characterized by missing values; since nodes associate with neighboring values, missing data can be interpolated. Additionally, with the use frequency maps SOMs can provide synoptic data that is easily understood with known error. Furthermore, as demonstrated by Nigro and Cassano (2014), SOMs can be used to track

atmospheric patterns temporally. This study employed SOMs to track dominant wind patterns over the Ross Ice Shelf; they used the SOM mapping capabilities to produce SOM maps for each season as well as frequency maps. Seasonal frequency maps were then determined for each node present in the SOM. The ability to portion data sets into seasonal or periodic sections and compare them using the same method of analysis is another advantage of SOMs. Climatology is dynamic and can vary on several timescales; the ability to compare each nodes frequency during each season is an extremely beneficial tool for climate research and allows for further interpretation of climatology data sets (Nigro and Cassano, 2014).

Liu and Weisberg (2011) include a review of synoptic papers published using SOM methods. SOMs have been used to examine oceanic chlorophyll, sea surface temperatures, sea-floor roughness, monsoon variability, and extreme climate. The applicability of SOMs to several fields proves SOMs are a flexible and imperative tool for future synoptic climate analysis. As SOMs increase in popularity important pitfalls need to be addressed for future research. Since SOM node density, learning rate, and number of iterations are specific to each research project; the concepts behind choosing each should be understood completely. Another obstacle SOMs face is the aversion of employing this method due to the user-defined portion of SOM methodology (Liu and Weisberg, 2011). Regardless, the SOM is a versatile and capable tool for climate analysis that can ensure accurate and reliable results. The SOM has exceptional skill at depicting climate trends and atmospheric transitional states and will be a valuable tool for future climate research.

CHAPTER 3

DATA AND METHODS

3.1 Data

Hourly values of temperature, dew point temperature, and station pressure were collected from the National Oceanic and Atmospheric Administration's Integrated Surface Database from Chicago's O'Hare airport station. To ensure data homogeneity the metadata was analyzed and the data set was pre-processed using FORTRAN. Data values were collected hourly but not always exactly on the hour; to retain data quality, each observation was assigned to the nearest hour and six hourly averages were calculated. The data set was trimmed to span 1948-2014 from June 1st through September 15th to encompass early season moisture and late season heating. Synoptic data was extracted from National Center for Environmental Prediction/National Center for Atmospheric Research (NCEP/NCAR) Reanalysis website for 500 mb geopotential height and 850 mb specific humidity (Kalnay et al. 1996). The variable of geopotential height was chosen at the mid-tropospheric level to analyze extreme or anomalous values; this choice is consistent with Perkins (2015) who stated geopotential height anomalies associated with extreme heat are consistently detected at the 500 mb level. Geopotential height at 500 mb has also been chosen for analysis by several additional studies (Ciancarelli et al 2013; Horton et al, 2015; Pezza et al. 2012). Additionally, specific humidity was analyzed at the low-tropospheric level as a surrogate for low level moisture transport; this level is consistent with Ross and Elliot's (2001) analysis of water vapor trends in the Northern Hemisphere. Study area latitude and longitude coordinates were adopted from Rogers et al. (2007) who conducted one of the first studies of T_E in the context of large-scale circulation using data from Columbus, OH (Rogers et al. 2007). Longitude was extended east by ten degrees to allow for inclusion of antecedent synoptic

conditions and include development of large-scale features (Rogers et al. 2007); coordinates for this study were 105W to 70W, 25N to 50N. Reanalysis data was trimmed to extract the determined coordinates and meet the 1948-2014, June through September data range. Geopotential height and specific humidity values were processed with MATLAB to produce self-organizing maps. Node assignments for each day were determined and node frequencies were calculated. Additionally, a transitional analysis was completed to examine node transition patterns and synoptic conditions associated with the development of heat waves. To determine heat waves in the Chicago time series, the criteria of 8 consecutive observations exceeding the 95th percentile was established; data values were condensed into six-hour observations meaning 48 consecutive hours of extreme values were necessary to qualify as a heat wave. For each six hour observation the 95th percentile was calculated ensuring the percentile was representative of diurnal variations. Heat waves were defined as 8 consecutive six-hour observations that exceeded the 95th percentile and 5% minimum for node frequency was established to exclude low-frequency synoptic patterns. Node frequencies for both temperature and equivalent temperature heat wave days were calculated and trends were analyzed for significance.

3.2 Equivalent Temperature Methodology

Equivalent temperature was calculated from the Chicago O'Hare International Airport dataset values of station pressure, temperature and dew point temperature. Vapor pressure, represented as (e) was derived from dew point temperature using the Bolton (1980) relationship; results are in units of degrees Celsius.

$$e = 6.112exp\left(\frac{17.67T_d}{T_d + 243.5}\right) \qquad (6)$$

The next step, calculating specific humidity (kg/kg), was accomplished by using station pressure, vapor pressure, and the following equation:

$$q = \frac{0.622e}{P - 0.378e} \tag{7}$$

To determine the latent heat of vaporization the Fall et al. (2010) equation was employed (°C):

$$L_v = (2.5 - 0.0022T)x10^6 \tag{8}$$

Equivalent temperature values were then calculated for the Chicago O'Hare International Airport dataset 1948-2014 data set and graphed along with temperature values. To determine significance, median of pairwise slopes regression was used; this measure is considered robust and is minimally impacted by outlying data values (Lanzante et al., 1996). Observations of temperature and equivalent temperature exceeding heat wave criteria were located on the SOM to determine nodes responsible for heat wave generation.

3.3 Self-Organizing Map Implementation

SOMs were chosen to extract synoptic patterns from geopotential height 500 mb and specific humidity 850 mb for Chicago, IL. To determine the appropriate number of nodes, several SOMs were analyzed. SOMs of 4×4, 5×5, and 6×6 were implemented with node assignment percentages calculated. The 4×4 SOM produced 16 nodes with distinct synoptic patterns and high percentages of occurrence. However, 16 nodes did not allow for adequate representation of synoptic transitions. The 5×5 SOM contained 25 nodes with moderate percentages of occurrence; this ensured that data was distributed moderately between nodes and synoptic patterns were not over simplified. The 6×6 SOM contained 36 nodes with extremely low percentages; this SOM produced several nodes with little variation between synoptic patterns

signifying the number of nodes was too large. SOM parameters for this study were 25 nodes, initial learning rate of 0.5 that incremented to 0.1 over 500,000 iterations. Initial weights were random with an initial attraction of 3.0 that decreased to 0.01. These values are similar to Schuenemann et al. (2008) who employed a radius of 2 and a learning rate of .01 that decreased over one million iterations.

CHAPTER 4

RESULTS AND DISCUSSION

To identify a trend in temperature or equivalent temperature values, time series of both variables were constructed. Because missing values would artificially decrease averages and influence trend significance they were omitted from these calculations. Yearly summertime means for temperature and equivalent temperature were plotted to determine if a trend was present and median of pairwise slopes regression (Lazante 1996) was used to determine the slope. Chicago O'Hare International Airport dataset temperature time series trend was not found to be significant at the 0.05 level (Figure 4.1) and the equivalent temperature trend was similarly positive but not statistically significant at the 0.05 level (Figure 4.2).

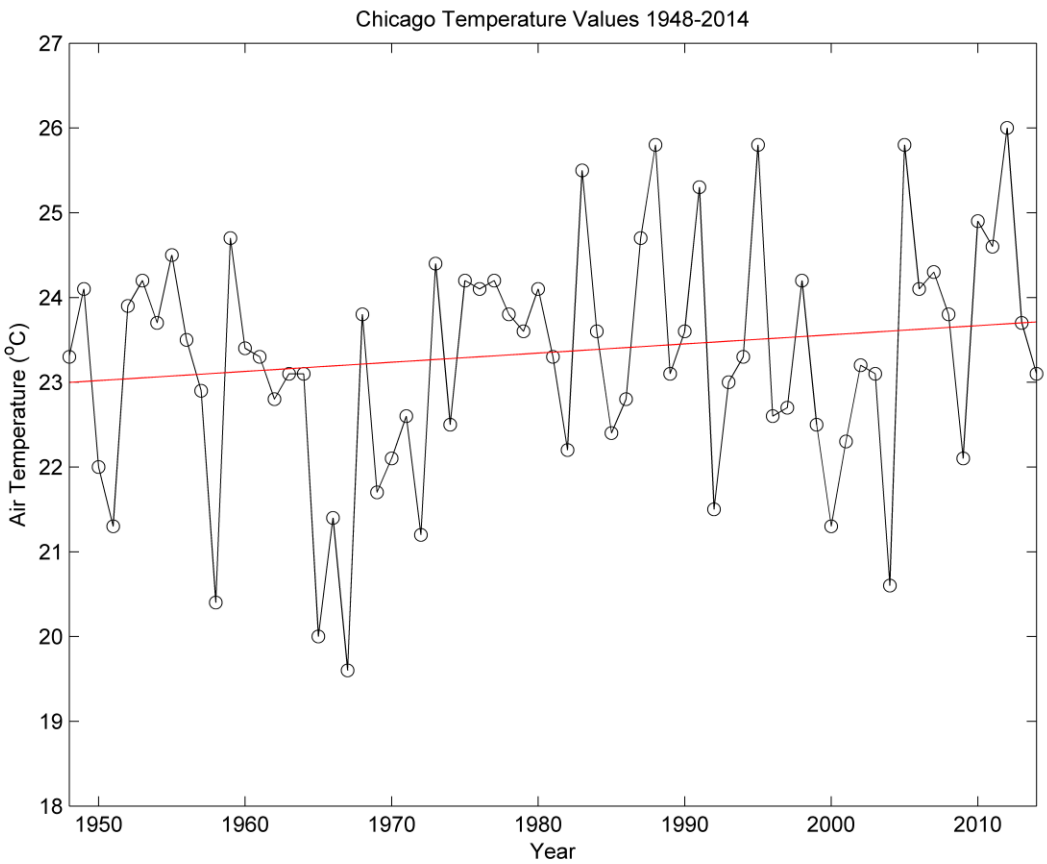

Figure 4.1: Chicago O'Hare International Airport dataset temperature time series using June 1st through September 15th 1948-2014 data set. Median of pairwise slopes was used to determine significance; the trend of 0.11°C per decade is not significant at the 0.05 confidence level with a p-value of 0.171.

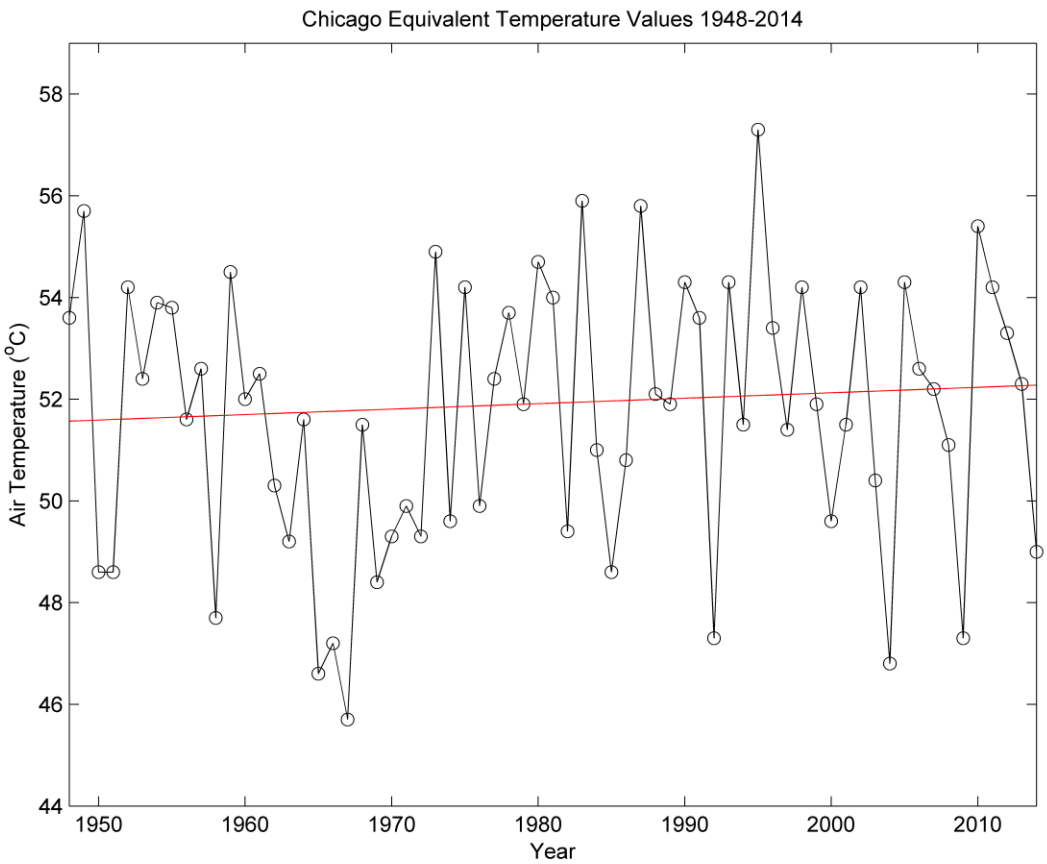

Figure 4.2: Chicago equivalent temperature time series using June 1st through September 15th 1948-2014 data. Median of pairwise slopes was used to determine significance; the trend of 0.11°C per decade is not significant at the 0.05 confidence level with a p-value of 0.480.

Additionally, time series of temperature and equivalent temperature were constructed for yearly summertime absolute maximum and absolute minimum values. Although Chicago temperature maximum values did not contain a significant trend minimum temperatures were found to be increasing with a significant trend at the 0.05 confidence level (Figures 4.3 and 4.4. respectively). These results are consistent with findings from additional research that discovered an increase in overall minimum temperatures (Schoof et al. 2014; Perkins et al. 2015). Equivalent temperature maximum values displayed a slightly decreasing trend that was not found to be significant while T_E minimum was increasing but was not found to be significant with a p-

value of 0.067 (Figures 4.5 and 4.6 respectively). Cooling nighttime temperatures provide relief from extreme conditions and allow recuperation from heat stress. The warming of overall minimum temperatures without an increase in maximum temperatures indicates a compact diurnal range minimizing nighttime temperature relief.

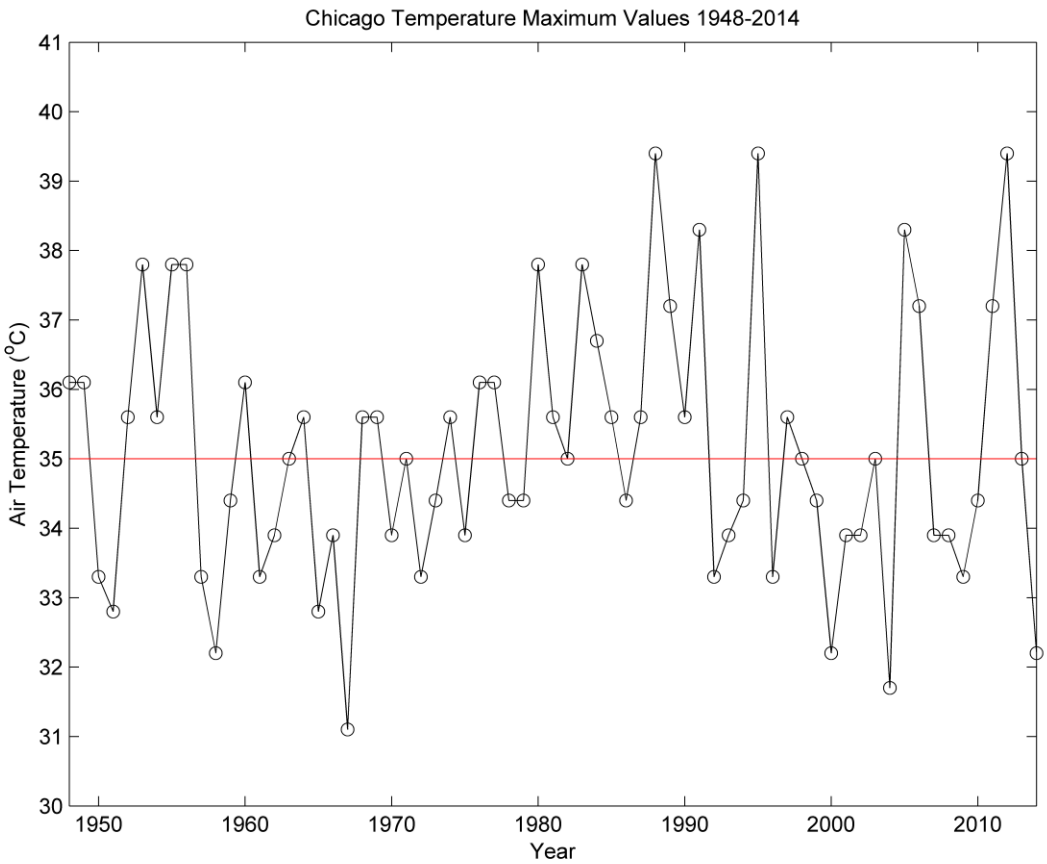

Figure 4.3: Chicago maximum temperature time series using June 1st through September 15th 1948-2014 data. Median of pairwise slopes was used to determine significance; the trend of 0.00°C per decade is not significant at the 0.05 confidence level with a p-value of 0.911.

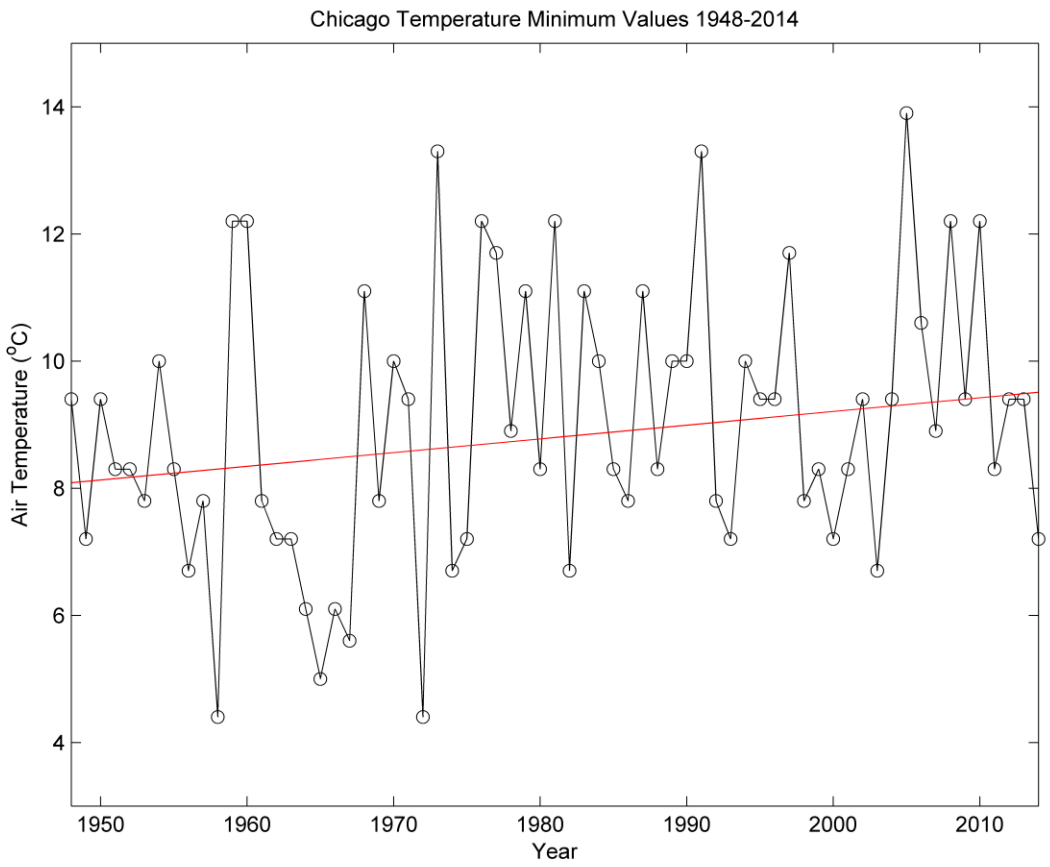

Figure 4.4: Chicago minimum temperature time series using June 1st through September 15th 1948-2014 data. Median of pairwise slopes was used to determine significance; the trend of 0.22°C per decade is significant at the 0.05 confidence level with a p-value of 0.042.

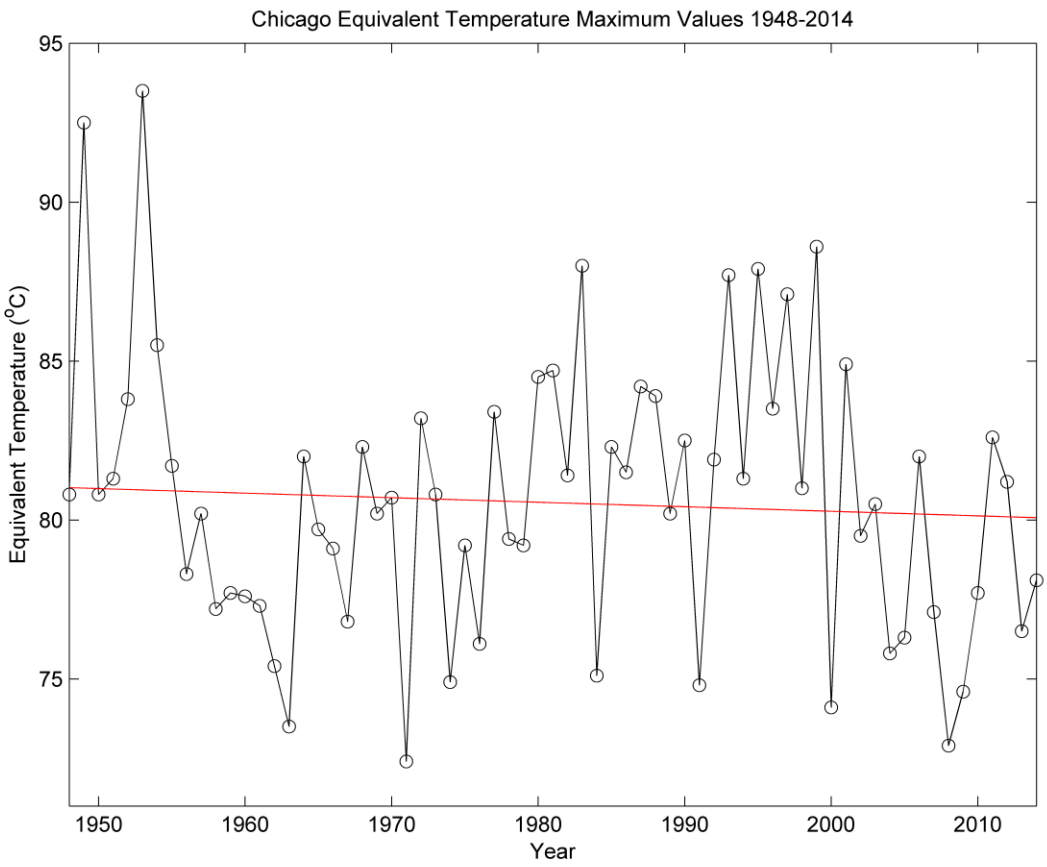

Figure 4.5: Chicago maximum equivalent temperature time series using June 1st through September 15th 1948-2014 data. Median of pairwise slopes was used to determine significance; the trend of -0.14°C per decade is not significant at the 0.05 confidence level with a p-value of 0.552.

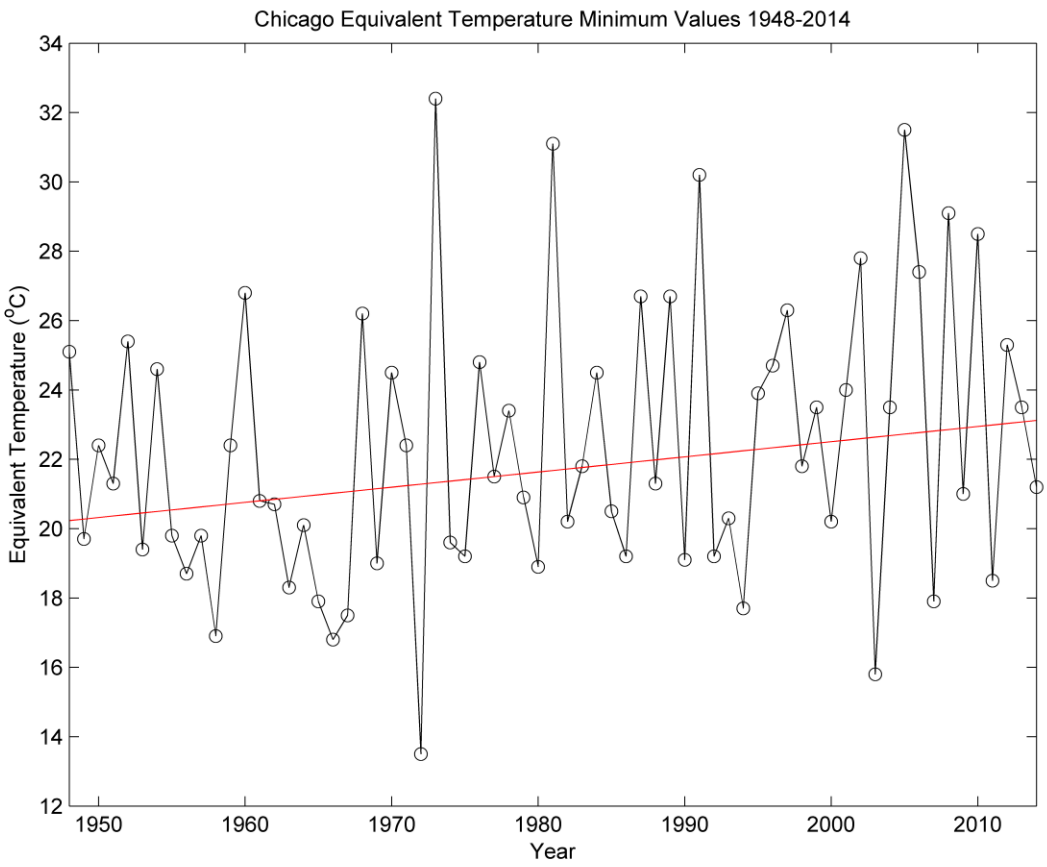

Figure 4.6: Chicago minimum temperature time series using June 1st through September 15th 1948-2014 data. Median of pairwise slopes was used to determine significance; the trend of 0.44°C per decade is not significant at the 0.05 confidence level with a p-value of 0.067.

4.1 Self-Organizing Map Patterns

SOMs were chosen to extract synoptic patterns from geopotential height 500 mb and specific humidity 850 mb for Chicago, IL (Figures 4.7 and 4.8, respectively) with frequencies calculated to determine the amount of observations assigned to each node. (Table 4.1 and 4.2, respectively).

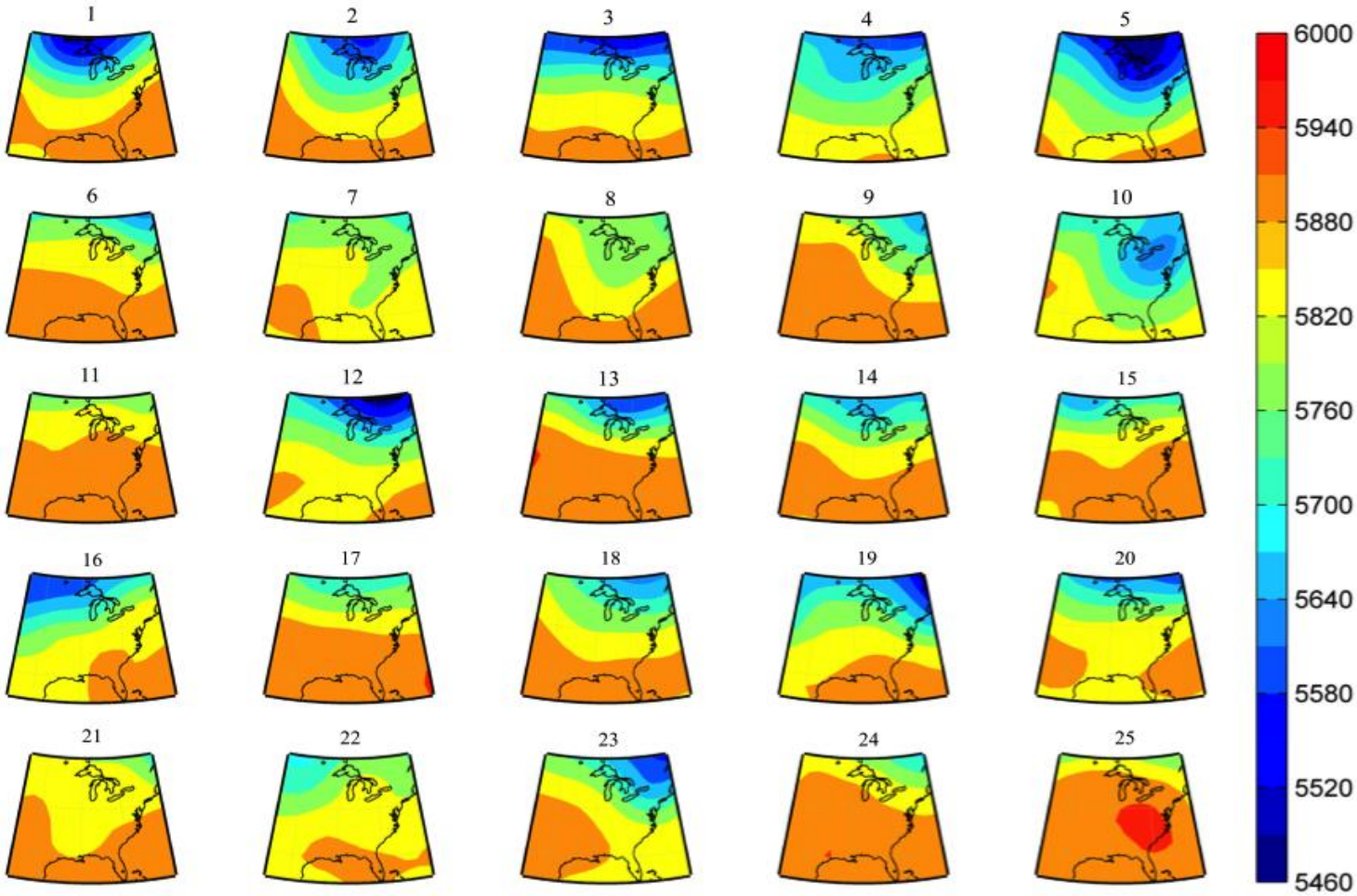

Figure 4.7: Self-organizing map of 500 mb geopotential height data for June through September 1948-2014; values are in meters.

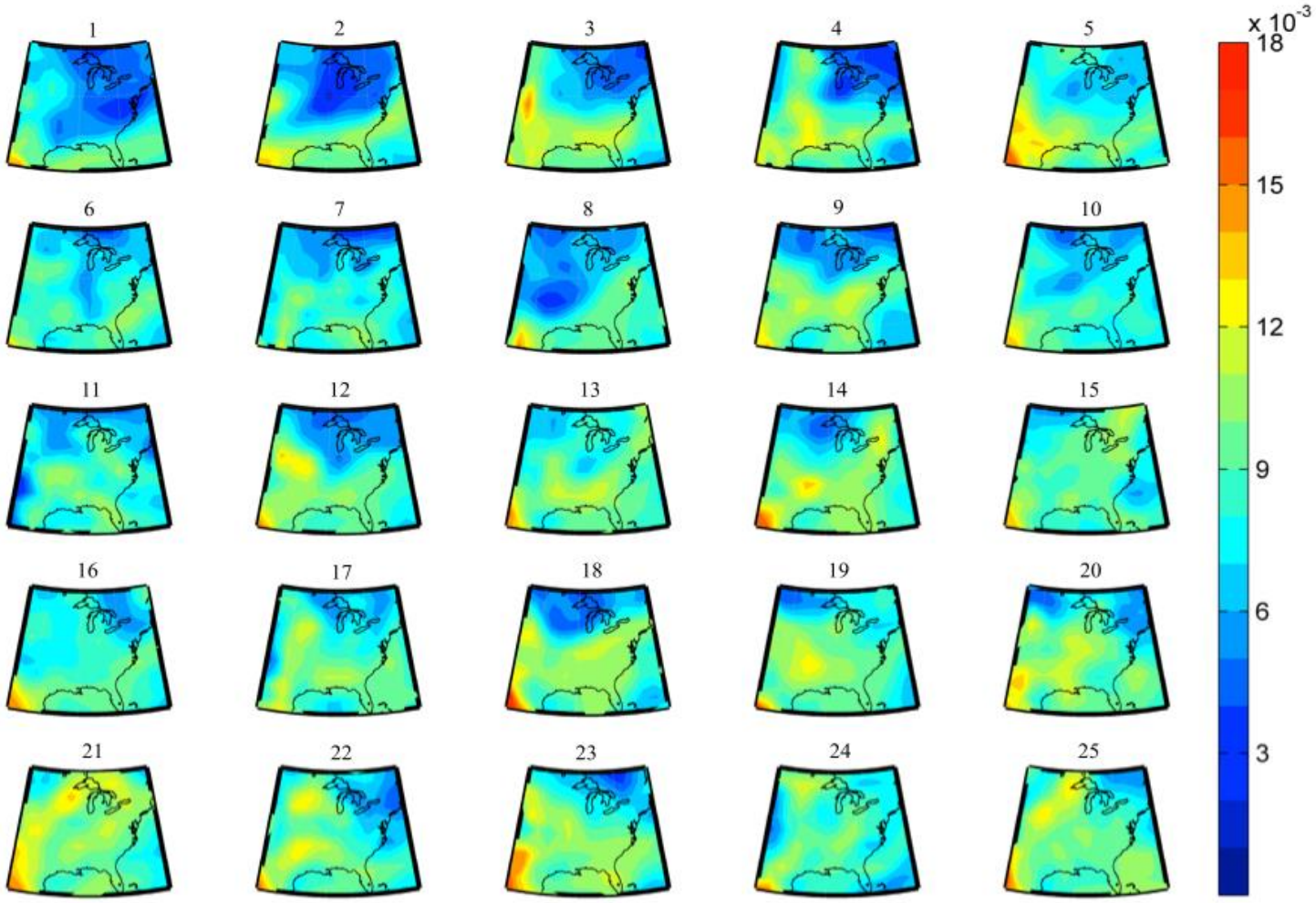

Figure 4.8: Self-organizing map of 850 mb specific humidity data for June through September 1948-2014; values are in kg/kg

Table 4.1: Calculated frequencies of 500 mb geopotential height 5×5 SOM observations.

Geopotential Height 5×5 SOM Node Frequencies				
Node 1	Node 2	Node 3	Node 4	Node 5
1.89%	3.17%	1.96%	2.12%	1.28%
Node 6	Node 7	Node 8	Node 9	Node 10
7.10%	2.56%	3.37%	6.32%	1.23%
Node 11	Node 12	Node 13	Node 14	Node 15
5.84%	4.18%	5.19%	6.12%	5.81%
Node 16	Node 17	Node 18	Node 19	Node 20
3.00%	6.09%	6.07%	2.34%	4.79%
Node 21	Node 22	Node 23	Node 24	Node 25
2.65%	3.52%	5.79%	5.03%	2.58%

Table 4.2: Calculated frequencies of 850 mb specific humidity 5×5 SOM observations.

Specific Humidity 5×5 SOM Node Frequencies				
Node 1	Node 2	Node 3	Node 4	Node 5
4.09%	2.44%	3.24%	2.00%	3.35%
Node 6	Node 7	Node 8	Node 9	Node 10
5.53%	4.14%	2.49%	5.43%	6.75%
Node 11	Node 12	Node 13	Node 14	Node 15
2.04%	6.56%	3.80%	4.32%	4.00%
Node 16	Node 17	Node 18	Node 19	Node 20
3.81%	4.00%	3.30%	6.40%	3.37%
Node 21	Node 22	Node 23	Node 24	Node 25
2.30%	5.47%	6.03%	2.06%	3.08%

To ensure each node was accurately descriptive of the assigned days, SOM map means and standard deviations were calculated. Each synoptic pattern present on the SOM is representative of an observation, or seed day, in the data set with each seed day replicating similar observations assigned to the node. A map of mean values for all days assigned to each seed day was produced to ensure the node was representative of the underlying observations; ideally, mean values should replicate the seed day with minor deviations. Mapped mean values for 500 mb geopotential height and specific humidity 850 mb were overall representative of SOM node synoptic patterns. Additionally, standard deviations from the seed day were summed and mapped to display areas where discrepancies may be present. High deviations can signify a seed day that is trying to represent too many patterns or outliers; low deviations assure a representative seed day with few variants in observations. Overall, a successful SOM contains low deviations among seed days and means that reproduce the node synoptic pattern. Standard deviations for geopotential height 500 mb and specific humidity 850 mb are low overall. Descriptions for each geopotential height and specific humidity SOM node are included below.

4.2 Geopotential Height SOM Node Descriptions

Geopotential height 500 mb values were mapped using the self-organizing map algorithm and twenty-five prominent weather patterns were extracted from NCEP/NCAR reanalysis data for the study area specified. Nodes containing observations that exceeded heat wave criteria at the 95th percentile for extreme temperature are nodes: 6, 9, 11, 15, 24 and 25. For equivalent temperature heat waves prominent nodes are: 6, 9, 11, 15, 17, 24, and 25.

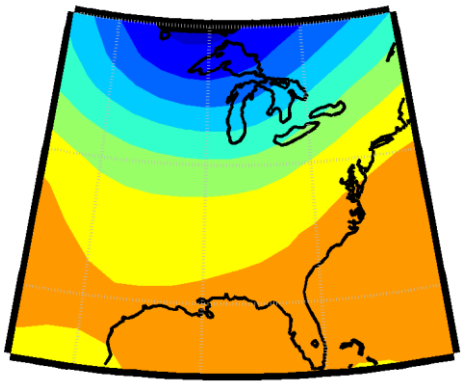

Figure 4.7.1: Geopotential height self-organizing map node 1.

1. In node one, a deep trough is present over the northern U.S. with height values gradually increasing southward. High height values of roughly 5880 meters encompass the extreme south and western portions of the study area. To determine the extent of node replication of input data, the mean and standard deviation of each value assigned to each specific node were calculated. For node one, the mean is very representative, almost indistinguishable from the SOM projected synoptic pattern. Standard deviation shows low values overall with higher discrepancies on the northern border of the study area.

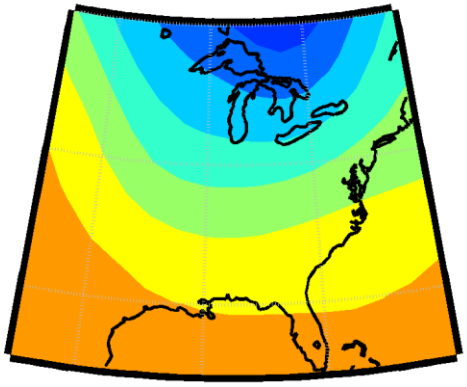

Figure 4.7.2: Geopotential height self-organizing map node 2.

2. Node two, being similar to node one, has a deep trough slightly off center in the northern portion of the study area with low heights in Chicago. Lowest values reach approximately 5560 meters with high height values covering the southwest. Mean value for all days assigned to the node represent the SOM projected node with slight variations. The map of mean days is characterized by a symmetrical trough that extends south into the study area. Standard deviation of days assigned to node two display the troughing pattern with overall low deviations. Highest standard deviation values occur on the northern boundary with two small ridges forming further south.

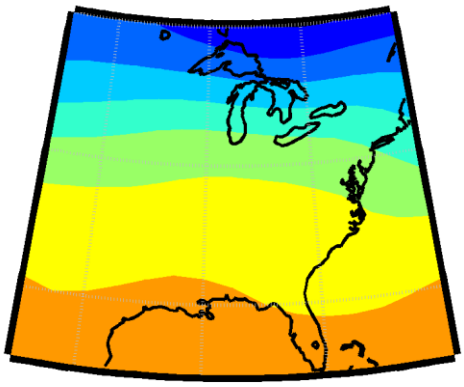

Figure 4.7.3: Geopotential height self-organizing map node 3.

3. Node three is characterized by zonal flow with slight ridge-trough fluctuations and low values across the northern boundary that decreases southward. Chicago is located in an area of semi-low heights. Mean values assigned to the node display suppressed variation and enhanced zonal flow. Standard deviations for node three are overall low values with the northeast containing the maximum values of roughly 60. Also present, small ridge of low deviations is positioned over the central east coast.

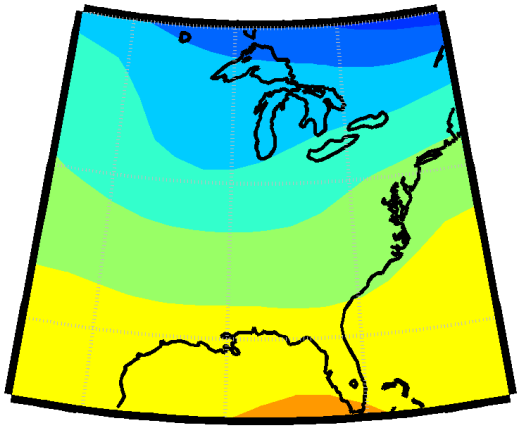

Figure 4.7.4: Geopotential height self-organizing map node 4.

4. In node four, the central portion of the study area is encompassed in a slight trough. Low height values extend southward with lowest values reaching roughly 5550 meters and high height values are located in the south. Node four mean values have several discrepancies. The overall trough pattern is apparent although more subdued and the lobe of high heights apparent in the southern portion of the SOM node is omitted from the mean. The lowest values, located in the northern portion of the SOM node, are less extreme. Standard deviations are highest on the northern border of the node with a small lobe of high values in the northeast. Maximum standard deviations reach approximately 70 while, further south, minimum values of roughly 20 cover the Gulf and Florida.

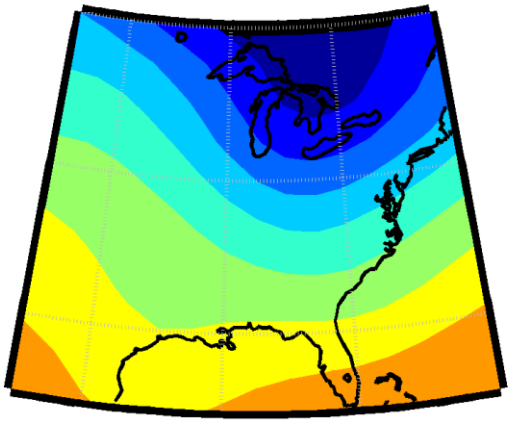

Figure 4.7.5: Geopotential height self-organizing map node 5.

5. Node five contains a deep low just east of Chicago with a short, steep gradient; this is the strongest and deepest trough apparent on the geopotential height SOM. Highest height values occur in southern Texas and the tip of Florida. Mean values are similar with a more organized, slightly reduced trough located in the northeast and a stronger gradient with high values is present in the southeast. Standard deviations for node five are highest for all nodes on the SOM with a large lobe of high values in the northeast extending southward. Overall, the standard deviation pattern mirrors SOM node and mean map with an eastward shift. Highest deviations occur in the northeast, where the SOM lowest values were concentrated.

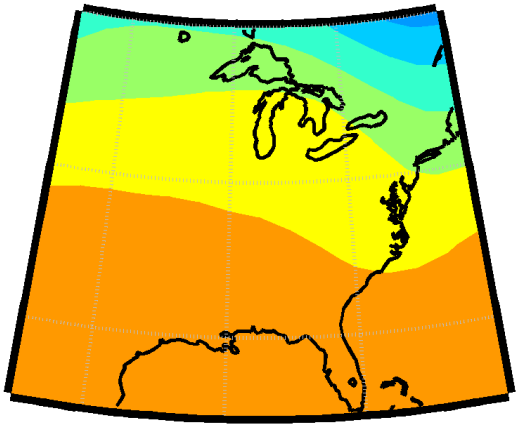

Figure 4.7.6: Geopotential height self-organizing map node 6.

6. Node six contains high heights over the south with a slow decrease northward and low heights concentrating in the northeast. Slight ridging is apparent signifying the potential to produce elevated temperatures consistent with Perkins (2015). Mean values for node six contain similar- if not identical- values with an intensified, more organized ridge over the western portion of the study area. Standard deviations reveal a significant ridge centered in the node; this ridge has low values but spans a vast area of the United States. Higher values are present in the northern edge and extend down the eastern and western edges.

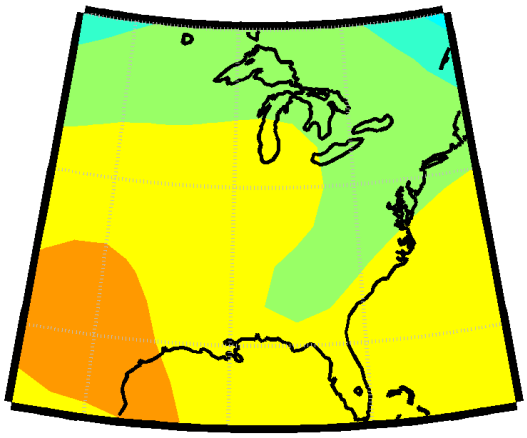

Figure 4.7.7: Geopotential height self-organizing map node 7.

7. In node seven, low heights are concentrated in the northeast and northwest. Heights of roughly 5800 meters reach the great lakes with a lobe extending southward covering the eastern coast of the United States. High height values of approximately 5910 meters concentrate in the southwestern section of the node. Mean values for node seven retain overall similarity but truncate the southward extending lobe; the region of high heights is drastically reduced in size and shifted to the southwest. Standard deviations show low values over the southern portion with a slow gradient northward to higher values. Highest deviations are located in the northeast.

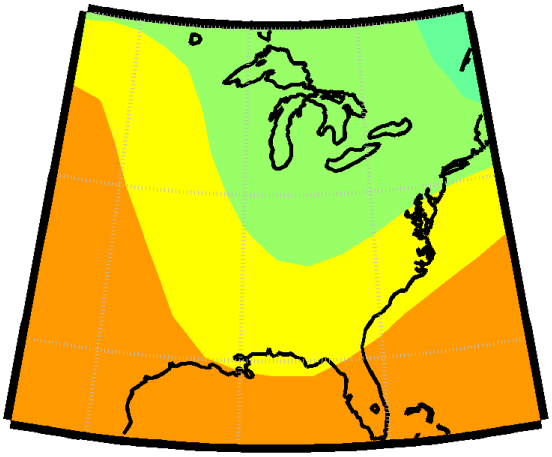

Figure 4.7.8: Geopotential height self-organizing map node 8.

8. In node eight, moderately low height values form a ridge-trough-ridge system. The western portion of the first ridge is in the northwest with a subsequent deep trough; the next ridge covers the eastern states and extends off the coast. Mapping the means of node eight shows a consistent pattern with the most extreme values reaching further east and expanding. For standard deviations, a lobe of low values extends up the western boundary. On the southern boundary, deviations are effectively zero and increases northward; maximum values are 50.

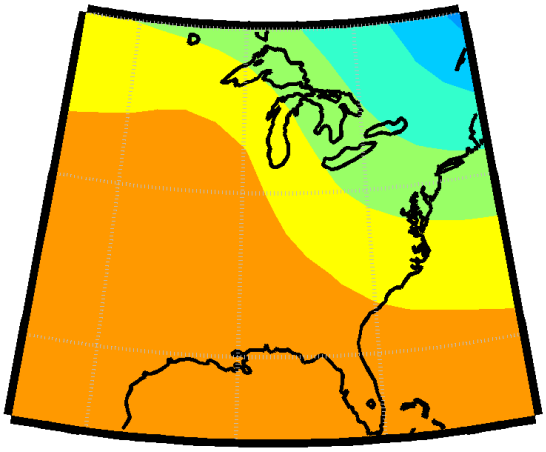

Figure 4.7.9: Geopotential height self-organizing map node 9.

9. Node nine has an apparent deep trough located in the northeast and extending across the top of the node. High geopotential height values cover the southern edge and expand up the western boundary. A strong ridge is positioned over Chicago with associated elevated height values. Amplified ridging is identified in Livezey and Tinker (1996) as causing the extreme temperatures responsible for the Chicago 1995 heat wave indicating node 9 contains conditions associated with the production of extreme events. Mean values display a map that is exceptionally representative of the SOM node. When analyzing mapped standard deviations, a ridge of low values occurs just off the western boundary with values of 20 covering the majority of the study area. Highest deviation values in the northeast gradually decrease toward the southwest.

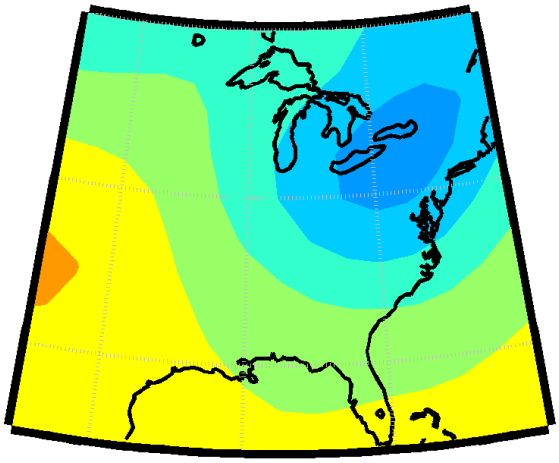

Figure 4.7.10: Geopotential height self-organizing map node 10.

10. A trough is located over the northeastern United States in node ten with a closed lobe of low heights is centered over northern Pennsylvania. High height values extend north from the southern boundary with an anomalous lobe of high heights on the western edge that is approximately 5890 meters. Mean values for node ten are overall representative of the SOM pattern with a few alterations. The lobe of low values is further east encompassing the northeastern edge of the states and continuing out of the study area while the parcel of high heights apparent in the SOM is omitted from the mean. Additionally, the trough has shifted eastward with a decrease in range.

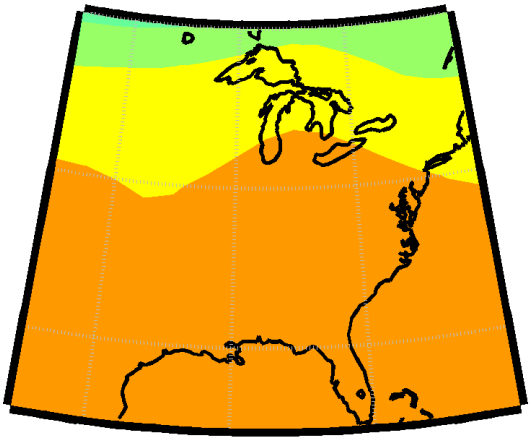

Figure 4.7.11: Geopotential height self-organizing map node 11.

11. In node eleven, consistent and high height values cover the majority of the study area with large transitional bands that decrease in height with latitude. A ridge occurs around the Great Lakes region with a proceeding trough. Elevated height values and ridging are upper atmospheric features determined by Perkins (2015) to produce extreme conditions indicating node 11 as a potential pattern for the production of extreme conditions. Mean values display a similar pattern with a slight area of low values occurring in the northeast and a decrease in the extent of the western ridge. Standard deviation map is similar to standard deviation values of node six, directly above. Low deviations cover the southern and middle portions with higher values expanding southward from the northern boundary.

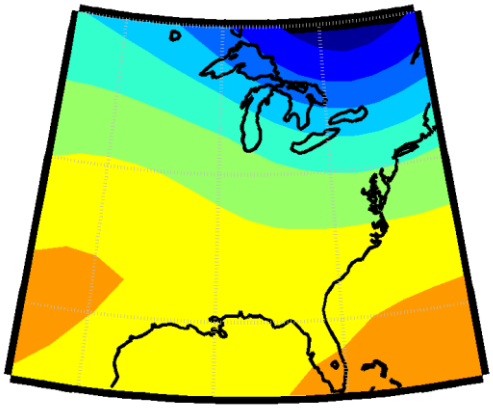

Figure 4.7.12: Geopotential height self-organizing map node 12.

12. Node twelve produces a deep, organized trough encompassing the northeast with heights increasing as latitude decreases. Values of 5700 meters extend as far south as Carolina with minimum values reaching 5460 meters at the center of the trough. A lobe of roughly 5900 meters occurs off the southwest covering portions of Florida and the Atlantic with an additional, smaller lobe extending from the southwestern edge. Mapping mean values presents a trough of the same magnitude but shifted northward decreasing the amount visible in the study area. Instead of two lobes of high height values, a band of high heights covers the southern boundary and extends upward on both the eastern and western edges. Standard deviation shows low values across the southern half with high values in the northeast where the SOM low is present.

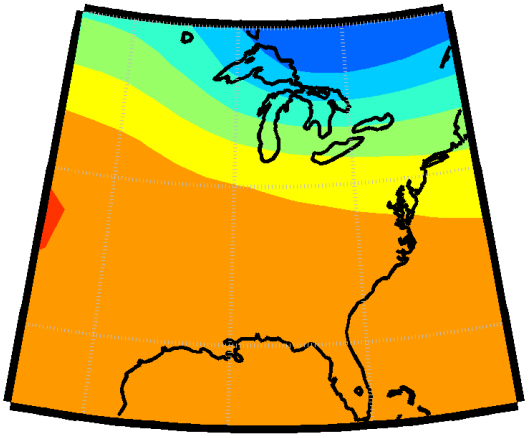

Figure 4.7.13: Geopotential height self-organizing map node 13.

13. Node thirteen displays an area of low height present in the northeast extending southward. Slight troughing is apparent on the northern boundary with flow transitioning to zonal with decreasing latitude. High height values of 5900 meters cover the majority of the node with a lobe of high heights occurring in the central region of the western boundary; this area reaches heights of approximately 5980 meters. Mapping mean values displays a stronger trough with slightly more variable flow. Most notably, the lobe of high heights is absent from the mean. Standard deviations have a ridge-trough-ridge pattern emerging just south of the great lakes; highest deviations occur in the north and northeast with a large majority of deviations being roughly 20.

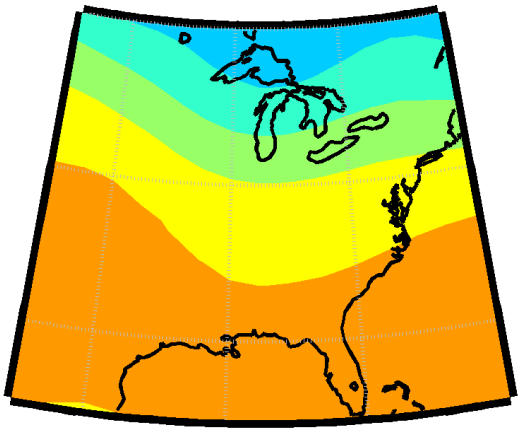

Figure 4.7.14: Geopotential height self-organizing map node 14.

14. Node 14 has an extensive trough on the northern boundary with large transitional bands to higher heights on the southern edge. Slight ridging occurs on either side of the feature with a small anomalous lobe on the western side of the southern boundary. Mean values replicate the SOM pattern with smoothened features and the omission of the anomalous low. The ridge-trough-ridge pattern is exaggerated in the map of standard deviations. Overall, standard deviation values are subdued for this node with a maximum value of 40.

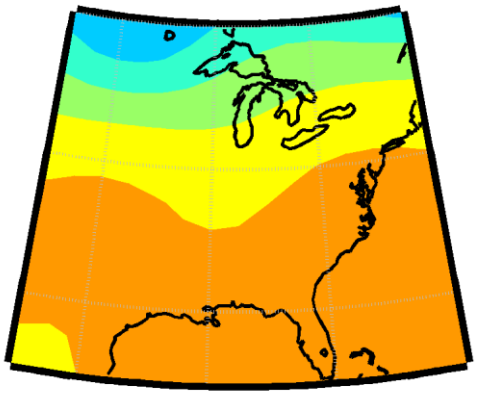

Figure 4.7.15: Geopotential height self-organizing map node 15.

15. Node fifteen is characterized by moderately low heights in the northwest with high height values of 5900 meters covering the majority of the south. The high height values reach northward in two peaks; one slightly off the western boundary and one on the eastern coast. Additionally, the southwest contains an anomalous low. Mapping the mean shows a depressed trough with high height values over the entire southern half of the node. The peaks of high height are smoothed and the low in the southwest of the SOM is excluded from the mean. Standard deviation highest values are located in the northwest and northeast; low values replicate the two peaks of height values in the SOM node.

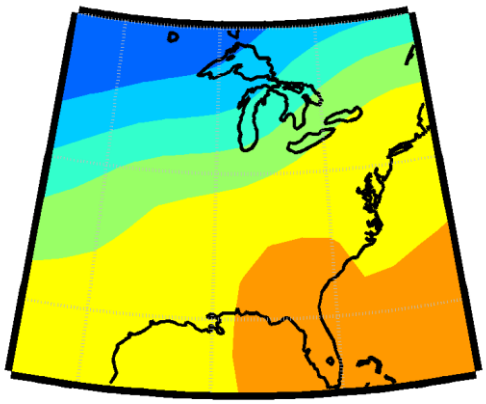

Figure 4.7.16: Geopotential height self-organizing map node 16.

16. In node sixteen, low heights concentrate in the northwest and gradually decrease in a southeast direction; high heights extend from the southeast. Mean values mapped to the node contain the southeastern decreasing pattern with high values in the southeast. However, in the mean, the high height values span a larger area and a small area of high values emerges on the western edge of the southern boundary. Standard deviations have overall low values across the southern portion with and increase toward the northern boundary. Highest values extend southward from the northeast.

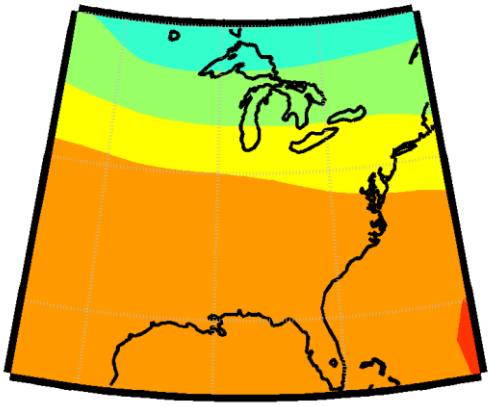

Figure 4.7.17: Geopotential height self-organizing map node 17.

17. Node seventeen has zonal flow with low height values spanning the northern edge and gradually increasing southward. High height values cover the southern portion. A small lobe of high pressures, roughly 5950 meters, occurs off the southern side of the eastern boundary. Mapped mean values omit the lobe of high height but replicate the SOM node pattern of zonal, southerly increasing flow almost identically. Mapped standard deviations have low values across the southern boundary of the node with a gradual increase northward. Highest values occur in the northwest and northeast and reach southward.

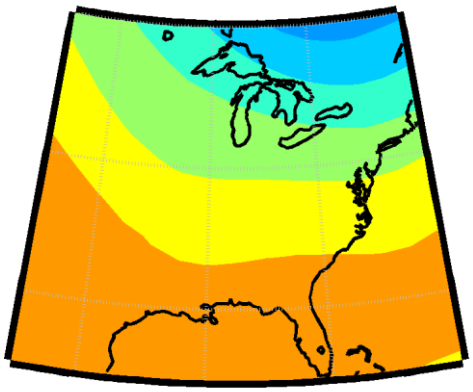

Figure 4.7.18: Geopotential height self-organizing map node 18.

18. In node eighteen, a moderate trough occurs in the northeast with heights decreasing southward. High heights encompass the southern portion of the node with areas of northward expansion. A small, anomalous lobe of low height values occurs in the southeast. Mean values exclude the lobe of low heights and present a more organized, smoother pattern of a trough in the northeast with low values extending further south. Standard deviations have low values in the south with two large peaks northward in the center of the node; highest deviations can be found in the northeast.

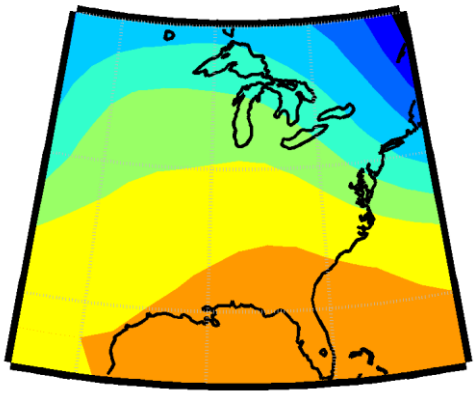

Figure 4.7.19: Geopotential height self-organizing map node 19.

19. Ridging dominates the center of node nineteen with a subsequent deep trough in the northeast. High heights are concentrated in the southeast with a decrease in height as latitude increases. Node map of mean values has a stronger ridge-trough pattern with less variability. The trough has decreased in strength and shifted north, ridging is more apparent and the height values are suppressed in the south. Standard deviations replicate the SOM pattern with low deviations covering the ridge and highest values in the northeast overlaying the trough.

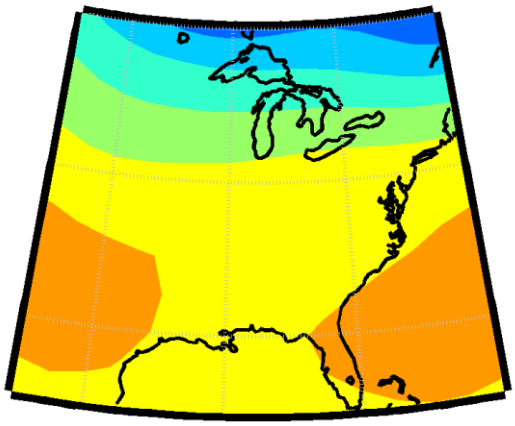

Figure 4.7.20: Geopotential height self-organizing map node 20.

20. In node twenty, high height values occur in two lobes on the southern portion of the eastern and western boundaries. Low heights encompass the northeastern portion of the node with small, tight bands that decrease in height southward. Moderate values of roughly 5850 meters extend from the southern boundary and cover the central U.S. Mapped means values diverge considerably for node twenty. The overall flow is more zonal and higher height values occur in the southern half of the node. Instead of two high pressure lobes, one large area of high heights spans the southern portion with a small lobe of lower values on the western edge of the southern boundary. Standard deviation has a value of 20 across the majority of the study area with higher values in the north of the great lakes and highest on the north boundary.

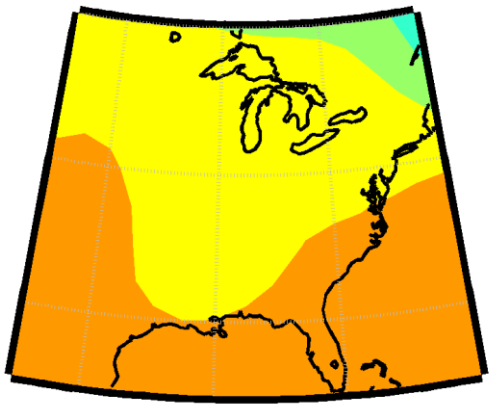

Figure 4.7.21: Geopotential height self-organizing map node 21.

21. High height values dominate node twenty-one. Highest values occur in the south with northward expansion across the eastern and western boundaries. Values of 5850 meters begin in the center of the node and expand north with lowest heights covering the northeast. Mean values display a similar pattern with the areas of high heights being pushed slightly further south and an increase in the low values found in the northeast. Standard deviations display a dissimilar pattern with lowest values in the south peaking in two distinct areas; moderate values then spread north with a lobe of high deviations located over the eastern great lakes. Highest deviations occur in the northwest and northeast.

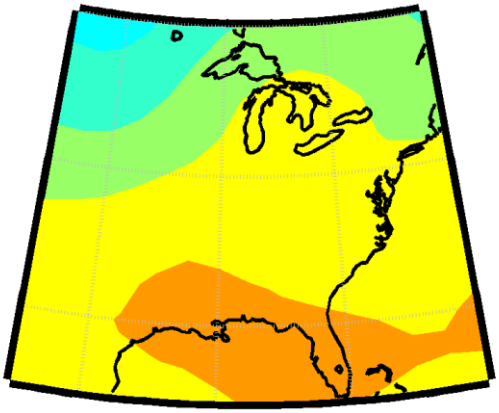

Figure 4.7.22: Geopotential height self-organizing map node 22.

22. Node twenty-two has an apparent trough-ridge pattern. The weak trough emerges from the northwest and ridges over the great lakes. High heights occur in a large lobe just off of the southern boundary. High values cover portions of the Gulf, extend into the United States, and a small portion of the Atlantic. Mapped means replicate the trough-ridge pattern with high heights that extend slightly north from the southern boundary. Highest standard deviations occur in the north and extend a significant distance down the eastern and western boundaries. Low values cover a large portion of the south with moderate deviations expanding northward, covering the great lakes.

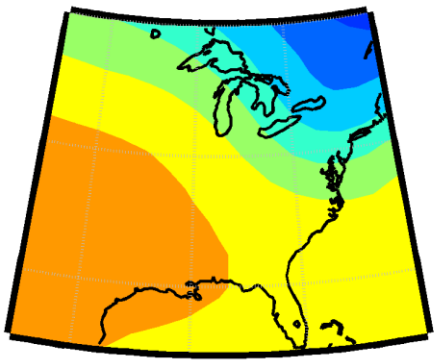

Figure 4.7.23: Geopotential height self-organizing map node 23.

23. In node twenty-three deep troughing is apparent in the northwest with large, southward decreasing bands and a lobe of high heights in the west. Mapped mean values display a deeper, more organized trough with high heights spanning the entire southern boundary and forming a distinct ridge-trough pattern not apparent in the SOM node. Standard deviations have a large ridge of low values in the west with higher values in the north and extending southward from the northeast.

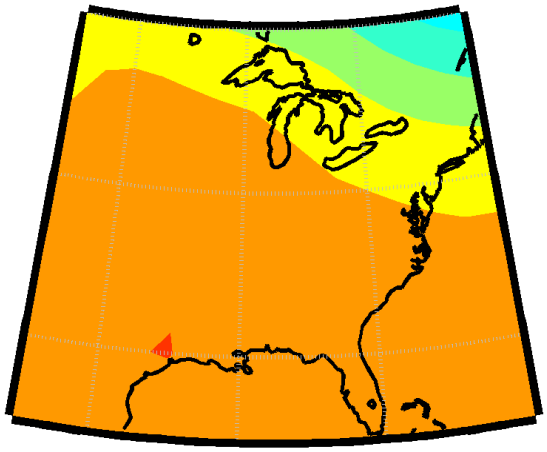

Figure 4.7.24: Geopotential height self-organizing map node 24.

24. A ridge-trough pattern with moderate values encompasses node twenty-four. High heights cover the majority of node with a small area of increased height values located in eastern Texas; lowest values are located in the northeast. Mapped mean values adequately replicate the SOM node however, omit the lobe of high heights. Standard deviations have low values of 10 across the southern boundary with an increase northward with highest values in the northeast.

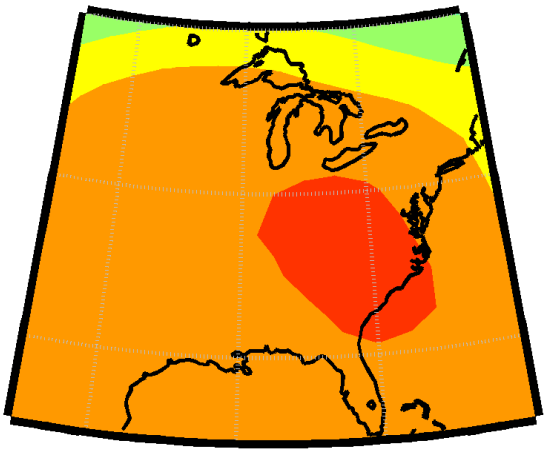

Figure 4.7.25: Geopotential height self-organizing map node 25.

25. Node twenty-five is characterized by large expanses of elevated height values. High heights span the United States with a large lobe of increased heights, approximately 5960 meters located along the eastern coast. Elevated heights accompanied by atmospheric riding are features determined to generate heat waves (Perkins 2015) indicating nodes 24 and 25 are likely to produce extreme temperatures. Lowest height values of roughly 5730 meters occur in the northeast and northwest. Mapped mean values for node twenty-five exclude the lobe of high values but replicate the large decreased northern bands. Standard deviations are dominated by low values in the south increasing toward the north with an anomalous lobe of elevated values in the central U.S.

4.3 Specific Humidity Self-Organizing Map Node Descriptions

Specific humidity 850 mb values were mapped using the self-organizing map algorithm and twenty-five prominent weather patterns were extracted from NCEP/NCAR reanalysis data for the study area specified. Nodes containing observations that exceeded heat wave criteria at the 95th percentile for extreme temperature are nodes: 14, 18, 19, 20, 24, and 25. For equivalent temperature heat waves prominent nodes are: 5, 14, 15, 19, 20, 24, and 25.

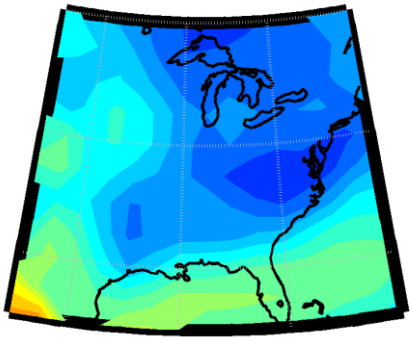

Figure 4.8.1: Specific humidity self-organizing map node 1.

1. Specific Humidity node one lowest values are located on the eastern coast and extend northwest. Highest humidity occurs in the southwest with elevated values along the southern boundary. Mapped mean values display an organized, weak trough with lowest values in the northeast and highest values in the southwest. When mapped, highest standard deviations are located in southwest and extend north; moderate deviations occur in two lobes in the central U.S and off the eastern coast.

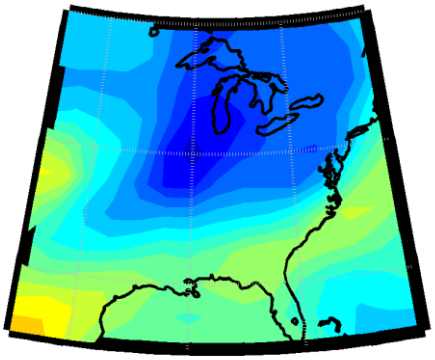

Figure 4.8.2: Specific humidity self-organizing map node 2.

2. In node two, a concentrated area of low heights occurs just east of Chicago with highest values located over southern Texas and extending north. A lobe of high humidity covers northern Florida and portions of the east coast before reaching over the Atlantic. Node two mapped mean values are dissimilar from the SOM node. Lowest humidity values are in the north and increase toward the west and south; highest humidity is located in the southwest and extends north. Standard deviation values are highest along the western boundary with lowest values in the south. A lobe of increased deviations is located along the east coast with moderate values spanning the southern and eastern United States.

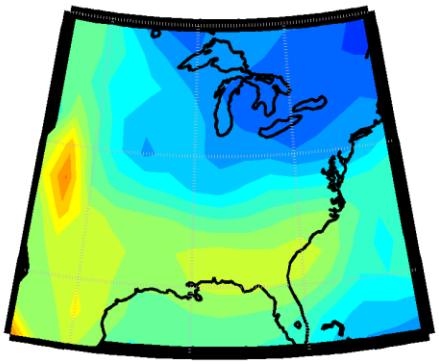

Figure 4.8.3: Specific humidity self-organizing map node 3.

3. Node three's highest humidity values are concentrated in a small lobe just off the western boundary and extend to the south and east. Lowest humidity is found in the northeast with an additional small lobe located in the southeast and moderate values are located in northern Florida and several Gulf states. Mapped mean values have an area of low humidity located on the northern boundary with an additional lobe over southern Illinois; high humidity is concentrated in the southwest extending north and south with parcels of high values in Kansas and Florida. Standard deviations have highest values in the southwestern and expand north. A small expanse of deviations, roughly, 2×10^{-3} kg/kg, occurs just off the eastern coast with low deviations encompassing the extreme southeastern portion.

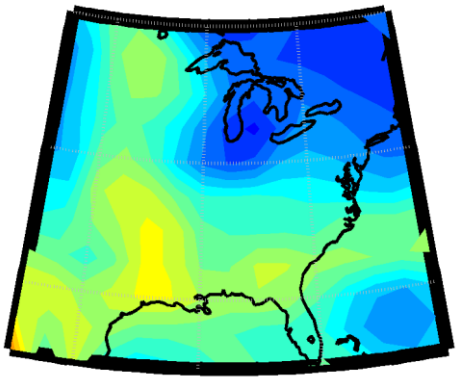

Figure 4.8.4: Specific humidity self-organizing map node 4.

4. In node four, lowest humidity is focused in the northeast with additional lobes of low values in the northwest and southeast. A small area of high values is located in the southwest with several lobes of approximately 13×10^{-3} kg/kg reaching north and east. Mapped mean values shift the high humidity lobes east with an overall decrease in values. Low mean humidity values converge in the northeast with a small lobe appearing in the southwest. Lowest standard deviations are present in the south with moderate values throughout; highest deviations occur in the west.

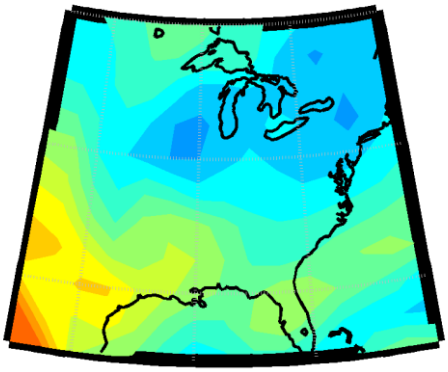

Figure 4.8.5: Specific humidity self-organizing map node 5.

5. High specific humidity values of roughly 15.5×10^{-3} kg/kg encompass the southeastern edge of node five; these values decrease toward the north and east with a small lobe of increased humidity over Florida. Low humidity values concentrate in three lobes that span the northeast. Mapped mean humidity displays a similar pattern with decreased values overall with an increase in area; moderate values span the southern United States and extend north slightly east of the Great Lakes. Additionally, low humidity values present in the SOM node have developed into a singular mass and shifted east. Standard deviations have moderate values in the eastern portion of the node and off the northeast coast; lowest values are located on the western boundary of the node.

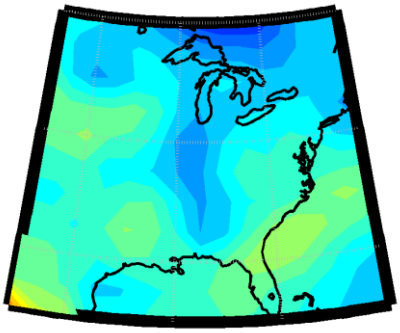

Figure 4.8.6: Specific humidity self-organizing map node 6.

6. Node is six characterized by low humidity values in the north with several lobes extending south and two small locations of low humidity in the southwest and southeast. Moderately low humidity values cover the southwestern and southeastern portions of the node with higher values in the extreme southwest and over Florida. Mapped mean values have two extreme low values just north and south of the great lakes; low values span the entire northern half of the node. High humidity is located in southern Texas with moderate values over Florida. Standard deviations show high values occurring in three areas: over Louisiana, off the northeast coast, and on the western boundary. Low values occur over the southeastern portion of the great lakes and on the southeastern edge of the node.

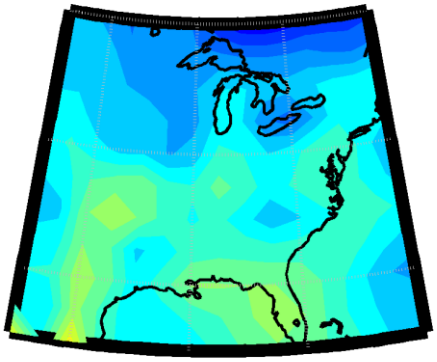

Figure 4.8.7: Specific humidity self-organizing map node 7.

7. In node seven, lowest humidity is located in the north with low values extending south in several lobes over the Great Lakes, southern Atlantic, and two small locations in the western portion of the node. Highest values encompass Texas and western Florida with northward extensions. Mapped mean values are higher and positioned in the southwest with moderate values over the southern states. Lowest values concentrate in the north spanning south slightly east of the great lakes. Highest deviations occur on the western boundary with moderate values off the northeastern coast and several Midwestern states; lowest deviations are located in the southeast and extend west.

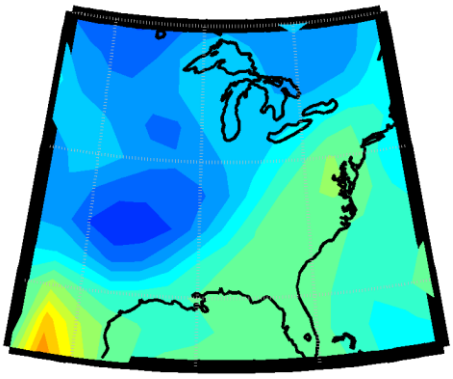

Figure 4.8.8: Specific humidity self-organizing map node 8.

8. Node eight highest humidity occurs over southern Texas with moderate values over Florida and extending up the eastern coast. Lowest humidity is located over Missouri and Arkansas and spreads northward with several isolated concentrations of low values. The mean humidity maps displays lowest humidity reaching south and west from a lobe positioned in the northeast. Moderate values cover the central United States with highest values over southern Texas. Mapped standard deviations show two lobes of high values. The largest lobe consequently contains the highest values of deviations and resides on the western boundary of the node; the second lobe is located just west of the Great Lakes. Lowest deviations are in the southwest of the node and extend west.

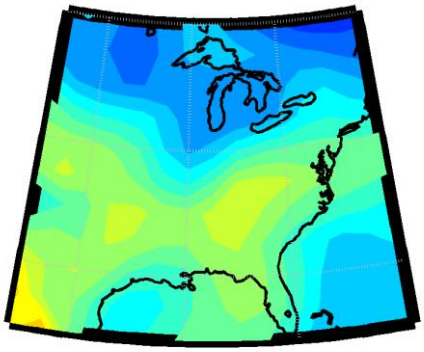

Figure 4.8.9: Specific humidity self-organizing map node 9.

9. Node nine is characterized by low humidity values in the north and a lobe of low humidity the southeast. Highest humidity occurs over southern Texas with high values dispersed throughout the central United States. Mean values replicate the high moisture values over southern Texas however the values are significantly more expansive and increased in magnitude. Moderate values cover the central United States in a large band with lowest values concentrating on the northern boundary. Highest deviations occur in the west with low deviations across the southwestern edge extending northward to Florida and portions of South Carolina.

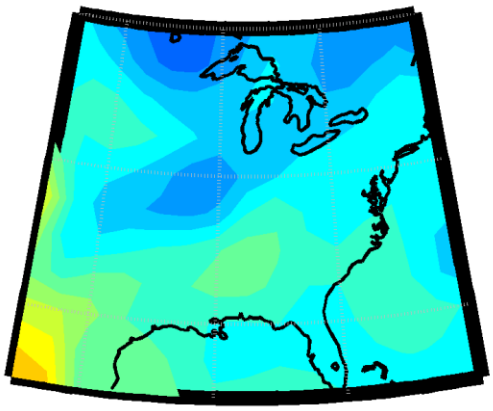

Figure 4.8.10: Specific humidity self-organizing map node 10.

10. Node ten has three distinct lobes of low humidity that are located in the north. Two lobes extend from the northern boundary with the last being slightly south and west of the Great Lakes. Highest humidity occurs in the southwest and extends slightly outward with small areas of moderate humidity located east of Louisiana. Mapped mean values show highest humidity in the southwest extending northward and gradually decreasing with latitude. Moderate humidity values expand across the southeastern United States with lowest values concentrating in the northeast. Mapped deviations are similar to deviations of node nine with highest values on the western boundary and lowest values spanning the southeastern edge and encompassing Florida and the Gulf. However, in node ten, deviations are higher and moderate values extend to the northern boundary and east; an additional small lobe of moderate values can be found of the eastern coast of the United States.

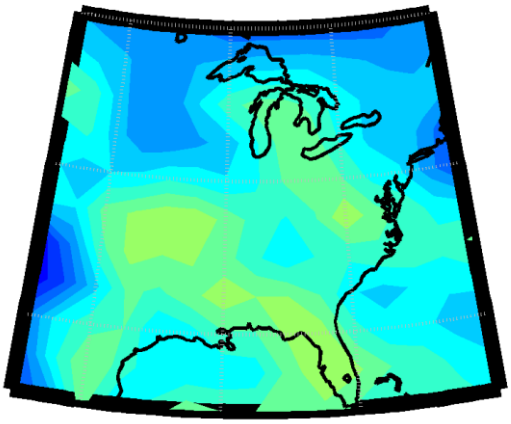

Figure 4.8.11: Specific humidity self-organizing map node 11.

11. Highest humidity values are dispersed in small lobes over the central United States in node eleven. However, the southwest which generally contains elevated moisture is the location of node eleven's lowest humidity values. Low humidity extends south from the northern boundary with significant values along the northern east coast. Mapped means show a large, deep trough of low humidity in the north; this system gradually increases in humidity as latitude decreases. Highest values are concentrated in the southwest with a moderate lobe over southern Mississippi, Louisiana, Alabama, and portions of Florida. Standard deviations show two distinct areas of low values centered on opposing boundaries. Extending from the northern edge, the low reaches the tip of Lake Huron; spanning northward, the southern lobe covers the Gulf, Florida, and portions of the southern states. Highest deviations are located in the west with a lobe occurring over the central United States and a moderate lobe off the eastern coast.

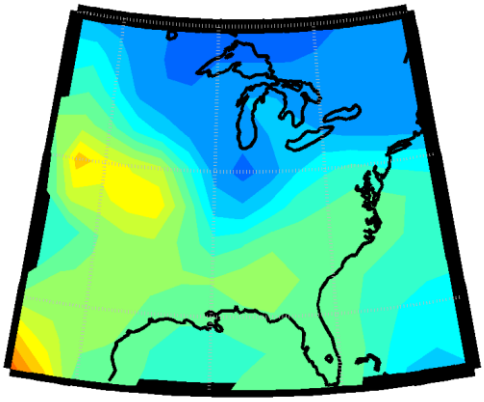

Figure 4.8.12: Specific humidity self-organizing map node 12.

12. In node twelve, decreased humidity occurs in the north with lowest values centered above the great lakes. High moisture is concentrated in southern Texas with a sizeable lobe in the northwest and moderate values spanning the south. Mapped mean values contain a deep trough of low humidity west of the great lakes. Highest humidity is located in the southwest with moderate values extending across the southern edge and eastern coast of the United States. Standard deviations for node twelve are highest on the western boundary with values of 3 occurring over expansive areas. Moderate values extend eastward with a lobe of high values over north of Louisiana. Lowest deviations are located west of the great lakes and southeast portions of the gulf.

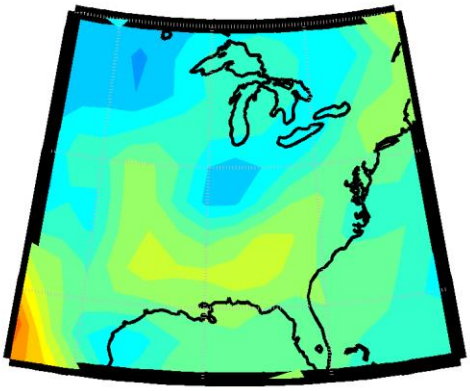

Figure 4.8.13: Specific humidity self-organizing map node 13.

13. Node thirteen contains overall high values of humidity with expansive lobes spanning the southern states and extending across the eastern coast. Highest humidity values concentrate in the southwest reaching values of approximately 16×10^{-3} kg/kg. An anomalous lobe of low humidity is present directly below the great lakes with an additional area of low values in the northwest. Lowest mean values are located across the northern border and extend slightly southward. Highest values extend from the southwest and reach across the central United States. Standard deviations are highest on the western border with high moderate values east of the great lakes; lowest values cover the gulf and extend up the eastern coast.

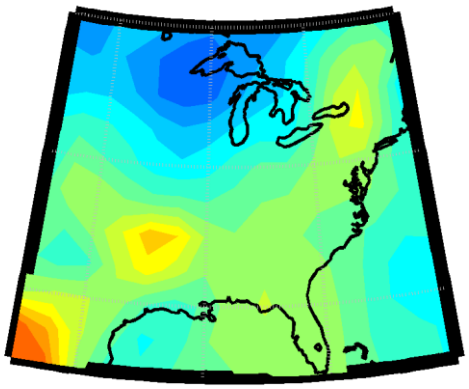

Figure 4.8.14: Specific humidity self-organizing map node 14.

14. In node fourteen, low humidity is concentrated in a closed center east of the great lakes extending west. Highest humidity is positioned in the southwest with two additional lobes of elevated values. The first lobe is located over Louisiana with a prominent center and moderate values spanning south and east; the second lobe is positioned east of the great lakes and extends south. Mapped mean values display a trough of low humidity in the north with highest humidity in the southwest and moderate values spanning the United States. Highest deviations extend east from the western boundary with low values of approximately 4 covering the northeastern coastal states. Lowest deviations are positioned in the south and encompass Florida and southern portions of several Gulf States; low deviations also occur on the western portion of the northern boundary.

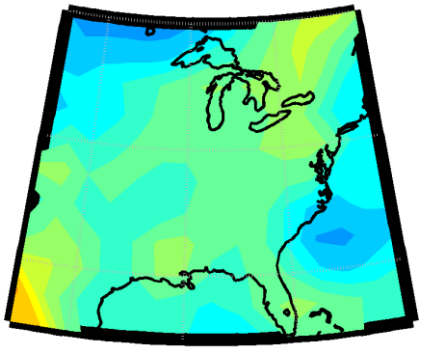

Figure 4.8.15: Specific humidity self-organizing map node 15.

15. In node 15, high specific humidity values of roughly 14×10^{-8} kg/kg are located over southern Texas with several moderate closed lobes across the states including moderate values over Chicago. Excessive available moisture is required for extreme equivalent temperature events indicating node 15 is likely to produce high T_E observations (Davey et al. 2006). Lowest humidity is located in two positions: off the coast of South Carolina and northeast of the Great Lakes. Mean values mapped for node 15 show a deep, closed lobe of low humidity northeast of the Great Lakes with values decreasing southward. Highest humidity is similar to the SOM pattern with elevated moisture in southern Texas. Moderate values have coalesced to produce a lobe of high humidity values over Iowa and Missouri with elevated moderate values situated over much of the United States. Standard deviations are lowest across the southeastern boundary and spread north covering southern Louisiana and east to portions of North Carolina.

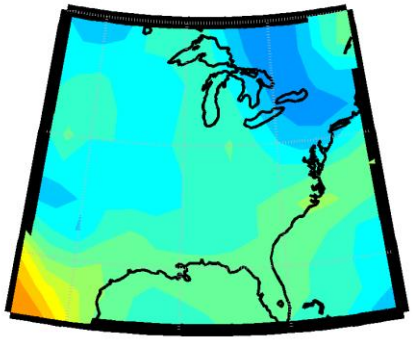

Figure 4.8.16: Specific humidity self-organizing map node 16.

16. Highest humidity is situated in the southwest of node sixteen with values reaching 15×10^{-8} kg/kg. Moderate values of approximately 10×10^{-8} kg/kg are positioned over southern Louisiana, Missouri, Alabama, Florida, Georgia and extend up the east coast to North Carolina where they transition into the Atlantic. Lower values cover the Midwestern states with lowest humidity east of the Great Lakes. Mean values for node 16 are markedly different from the SOM pattern; moderate values cover the east coast, Texas, and portions of the Gulf. Lowest values span the north and extend south with small closed lobes of low humidity positioned over eastern Louisiana and Texas. Mapped standard deviations show largest values over eastern Texas and Louisiana with elevated deviations over large portions of the Midwest and southern states. Moderate deviations occur off the east coast while lowest deviations are located on the tip of Florida.

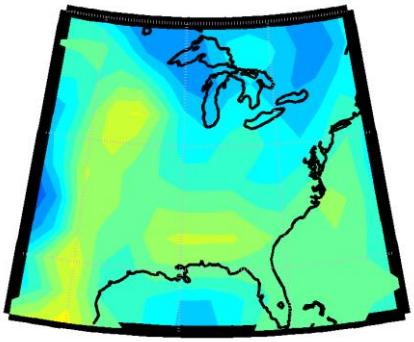

Figure 4.8.17: Specific humidity self-organizing map node 17.

17. Low humidity is apparent in three locations in node 17. A large lobe of low values in the north separates and forms two extensions around the Great Lakes with a small center of slightly higher values. The additional lobes are located across the western boundary and in the Gulf of Mexico. High humidity is concentrated in several areas; closed lobes of high values are positioned over Texas, Alabama, Mississippi, and Iowa and off the eastern coast. Mapped mean highest humidity values are located in southern Texas with a small concentration over Mississippi and Louisiana. Moderate values cover the southern United States with exception of a small intrusion of low values on the western boundary north of Texas. Lowest humidity is present in large bands across the north. Mapped standard deviations are lowest over the Gulf of Mexico and extend northeast to cover Florida and portions of Mississippi, Alabama, Georgia and the Carolinas. Highest deviations concentrate in southern Texas and expand north. Moderate values are located east of the Great Lakes and off the northeastern coast.

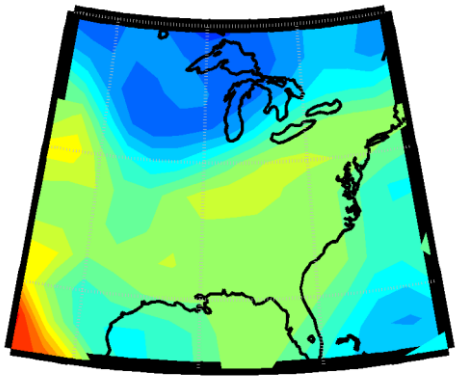

Figure 4.8.18: Specific humidity self-organizing map node 18.

18. In node eighteen, significantly elevated humidity values of 17×10^{-8} kg/kg are located in the southwest. Moderate to high values cover the majority of the United States with a small intrusion of low values in eastern Texas. Closed lobes of high values are located south of the Great Lakes and across the western boundary. Lowest humidity occurs north of the Great Lakes with a small inclusion of low values off the coast of Florida. Mapped mean values are suppressed over the node with highest values in the southwest. Lowest values are positioned off the eastern coast with an additional lobe in the northeast. Standard deviations are lowest across the southern border and include portions of Florida and Louisiana. Highest deviations are in the west with moderate values spanning the northern United States and extending down the east coast.

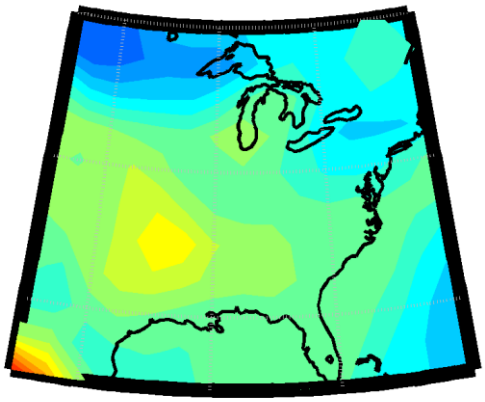

Figure 4.8.19: Specific humidity self-organizing map node 19.

19. Node nineteen's highest humidity values are located in the southwest with a large inclusion of 13×10^{-8} kg/kg positioned over Louisiana and elevated values in the southern Great Lakes. Moderate values cover the majority of the United States with low humidity in the northwest and southeast. Mean values have suppressed, albeit still high values in southern Texas and a small lobe of moderate values extending from the western boundary. Highest deviations are concentrated on the western boundary with lowest deviations in the Gulf and across the eastern coast.

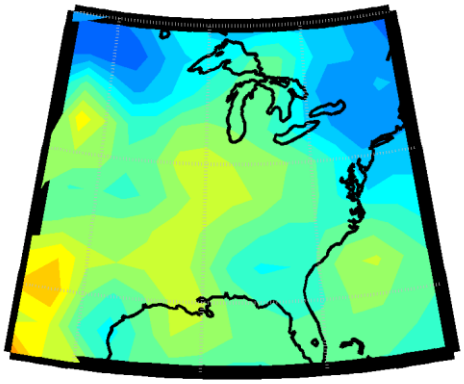

Figure 4.8.20: Specific humidity self-organizing map node 20.

20. Node twenty is characterized by high specific humidity values of approximately 13×10^{-8} kg/kg in the southwest with additional lobes of similar magnitude present over Louisiana, Arkansas, Missouri, and the eastern coast. Elevated specific humidity values in nodes 19 and 20 suggest these nodes will be associated with development of extreme equivalent temperature heat waves (Davey et al. 2006). Lowest humidity occurs in two distinct lobes in the extreme northeast and northwest. Mapped means produce a ridge of low humidity over the Great Lakes with low values present in the southern Atlantic. Highest humidity values are positioned over Texas and extend northeast. Lowest standard deviations are positioned in the Gulf and portions of Florida. Highest deviations are located on the southern edge of the western boundary extending north with moderate values spanning large portions if the northern boundary.

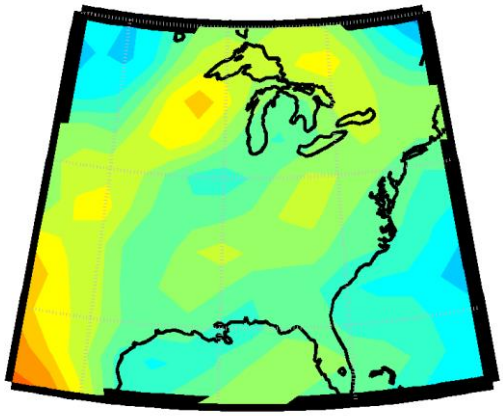

Figure 4.8.21: Specific humidity self-organizing map node 21.

21. In node twenty-one highest humidity is located in the southwest with northern and eastern expansion. Several additional lobes of elevated moisture occur over the states with a deep isolated lobe west of the Great Lakes. Lowest humidity is apparent in the northeast with small concentrations in the northwest. Mapped means show lowest humidity across the northern, eastern, and portions of the western boundaries with moderate values encompassing the Gulf and the majority of the states. Standard deviations have lowest values occurring south of the Gulf and extending north across Mississippi, Florida and traveling inland. Standard deviations of 2.5 occur in two distinct areas: just off the western border and in the Atlantic off the east coast. Deviations of roughly 2 extend down the eastern coast and portions of the western states.

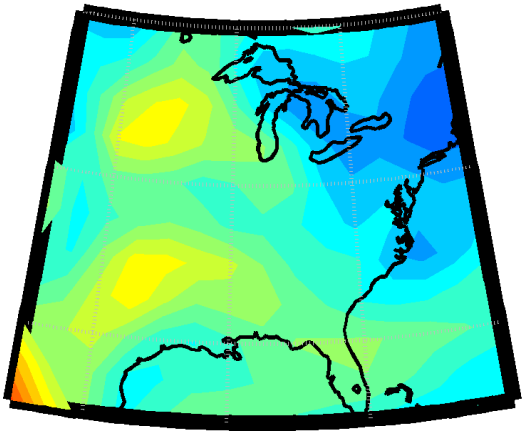

Figure 4.8.22: Specific humidity self-organizing map node 22.

22. Node twenty-two's highest humidity occurs in the southwest with two additional closed lobes of 13×10^{-8} kg/kg located over Louisiana and Minnesota. Lowest humidity is positioned over the northeastern United States and extends over the Great Lakes. Mapped mean values show a significant center of low humidity north of the Great Lakes. Low values gradually increase with decreases in latitude. No extreme high humidity values are present on this node. Slightly higher values of roughly 10×10^{-8} kg/kg are situated over southern Florida, Texas and Missouri. Low deviations are present over southern Florida and in the northwest. Highest standard deviations are located west of the Great Lakes and just off the western boundary extending south.

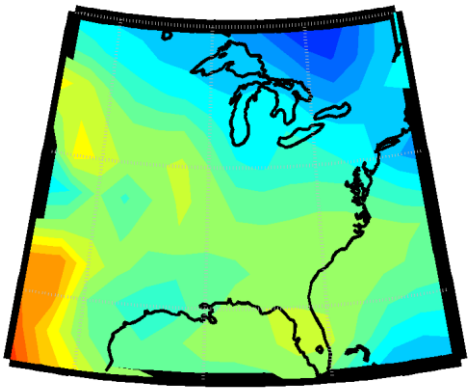

Figure 4.8.23: Specific humidity self-organizing map node 23.

23. In node twenty-three highest humidity occurs in a large expanse of Texas with values of 14×10^{-8} kg/kg-16×10^{-8} kg/kg. Several isolated small lobes of high values, roughly 13×10^{-8} kg/kg are situated over southern Florida, Missouri, and off the western boundary. Lowest humidity occurs northeast of the Great Lakes and off the northeastern coast. Mapped mean values have highest values concentrated in the southwest with moderate values covering the central and southern states. Low mean humidity values are present in a large, organized trough that extends south from the northern edge of the node. Lowest standard deviations spread across the Gulf and several southern states with small areas of low deviations are present over North Carolina and Texas. Highest values are focused on the western boundary with moderate values extending west to the Great Lakes.

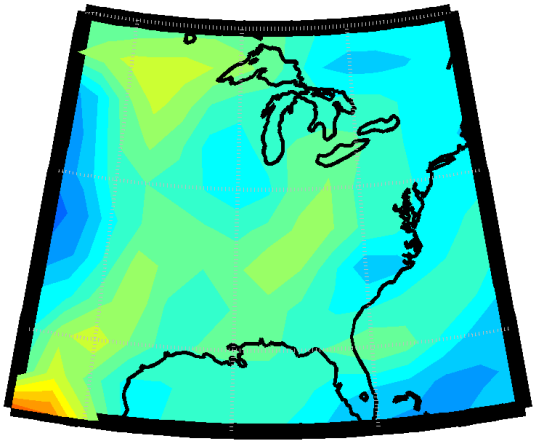

Figure 4.8.24: Specific humidity self-organizing map node 24.

24. In node twenty-four humidity values are highest in the southwest with several areas of moderate values scattered across the states. Lowest values are located on the western boundary, north of the Great Lakes, south of Florida, and over South Carolina. Mapped means have lowest values in the northwest and highest values in the southwest with moderate values extending west across the southern states. Lowest standard deviations span the western portions of the Gulf, across Florida and up the eastern coast. Highest deviations occur on the southern portion of the western edge.

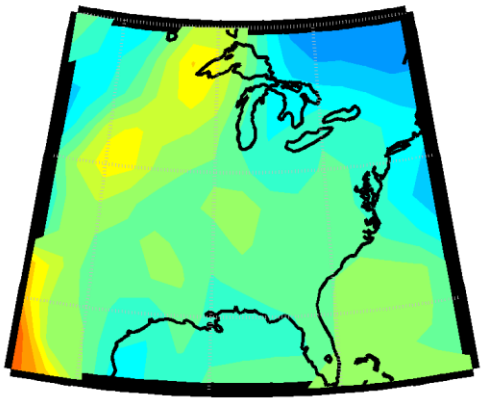

Figure 4.8.25: Specific humidity self-organizing map node 25.

25. Highest humidity in node twenty-five is located in the southwest with values of roughly 15×10^{-8} kg/kg. Two additional lobes of high values, 13×10^{-8} kg/kg, are west and southwest of the Great Lakes. Elevated specific humidity values over Chicago indicate the potential for extreme equivalent temperature heat waves to form from node 25 (Davey et al 2006). Moderate values cover the southern states and southeast with low humidity situated in the northeast and extending slightly down the eastern border. Mapped mean values have no large areas of significantly low humidity; however, a moderately valued area is present in the northwest. Highest values are positioned in the southwest and continue northeast to the Great Lakes; this extension of higher values leads to a slow decrease of humidity values across the study area. Lowest deviations are positioned over the Gulf with two large lobes over the Carolinas and Mississippi. Highest deviations span the western border and extend northeast with a small portion protruding down the east coast.

4.4 Self Organizing Map Patterns Associated with Heat Wave Development

4.4.1 Temperature

For the Chicago O'Hare International Airport dataset, high temperature heat wave criteria generated 363 observations. Geopotential height nodes containing observations that exceeded heat wave criteria were nodes 6, 9, 11, 15, 24 and 25 (Figure 4.9). The lowest SOM heat wave frequencies were assigned to nodes 9 and 6 with less than 30 observations occurring on each node. Node 9 contains a ridge that is located west of Chicago with moderate heights and a SOM frequency of 6.61% while node 6 presents more zonal flow and weak riding with an associated SOM frequency of 7.99%. Node 11's SOM frequency was 24.52% indicating this synoptic pattern is the dominant node for the production of extreme temperature heat waves. In node 11, a prominent ridge is situated west of Chicago with associated high geopotential height values. Also displaying ridging, node 15 presents a ridge-trough-ridge pattern in the south with more zonal flow in the north; ridging occurs east of Chicago with moderate heights over the city. Also noteworthy with a frequency of 17.63%, node 24 contains a synoptic pattern of ridge-trough flow with Chicago located west of the trough axis. Node 25 is the warmest node on the geopotential height SOM with a frequency 21.21%. In this node, elevated geopotential height values span the entire United States with a lobe of high heights located southeast of Chicago and extending over the eastern coast. These extreme geopotential height values are accompanied by a wide, defined ridge over the great lakes. Geopotential height nodes associated with extreme temperature heat wave formation exhibit heat wave characteristics of varying magnitude. Several nodes contained strong ridging with elevated geopotential height values, features that are consistent with identified large-scale heat wave patterns in Perkins (2015) and occurred in both the historic Chicago 1995 and 1999 events (Kunkel et al. 1996; Palecki et al. 2001).

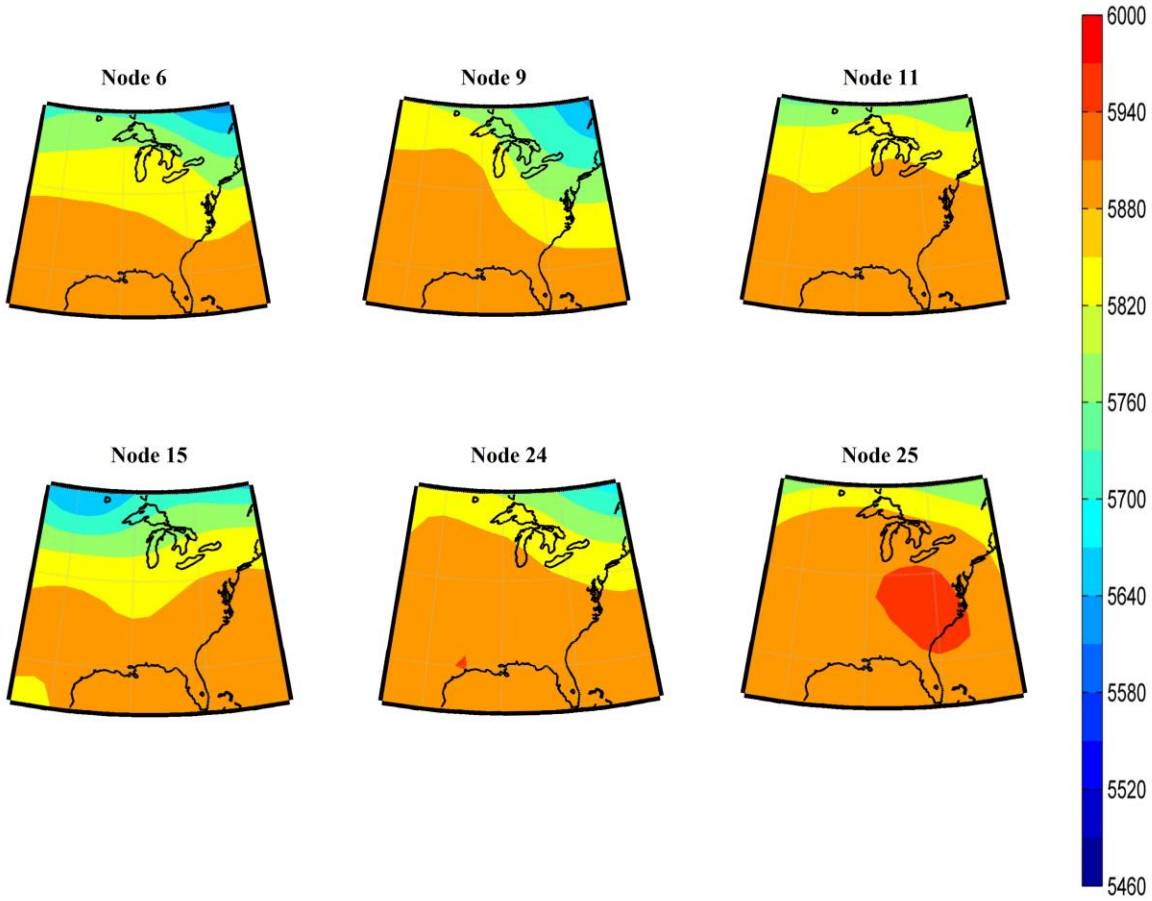

Figure 4.9: Geopotential height nodes responsible for extreme temperature heat wave development. Nodes included in the figure are nodes: 6, 9, 11, 15, 24, and 25 and values are in meters.

For specific humidity, heat wave nodes with greater than 5% SOM frequency were: 14, 18, 19, 20, 24, and 25 (Figure 4.10). Observations exceeding heat wave criteria concentrate on node 19 with 26.34% occurrence, node 20 with 12.67% occurrence, and node 25 with 20.11% occurrence. Node 14 presents low values over Chicago with moderate values to the south, the associated SOM frequency was 8.26%. Extremely low values encompass Chicago in node 18 where depressed specific humidity extends south into northern Illinois. Node 18 is exclusive to extreme temperature heat wave formation and contains a SOM frequency of 5.79%. In node 19

high humidity values are positioned over the central United States with elevated specific humidity values centered over Chicago and the southern portion of Lake Michigan. Node 20's SOM frequency was 12.67% and contained a large lobe of elevated specific humidity values that span the central United States and extend to the Great Lakes; in this node, elevated humidity located directly over Chicago. Node 24 contains a frequency of 8.82% with low humidity values over the Chicago region and moderate values surrounding the city. Node 25's synoptic pattern displays moderate values over the Chicago area; elevated values are located directly to the north and east; the associated frequency for this node was 20.11%

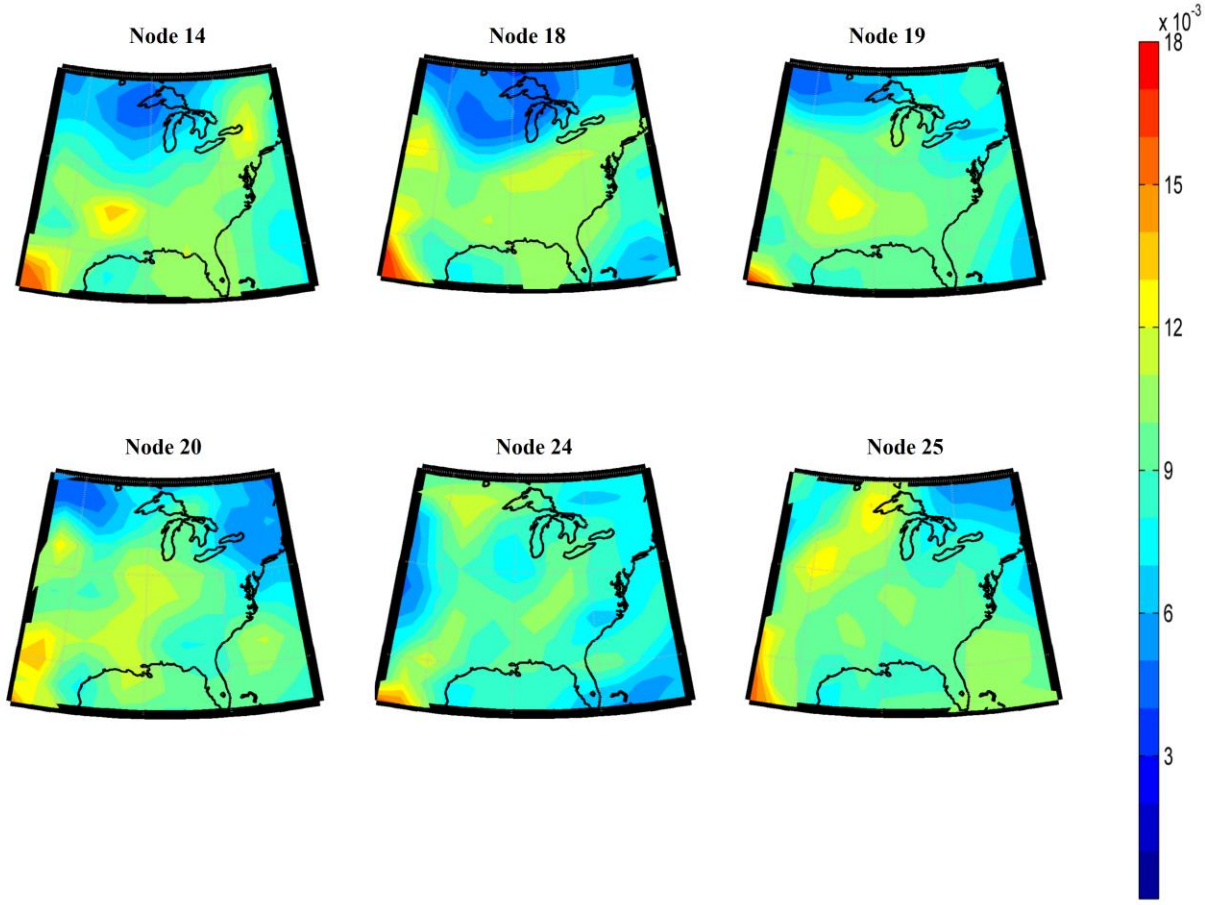

Figure 4.10: Specific humidity nodes responsible for extreme temperature heat wave development. Nodes included in the figure are nodes: 14, 18, 19, 20, 24, and 25.

4.4.2 Equivalent Temperature

Geopotential height SOM nodes 6, 9, 11, 15, 17, 24, and 25 are responsible for development of high equivalent temperature heat waves (Figure 4.11). Nodes 15 and 17 account for the two lowest SOM frequencies and contain relatively weak patterns. However, nodes 6, 9, 11, 24, and 25 contain elevated height values with prominent ridging. Node 11 is responsible for 34.66% of observations exceeding equivalent temperature heat wave criteria indicating node 11 is the dominant synoptic pattern for high equivalent temperature observations. The synoptic pattern represented by node 11 is distinct ridging over Illinois and Indiana with elevated height

values that extent north. Node 6, being a neighboring node, is similar to node 11 however, the ridge is weaker and less organized with lower geopotential height values present in the north; the SOM frequency for node 6 is 8.52%. Node 9's frequency is 10.80% with a synoptic pattern displaying a ridge located west of Chicago with moderate values in the study area. Node 25's synoptic pattern presents a wide ridge spanning the study area with a lobe of elevated high height values south east of the Great Lakes; this node is responsible for 18.18% of SOM heat wave observations. Node 17, exclusive to equivalent temperature heat waves, contains relatively zonal flow, with moderate height values over Chicago and slight troughing over the Great Lakes; this node accounts for 6.82% of geopotential height equivalent temperature heat wave observations. The majority of equivalent temperature nodes display appropriately located features responsible for heat wave development and indicate extreme temperatures associated with these events.

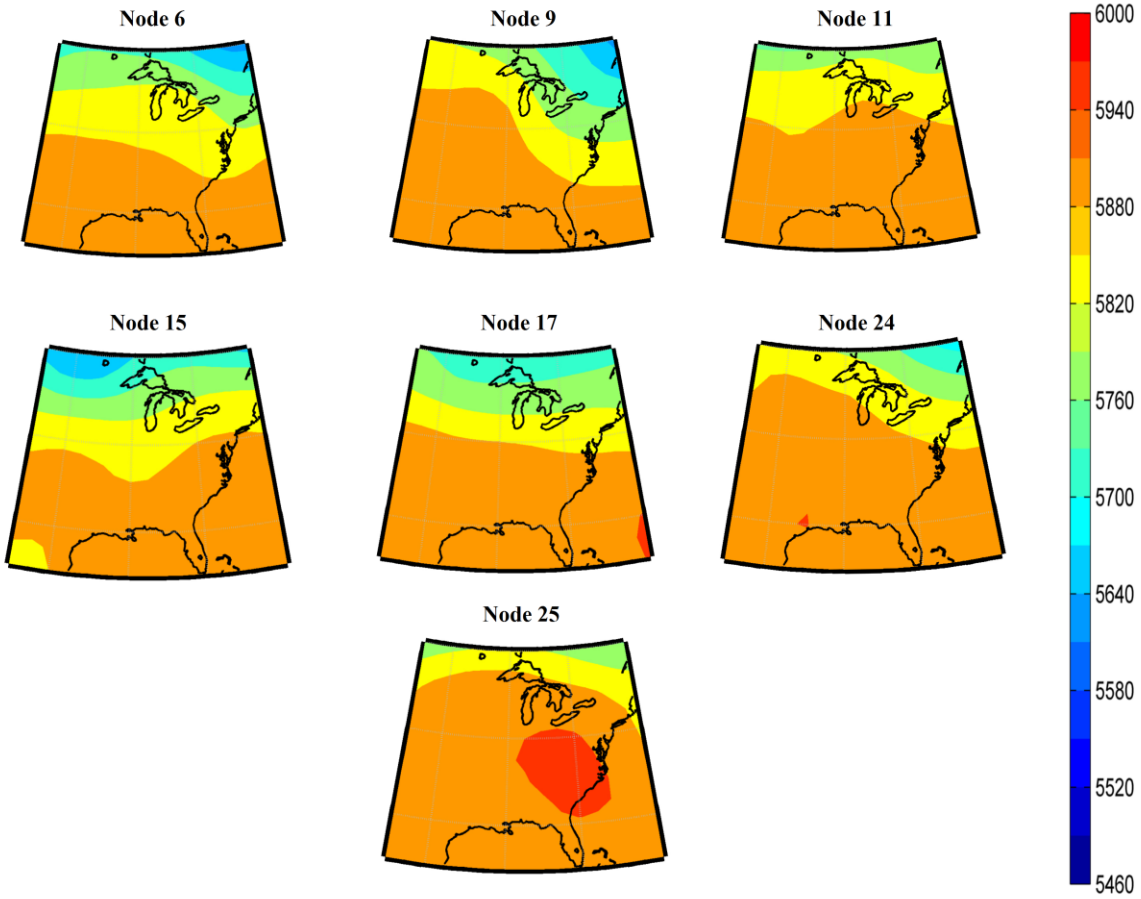

Figure 4.11: Geopotential height nodes responsible for extreme temperature heat wave development. Nodes included in the figure are nodes: 6, 9, 11, 15, 17, 24, and 25 and values are in meters.

For specific humidity SOM equivalent temperature heat wave observations are represented by nodes: 5, 14, 15, 19, 20, 24, and 25 (Figure 4.12). Specific humidity node 5 synoptic pattern displays low heights over Chicago with a concentrated lobe of low values located directly west. Nodes 5, 14, and 15 were responsible for 5.11% of SOM extreme temperature observations with 9 observations occurring on each node. Node 14's synoptic pattern displays low specific humidity values over Chicago with a concentrated center of elevated height values to the southwest and northeast. In node 15, the moderate values have

expanded to encompass Chicago with a lobe of excess moisture in the northeast. Node 19, with a SOM frequency of 25.34% was identified as the most significant node for equivalent temperature heat wave development. Node 19, as described above, contains available moisture for the Chicago region with elevated values in the southeast. Elevated moisture values persist in neighboring node 20 with a large expanse of high specific humidity values located over Chicago and extending south. Nodes 24 and 25 contain SOM frequencies of 5.11% and 21.02% respectively with node 24 displaying moderately low humidity over Chicago and node 25 characterized by elevated humidity over the city.

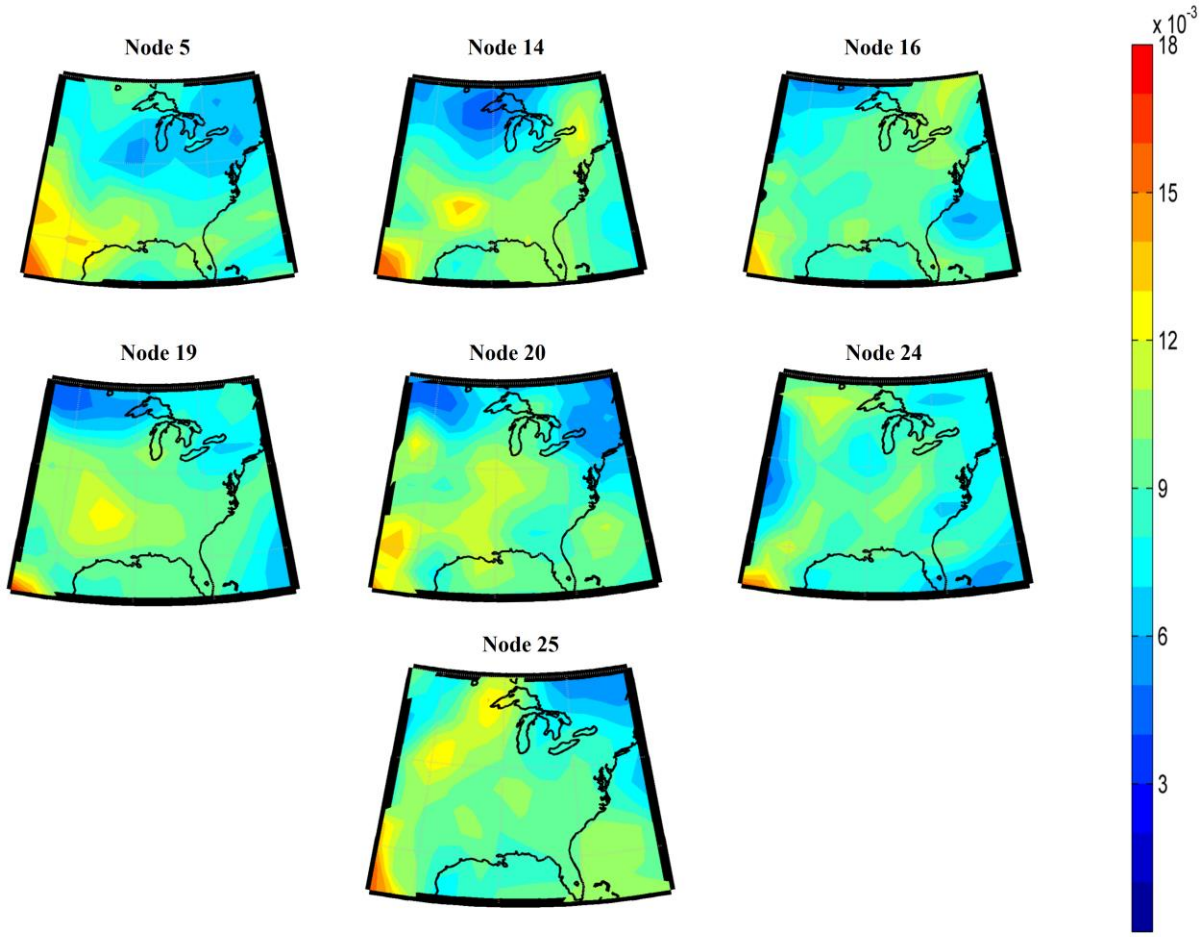

Figure 4.12: Specific humidity nodes responsible for extreme temperature heat wave development. Nodes included in the figure are nodes: 5, 14, 18, 19, 20, 24, and 25 and values are in kg/kg.

High temperature events are concentrated on nodes with heat wave characteristics such as elevated geopotential height values and ridging with the potential for association with conditions of available moisture. For geopotential height, temperature and equivalent temperature observations clustered on nodes 11, 24, and 25. Equivalent temperature observations also associated with height node 17 at a frequency of 6.82%. For specific humidity heat wave observations for both temperature and equivalent temperature concentrated on nodes 19, 20, and 25. Specific humidity node 18, exclusive to temperature heat waves, occurred at a frequency of

5.79% and contained a moisture deficit over Chicago. Equivalent temperature observations also exclusively included nodes 5 and 15. Node 5 contained low moisture values over Chicago while 15 possessed moderate available moisture. Overall, temperature and equivalent heat wave associated nodes are similar with several nodes associated with production of both extreme events. Extreme temperature events include two nodes with depressed humidity values indicating extreme temperature events can occur without the presence of available moisture. Nodes 14 and 18 contain low specific humidity values for the Chicago region with node 18 being extremely low; the associated SOM frequencies are 8.26% and 5.79%. Equivalent temperature includes nodes 5 and 14 both characterized by low humidity however, the frequencies are a reduced 5.11% for both variables. Additionally, an analysis of heat wave observations for equivalent temperature shows nodes 5 and 14 occurring only in the initial or ending stages of heat wave development and occurring no more than twice consecutively. This analysis signifies nodes 5 and 14 may be relevant to onset and dissipation of heat wave conditions but are not responsible for peak heat wave conditions. Conversely, for temperature, nodes 14 and 18 are responsible for the production of two distinct heat waves and occur up to ten times consecutively. Therefore, temperature and equivalent temperature heat waves form with overall similar synoptic characteristics however; excessive moisture is necessitated for equivalent temperature heat waves while extreme temperature events can occur with a moisture deficit.

4.5 Transitional Analysis

Recurrence of heat wave associated nodes is significant because persistence of extreme suppressive conditions is essential for heat wave development. Gershunov et al. (2009) determined heat wave severity is dependent on intensity and duration and Perkins (2015) states mortality associated with extreme heat events drastically increases after the second consecutive

day of oppressive conditions. Once established, heat wave features such as stationary blocking highs can generate stagnant conditions where warm air intensifies and northern cooler air is blocked from descending into the area. Several historic heat waves such as the Russia's 2010 heatwave, Chicago's heat wave in 1995, and the European heat wave in 2003 developed from stationary high pressure systems. Elevated node recurrence for extreme temperature and equivalent temperature associated synoptic patterns indicates long-lasting heat waves with high probability for heat caused mortality

Transitional analysis, or return frequency, was calculated for each node. Frequencies were divided into three categories: recurrence of the measured node, transitioning to a neighboring node, and transitioning to a non-neighboring node; neighboring nodes were defined as nodes that bordered the pattern being analyzed. For both geopotential height and specific humidity SOMs, the highest percentage was recurrence of the measured node (Table 4.3). For example, geopotential height SOM node one return frequency is 69.56% meaning there is a 69.56% likelihood of the same synoptic pattern occurring for the next observation. Because SOMs are organized by similarity, a neighboring node frequency was calculated as well; this determines the probability of a similar synoptic pattern occurring on the following observation. For node one, neighboring nodes are node two, node six and node seven. The probability of node one transitioning to a neighboring node is 10.52%. Non-neighboring nodes are all other SOM patterns that are not adjacent to node one; the probability of a node one transitioning to any non-neighboring node is 19.93%. Frequencies for nodes associated with heat wave development as well as recurrence were determined for geopotential height and specific humidity.

Table 4.3: Geopotential height SOM node transitions represented as three percentages: node recurrence, transition to a neighboring node, or a non-neighboring node transition.

Geopotential Height Node Transitions				
Node 1	Node 2	Node 3	Node 4	Node 5
69.56%	67.73%	67.62%	70.72%	84.97%
10.52%	2.64%	9.07%	9.05%	4.37%
19.93%	29.63%	23.31%	20.23%	10.66%
Node 6	Node 7	Node 8	Node 9	Node 10
61.39%	61.31%	74.72%	73.16%	80.23%
6.43%	15.26%	10.67%	2.65%	2.54%
32.17%	23.43%	14.61%	24.19%	17.23%
Node 11	Node 12	Node 13	Node 14	Node 15
70.57%	71.39%	67.00%	61.94%	69.03%
7.82%	6.34%	18.41%	22.34%	10.20%
21.61%	22.27%	14.58%	15.73%	20.77%
Node 16	Node 17	Node 18	Node 19	Node 20
75.32%	62.54%	65.10%	68.30%	58.11%
3.14%	10.31%	14.75%	12.65%	16.73%
21.54%	27.15%	20.15%	19.05%	25.16%
Node 21	Node 22	Node 23	Node 24	Node 25
66.71%	69.87%	74.53%	68.56%	72.60%
1.84%	6.05%	8.13%	3.05%	9.45%
31.45%	24.08%	17.34%	28.38%	17.95%

Geopotential height extreme temperature and equivalent temperature heat waves concentrated on nodes 6, 9, 11, 15, 17, 24, and 25. Node 11 contains 89 observations with a SOM frequency of 24.52% making this node the primary synoptic pattern for the production of extreme temperature and equivalent temperature heat waves. The return frequency for node 11 is 70.57% signifying pattern persistence once established. However, low neighboring transition probabilities in combination with higher non-neighboring transition values signify once disrupted

the synoptic pattern will likely transition to a distinct, non-similar pattern. Nodes 6, 15, and 24 contained recurrence percentages that exceeded 60% while nodes 9, 11, and 24 percentage of recurrence exceeded 70%. Overall, geopotential height nodes contained highest percentage for recurrence of the measured pattern indicating once a pattern is established persistence is highly probable. However, neighboring frequency was significantly lower than non-neighboring pattern probability signifying pattern disruption occurs more frequently than neighboring transitions.

For specific humidity high temperature and equivalent temperature heat waves observations clustered to nodes 5, 14, 15, 18, 19, 20, 24, and 25 (Table 4.4). Node 19 being the dominant node of extreme heat wave production for both variables has a recurrence rate of 63.43% with 26.25% neighboring node probability. Node 25 is responsible for 21.21% of extreme temperature observations and 18.18% of equivalent temperature has a recurrence probability of 52.71%. Node 18 is exclusive to extreme temperature heat waves; the SOM frequency for this node 5.79% with a recurrence rate of 65.10%. Overall, specific humidity return frequencies are lower than geopotential height SOM values; however, probabilities continue to exceed 50% for the majority of nodes for temperature and equivalent temperature events indicating pattern persistence for synoptic states. However, specific humidity nodes have higher neighboring node frequencies signifying once the heat wave pattern is disrupted, similar synoptic patterns are probable.

Node repetition is apparent in temperature and equivalent temperature heat waves for both variables of geopotential height and specific humidity; therefore pattern persistence is similar for both measures. However, differences are apparent in geopotential height and specific humidity node transitions. Overall geopotential height nodes retain a higher recurrence percentage compared to specific humidity recurrence rates, while specific humidity nodes are

more likely to transition to a neighboring node. For example, geopotential height nodes 11, 24, and 25 are the three most prominent nodes for production of both temperature and equivalent temperature heat waves; the rate of recurrence for all three nodes exceeds 68% with neighboring node transitions less than 10%. For specific humidity nodes 19, 20, and 25 are the top three nodes for generation of heat wave observations for both temperature and equivalent temperature. The recurrence frequencies for these nodes are lower with rates of: 63.43%, 54.29%, and 63.95% respectively. However, specific humidity nodes contain increased neighboring transition frequencies; for the three nodes specified neighboring transitional percentages all exceed 25% with node 20's frequency at 32.32%. Therefore, geopotential height nodes are likely to persist but when disrupted transition to a dissimilar pattern while specific humidity recurrence rates are depressed but increased neighboring node frequencies indicate transitions to similar patterns are likely.

Table 4.4: Specific humidity SOM node transitions represented as three percentages: node recurrence, transition to a neighboring node, or a non-neighboring node transition.

Specific Humidity Node Transitions				
Node 1	Node 2	Node 3	Node 4	Node 5
59.30%	43.25%	43.16%	35.23%	54.77%
11.21%	13.94%	24.06%	6.09%	2.63%
29.49%	42.81%	32.78%	58.68%	42.60%
Node 6	Node 7	Node 8	Node 9	Node 10
72.17%	57.74%	60.48%	56.93%	46.19%
18.70%	15.74%	11.95%	19.76%	17.12%
9.13%	26.52%	27.57%	23.30%	36.69%
Node 11	Node 12	Node 13	Node 14	Node 15
64.60%	58.34%	54.75%	52.71%	64.14%
12.84%	29.12%	24.66%	27.76%	15.45%
22.57%	12.54%	20.59%	19.53%	20.42%
Node 16	Node 17	Node 18	Node 19	Node 20
69.46%	57.40%	58.43%	63.43%	54.29%
11.09%	13.14%	16.86%	26.25%	32.32%
19.46%	29.45%	24.71%	10.31%	13.39%
Node 21	Node 22	Node 23	Node 24	Node 25
55.99%	70.17%	54.60%	59.80%	63.95%
10.78%	9.29%	6.00%	9.92%	25.83%
33.23%	20.54%	39.40%	30.29%	10.22%

4.6 Node Pairing Analysis

An additional analysis was completed to determine node pairing between geopotential height and specific humidity SOM nodes. Geopotential height nodes are presented as paired specific humidity nodes to determine node pairing frequencies (Tables 4.5 and 4.7, respectively).

Similarly, specific humidity nodes are displayed with geopotential height node pairing frequencies (Tables 4.6 and 4.8, respectively). Self-organizing maps nodes included in this analysis were nodes that contained at least 5% of observations exceeding the 95th percentile for temperature and equivalent temperature. For example, in Table 4.5 all observations assigned to geopotential height node 6, shown in gray, pair with specific humidity node 1 2.36% of the time; highest paired nodes for geopotential height node 6 are specific humidity node 5 and 8; the two highest pairing frequencies for each variable have been highlighted.

For geopotential height temperature it is apparent nodes pair frequently with specific humidity nodes associated with extreme events. Geopotential height nodes 6, 9, and 24 pair frequently with specific humidity node 5. Geopotential height nodes 6 and 24 are characterized by strong ridging over Chicago with elevated height values while node 6 has weak ridging with moderate values; specific humidity node 5 contains minimal moisture over the Chicago region. This indicates for temperature heatwaves, geopotential height nodes have the capacity to pair with specific humidity patterns that do not display excessive available moisture. Additionally, geopotential height node 25 contains an elevated pairing frequency of 14.14% with specific humidity node 5. Geopotential height node 25 is responsible for 21.21% of extreme temperature heat waves and contains the highest geopotential height values on the SOM. Specific humidity nodes 19, 20, 24, and 25 contain elevated humidity values over the Chicago region and pair frequently with geopotential height patterns associated with extreme temperature generation. Notably, height node 25 pairs with humidity node 19 at a rate of 20.51% indicating they consistently occur in combination. For extreme temperature heat waves, pairing analysis indicates extreme temperature events can occur in combination with available moisture but do not necessitate elevated humidity values.

Specific humidity nodes associated with extreme temperature heat wave development pair most frequently with geopotential height patterns represented by nodes 11, 15 and 17. As mentioned in the node analysis, height node 11 is the dominant node for production of geopotential height temperature and extreme temperature heatwaves; the pattern represented is strong ridging with elevated geopotential height values and pairs frequently with humidity nodes with high humidity values over Chicago. Geopotential height node17 is exclusive to equivalent temperature events but pairs frequently with specific humidity temperature associated patterns. All specific humidity nodes associated with extreme temperature generation contain elevated moisture over Chicago except nodes 14 and 18.

Table 4.5: Geopotential height extreme temperature node pairing frequencies with specific humidity nodes. Geopotential height nodes associated with temperature heat wave development with more than 5% of observations at the 95th percentile located across the top of the table in columns with paired specific humidity nodes in rows; specific humidity nodes associated with the development of extreme conditions are highlighted in green; the top two node pairings for each geopotential height node are highlighted in blue.

	Geopotential Height Nodes Associated with Extreme Temperature Heat Waves						
	Node	6	9	11	15	24	25
Specific Humidity Nodes	1	2.36%	4.47%	0.90%	1.02%	0.90%	0.40%
	2	4.17%	3.31%	2.51%	1.38%	2.01%	2.02%
	3	4.57%	6.74%	1.07%	0.36%	4.09%	1.75%
	4	3.19%	2.15%	0.66%	1.02%	0.35%	1.08%
	5	9.28%	9.22%	10.27%	6.12%	10.62%	14.44%
	6	1.23%	2.71%	0.30%	0.30%	0.21%	0.00%
	7	5.45%	4.47%	4.54%	3.90%	3.96%	2.70%
	8	9.38%	14.19%	3.64%	2.46%	6.80%	2.29%
	9	4.86%	7.40%	1.01%	2.70%	5.07%	0.67%
	10	3.98%	5.36%	2.75%	0.42%	5.41%	2.02%
	11	0.25%	1.44%	0.06%	0.54%	0.21%	0.00%
	12	0.25%	0.33%	0.48%	1.68%	0.21%	0.00%
	13	2.26%	0.83%	2.27%	8.58%	2.36%	0.94%
	14	2.55%	1.60%	5.91%	6.60%	5.83%	4.72%
	15	8.94%	7.34%	2.09%	0.72%	7.56%	2.29%
	16	0.25%	0.28%	0.12%	0.42%	0.07%	0.00%
	17	7.27%	7.01%	1.43%	2.46%	3.89%	1.75%
	18	6.43%	2.54%	11.28%	10.08%	4.72%	8.23%
	19	6.34%	7.95%	12.84%	7.56%	17.77%	20.51%
	20	4.57%	1.44%	13.85%	8.52%	5.27%	9.31%
	21	0.64%	0.00%	0.24%	1.80%	0.00%	0.13%
	22	0.64%	0.39%	0.18%	0.06%	0.00%	0.00%
	23	7.12%	5.80%	0.78%	3.78%	3.61%	1.75%
	24	2.16%	2.54%	7.58%	11.40%	5.90%	5.26%
	25	1.87%	0.50%	13.25%	16.09%	3.19%	17.68%

Table 4.6: Specific humidity extreme temperature node pairing frequencies with geopotential height nodes. Specific humidity nodes associated with temperature heat wave development with more than 5% of observations at the 95th percentile are located across the top of the table in columns with paired geopotential height nodes in rows; geopotential height nodes associated with the development of extreme conditions are highlighted in green; the top two node pairings for each specific humidity node are highlighted in blue.

Geopotential Height Nodes	Specific Humidity Nodes Associated with Extreme Temperature Heat Waves					
Node	14	18	19	20	24	25
1	1.57%	0.36%	0.39%	0.10%	1.62%	0.57%
2	0.86%	0.18%	0.11%	0.10%	4.27%	0.09%
3	0.78%	0.27%	0.11%	0.10%	0.18%	0.09%
4	0.63%	0.09%	0.06%	0.00%	0.12%	0.00%
5	0.00%	0.00%	0.00%	0.00%	0.06%	0.00%
6	4.08%	11.69%	7.19%	9.73%	2.64%	3.60%
7	1.65%	2.32%	1.67%	1.67%	1.62%	0.28%
8	2.35%	0.98%	2.45%	0.52%	8.17%	0.66%
9	2.27%	4.10%	8.03%	2.72%	2.76%	0.85%
10	0.00%	0.00%	0.00%	0.00%	0.00%	0.00%
11	7.76%	16.86%	11.98%	24.27%	7.63%	21.00%
12	1.41%	0.09%	0.11%	0.00%	0.42%	0.00%
13	11.06%	2.23%	3.23%	1.36%	4.21%	0.28%
14	9.88%	2.77%	5.13%	2.62%	17.61%	3.97%
15	8.63%	14.99%	7.02%	14.85%	11.42%	25.35%
16	3.29%	3.93%	0.61%	2.30%	3.97%	7.10%
17	14.43%	10.08%	13.60%	7.95%	12.38%	7.66%
18	4.71%	1.52%	1.73%	0.31%	4.57%	0.38%
19	0.24%	0.80%	0.17%	1.46%	0.06%	0.28%
20	9.25%	4.64%	2.84%	3.56%	3.13%	1.42%
21	1.65%	1.52%	7.80%	2.41%	2.28%	3.03%
22	3.29%	7.76%	2.29%	8.58%	2.94%	6.53%
23	0.86%	1.34%	0.72%	0.21%	0.48%	0.09%
24	6.59%	6.07%	14.27%	7.95%	5.11%	4.35%
25	2.75%	5.44%	8.47%	7.22%	2.34%	12.39%

Table 4.7: Geopotential height equivalent temperature node pairing frequencies with specific humidity nodes. Geopotential height nodes associated with equivalent temperature heat wave development with more than 5% of observations at the 95th percentile located across the top of the table in columns with paired specific humidity nodes in rows; specific humidity nodes associated with the development of extreme conditions are highlighted in green; the top two node pairings for each geopotential height node are highlighted in blue.

Specific Humidity Nodes	Geopotential Height Nodes Associated with Equivalent Temperature Heat Waves						
Node	6	9	11	15	17	24	25
1	2.36%	4.47%	0.90%	1.02%	0.52%	0.90%	0.40%
2	4.17%	3.31%	2.51%	1.38%	1.89%	2.01%	2.02%
3	4.57%	6.74%	1.07%	0.36%	1.37%	4.09%	1.75%
4	3.19%	2.15%	0.66%	1.02%	0.63%	0.35%	1.08%
5	9.28%	9.22%	10.27%	6.12%	5.56%	10.62%	14.44%
6	1.23%	2.71%	0.30%	0.30%	0.00%	0.21%	0.00%
7	5.45%	4.47%	4.54%	3.90%	4.18%	3.96%	2.70%
8	9.38%	14.19%	3.64%	2.46%	1.95%	6.80%	2.29%
9	4.86%	7.40%	1.01%	2.70%	7.85%	5.07%	0.67%
10	3.98%	5.36%	2.75%	0.42%	2.46%	5.41%	2.02%
11	0.25%	1.44%	0.06%	0.54%	0.29%	0.21%	0.00%
12	0.25%	0.33%	0.48%	1.68%	1.43%	0.21%	0.00%
13	2.26%	0.83%	2.27%	8.58%	7.67%	2.36%	0.94%
14	2.55%	1.60%	5.91%	6.60%	10.54%	5.83%	4.72%
15	8.94%	7.34%	2.09%	0.72%	2.00%	7.56%	2.29%
16	0.25%	0.28%	0.12%	0.42%	0.11%	0.07%	0.00%
17	7.27%	7.01%	1.43%	2.46%	6.82%	3.89%	1.75%
18	6.43%	2.54%	11.28%	10.08%	6.47%	4.72%	8.23%
19	6.34%	7.95%	12.84%	7.56%	13.97%	17.77%	20.51%
20	4.57%	1.44%	13.85%	8.52%	4.35%	5.27%	9.31%
21	0.64%	0.00%	0.24%	1.80%	0.34%	0.00%	0.13%
22	0.64%	0.39%	0.18%	0.06%	0.06%	0.00%	0.00%
23	7.12%	5.80%	0.78%	3.78%	3.09%	3.61%	1.75%
24	2.16%	2.54%	7.58%	11.40%	11.80%	5.90%	5.26%
25	1.87%	0.50%	13.25%	16.09%	4.64%	3.19%	17.68%

Table 4.8: Specific humidity equivalent temperature node pairing frequencies with geopotential height nodes. Specific humidity nodes associated with equivalent temperature heat wave development with more than 5% of observations at the 95th percentile are located across the top of the table in columns with paired geopotential height nodes in rows; geopotential height nodes associated with the development of extreme conditions are highlighted in green; the top two node pairings for each specific humidity node are highlighted in blue.

Geopotential Height Nodes	Specific Humidity Nodes Associated with Equivalent Temperature Heat Waves						
Node	5	14	15	19	20	24	25
1	0.19%	1.57%	0.00%	0.39%	0.10%	1.62%	0.57%
2	0.51%	0.86%	0.13%	0.11%	0.10%	4.27%	0.09%
3	0.19%	0.78%	0.39%	0.11%	0.10%	0.18%	0.09%
4	0.06%	0.63%	0.00%	0.06%	0.00%	0.12%	0.00%
5	0.00%	0.00%	0.00%	0.00%	0.00%	0.06%	0.00%
6	12.11%	4.08%	23.82%	7.19%	9.73%	2.64%	3.60%
7	3.07%	1.65%	2.23%	1.67%	1.67%	1.62%	0.28%
8	3.72%	2.35%	0.26%	2.45%	0.52%	8.17%	0.66%
9	10.70%	2.27%	17.41%	8.03%	2.72%	2.76%	0.85%
10	0.13%	0.00%	0.00%	0.00%	0.00%	0.00%	0.00%
11	11.02%	7.76%	4.58%	11.98%	24.27%	7.63%	21.00%
12	0.32%	1.41%	0.00%	0.11%	0.00%	0.42%	0.00%
13	2.11%	11.06%	4.19%	3.23%	1.36%	4.21%	0.28%
14	3.40%	9.88%	2.09%	5.13%	2.62%	17.61%	3.97%
15	6.53%	8.63%	1.57%	7.02%	14.85%	11.42%	25.35%
16	1.41%	3.29%	0.52%	0.61%	2.30%	3.97%	7.10%
17	6.21%	14.43%	4.58%	13.60%	7.95%	12.38%	7.66%
18	3.72%	4.71%	2.62%	1.73%	0.31%	4.57%	0.38%
19	1.28%	0.24%	2.62%	0.17%	1.46%	0.06%	0.28%
20	2.24%	9.25%	5.50%	2.84%	3.56%	3.13%	1.42%
21	6.34%	1.65%	2.75%	7.80%	2.41%	2.28%	3.03%
22	5.89%	3.29%	1.83%	2.29%	8.58%	2.94%	6.53%
23	2.18%	0.86%	6.41%	0.72%	0.21%	0.48%	0.09%
24	9.80%	6.59%	14.27%	14.27%	7.95%	5.11%	4.35%
25	6.85%	2.75%	2.23%	8.47%	7.22%	2.34%	12.39%

Patterns associated with the development of extreme temperature and equivalent temperature events are similar with several nodes producing both extremes. For geopotential height equivalent temperature heat waves differ from temperature events with the inclusion of node 17. Geopotential height node 17 is characterized by zonal flow and moderate values over Chicago; this node pairs at a frequency of 13.97% with specific humidity node 19 and 11.80% with specific humidity node 24. Specific humidity equivalent temperature nodes differ from temperature heat wave nodes with inclusion of nodes 5 and 15 and exclusion of node 18. When analyzing Chicago, nodes 5 and 15 provide low humidity values while node 18 contains extremely low humidity. The alteration of nodes for specific humidity values indicates equivalent temperature requires, at minimum, low to moderate values of humidity for formation.

Heat wave observations were determined using Chicago O'Hare international Airport data for temperature and equivalent temperature; these heat wave events were then located on self-organizing map nodes to determine which pattern was producing the extreme values. Because heat waves were identified using the Chicago dataset, observations for temperature and equivalent temperature are the same, the difference is where they occurred on their respective SOM. Because these values are identical elevated pairing frequencies would be expected with the opposing measure. As expected, geopotential height heat wave nodes pair frequently with specific humidity heat wave nodes and specific humidity nodes pair frequently with geopotential height nodes. However, the observations included in this analysis are not limited to heat wave observations but all observations assigned to each node. For example, specific humidity equivalent temperature node 24 contains all observations assigned to node 24 in the summertime 1948-2014 dataset. This node pairs with geopotential height node 14 at a rate of 17.61% exemplifying that even though specific humidity node 24 is associated with heat wave

development frequent pairings can occur with non-heat wave associated nodes as well. Because all observations for each node are included in this analysis the elevated pairing frequencies with heat wave related nodes are significant. This indicates even in a non-heat wave scenario, if a heat wave related pattern were to occur, it would frequently pair with another heat wave associated pattern. This relationship signifies the increased likelihood of heat wave development when a prominent pattern occurs.

4.7 Node Trend Analysis

Nodes responsible for the production of extreme temperature or equivalent temperature events were analyzed to determine if the associated synoptic patterns are increasing in frequency. To establish if patterns are occurring more frequently, all observations assigned to nodes exceeding heat wave criteria were summed and analyzed for trend significance. Geopotential height node 17 was found to contain a significant trend with a p-value of 0.0001; this pattern is responsible for 6.81% of all equivalent temperature heat wave observations. For specific humidity, node 19 was increasing at the 0.05 confidence level; node 19 is a prominent node in both extreme temperature and equivalent temperature heat wave generation with frequencies of 25.34% and 26.14%; node 19's trend is increasing with a p-value of 0.0008 (Figure 4.13).

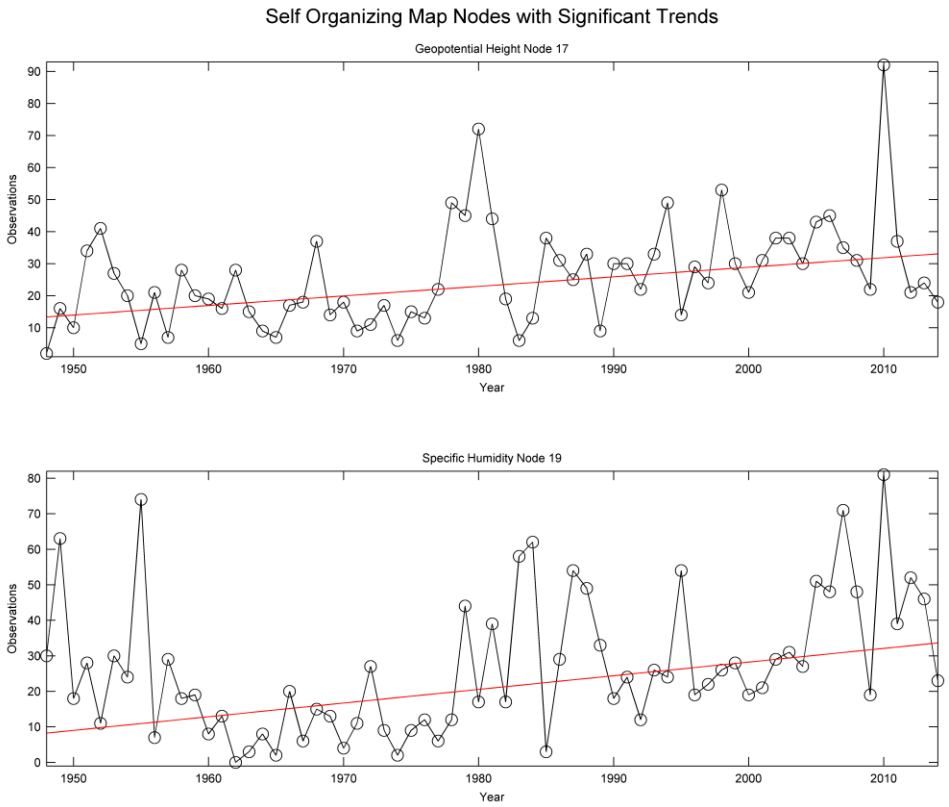

Figure 4.13: Self organizing map nodes displaying significant trends. Median of pairwise slopes was used to determine significance; the trends were significant at the 0.05 confidence level. Geopotential height node 17 is increasing by 2.98 per decade with a p-value of 0.0001. Specific humidity node 19 is increasing at 3.85 per decade with an associated p-value of 0.0008.

Additionally, all nodes identified as responsible for heat wave production for both variables of temperature and equivalent temperature were summed and assessed for trend significance. Therefore, for geopotential height temperature heat waves, all counts were summed for nodes 6, 9, 11, 15, 24 and 25; the trend was then assessed for significance using median of pairwise slopes regression (Figure 4.14). Geopotential height nodes associated with equivalent temperature heat wave development were found to be increasing with a significant trend and associated p-value of 0.0447 (Figure 4.15). Both specific humidity temperature and equivalent temperature nodes associated with heat wave development were found to be increasing with

significant trends and p-values of .00407 and 0.017 respectively (Figures 4.16 and 4.17, respectively). Increasing trends signify the associated patterns are becoming more prevalent and conditions favorable for extreme temperature or equivalent temperature heat waves are occurring more frequently. Additionally, because of high recurrence frequencies, once established these synoptic patterns are likely to persist and increase the probability of extreme events occurring.

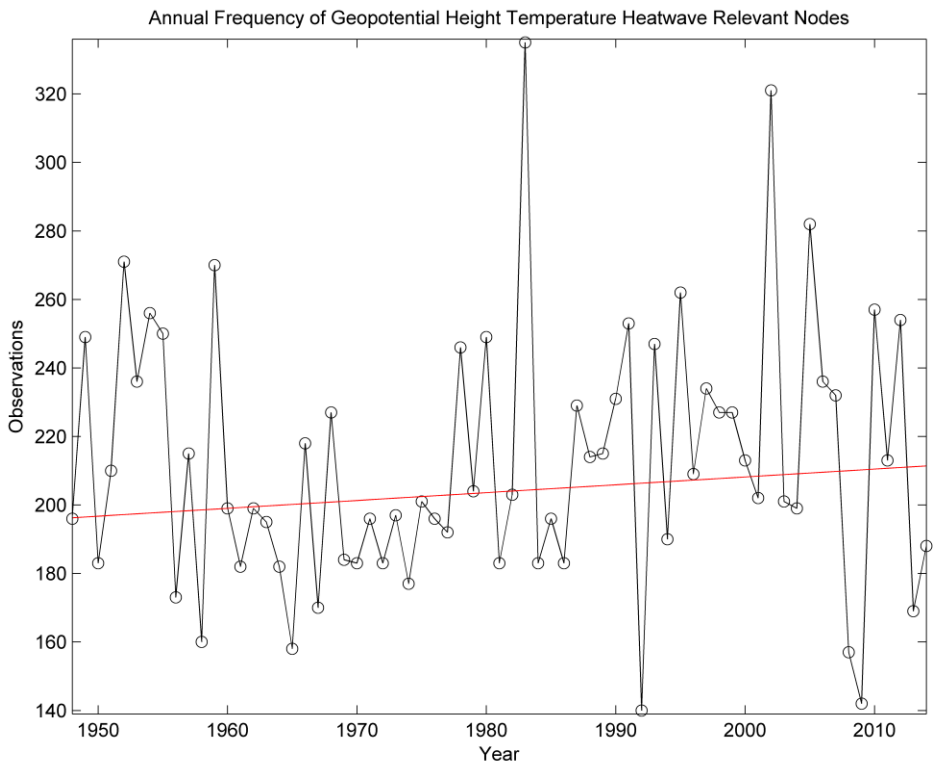

Figure 4.14: Geopotential height nodes associated with extreme temperature heat wave development. Median of pairwise slopes was used to determine significance; the trend of 2.29 per decade was not significant at the 0.05 confidence level with an associated p-value of 0.390.

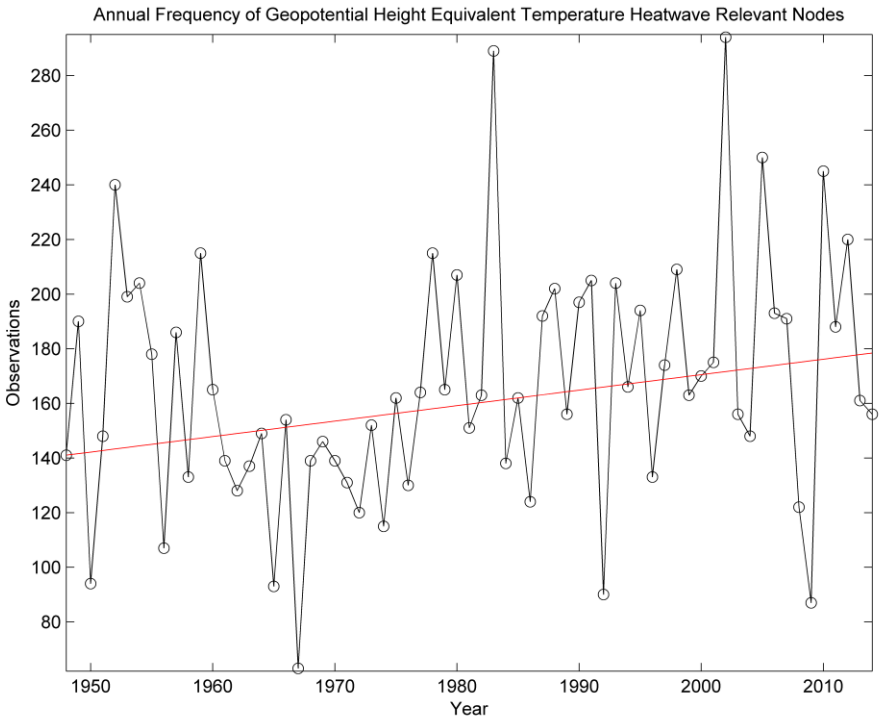

Figure 4.15: Geopotential height nodes associated with extreme equivalent temperature heat wave development. Median of pairwise slopes was used to determine significance; the trend of 5.67 per decade was significant at the 0.05 confidence level with an associated p-value of 0.0447.

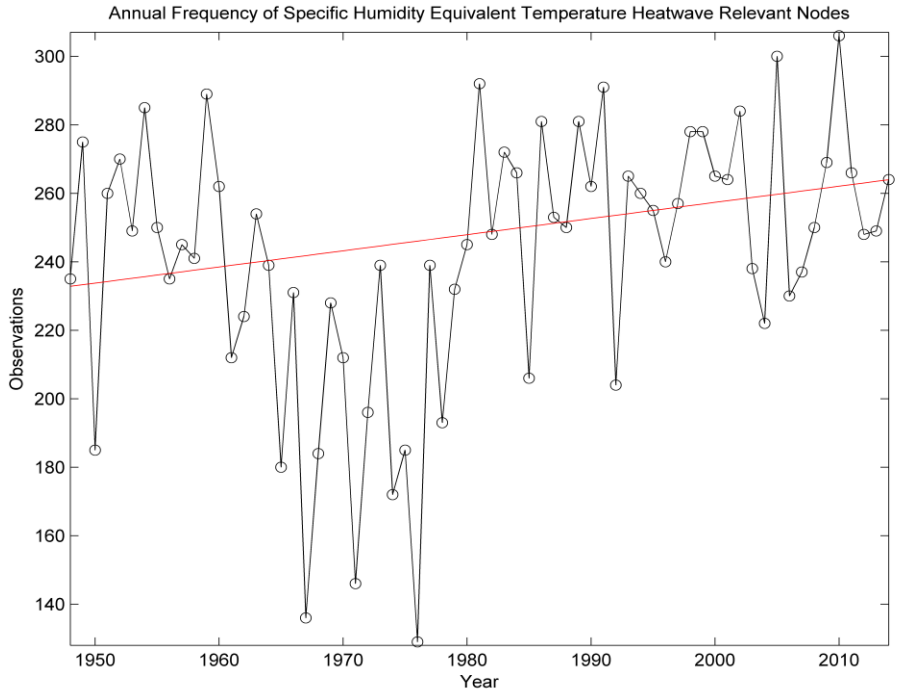

Figure 4.16: Specific humidity nodes associated with extreme equivalent temperature heat wave development. Median of pairwise slopes was used to determine significance; the trend of 5.60 per decade was significant at the 0.05 confidence level with an associated p-value of 0.011.

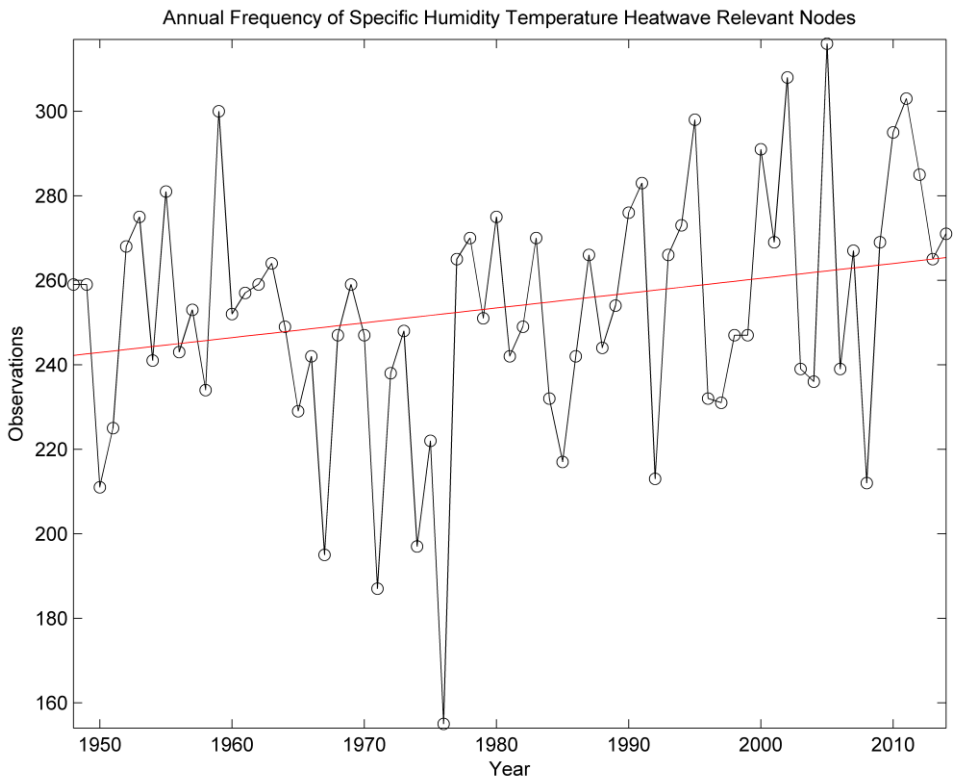

Figure 4.17: Specific humidity nodes associated with extreme equivalent temperature heat wave development. Median of pairwise slopes was used to determine significance; the trend of 7.42 per decade was significant at the 0.05 confidence level with an associated p-value of 0.0047.

CHAPTER 5

CONCLUSION

5.1 Evaluation of Research Questions

With rising minimum temperatures a more compact diurnal temperature range is apparent resulting in diminishing relief from oppressive heat wave conditions causing greater human heat stress. As temperatures increase heat waves are projected to become more intense, frequent, and longer in duration (Vavrus and VanDorn, 2009). Understanding heat wave development and large scale features associated with extreme events can improve understanding of Chicago heat waves and reduce mortality. For this study, analysis of self-organizing map patterns determined extreme temperature events were associated with heat wave characteristics of distinct ridging and elevated height values and can occur with excess moisture or moisture deficit. Conversely, equivalent temperature events are associated with heat wave characteristics and excessive available moisture. Several synoptic patterns for both variables displayed increasing trends signifying these patterns are becoming more prevalent. Additionally, patterns associated with development of extreme events for temperature and equivalent temperature contain elevated return frequencies indicating pattern persistence and the continuation of extreme events.

Q1: How have equivalent temperature extremes in Chicago changed over time?

Equivalent temperature June 1st through September 15th yearly summertime averages as well as yearly summertime absolute minimum and absolute maximum values were calculated for the 67 year study period; these values were graphed omitting missing values to determine if a trend was present. Equivalent temperature yearly summer averages and minimum values were found to be increasing but the trends were not found to be significant at 0.05 confidence level. Additionally, yearly summertime frequencies for all nodes containing observations at the 95th

percentile with greater than 5% occurrence were graphed individually. Results show for specific humidity node 19, responsible for 26.14% of equivalent temperature generation, increases with a significant trend at the 0.05 confidence level with a p-value of 0.0008. Nodes identified as contributing to the formation of equivalent temperature heat waves were summed to determine if an overall trend was apparent in all patterns associated with extreme event development. Nodes associated with equivalent temperature heat wave generation for both variables of geopotential height and specific humidity were increasing with a significant trend.

Since the synoptic patterns associated with extreme equivalent temperature heat waves are increasing in frequency; more extreme events are likely to occur. Increasing temperatures coupled with more frequent synoptic patterns associated with equivalent temperature extremes means potentially more frequent and more intense equivalent temperature heat waves.

Q2: What synoptic drivers are responsible for extreme equivalent temperature events? Are these features different from high temperature events?

Synoptic patterns associated with high temperature and equivalent temperature heat waves are interrelated but distinct. For geopotential height 500 mb SOM, synoptic patterns associated with extreme temperature heat wave generation were nodes 6, 9, 11, 15, 24, and 25. The majority of these patterns contain elevated height values or upper atmospheric ridging, conditions identified in previous studies as necessary for heat wave development (Perkins 2015; Black et al. 2004; Namias 1982). For geopotential height, observations that produced equivalent temperature heat wave events were concentrated on nodes 6, 9, 11, 15, 17, 24, and 25. Synoptic pattern repetition is apparent with nodes 6, 9, 11, 15, 24 and 25 producing both extreme temperature and equivalent temperature heat waves. However, extreme equivalent temperature

events concentrate on nodes with prominent and developed heat wave characteristics, while extreme temperature events encompass a larger range of SOM synoptic patterns including those with less developed heat wave features. For example, geopotential height node 17 is exclusive to equivalent temperature heat waves and contains a synoptic pattern of moderate values and relatively zonal flow.

Specific humidity nodes associated with extreme temperature heat wave events are nodes 14, 18, 19, 20, 24, and 25, with four patterns containing heightened humidity values for Chicago. Low humidity values are present in nodes 14 and 18 containing moderately-low and low humidity values over the Chicago region. Specifically, node 18 contains a strong lobe of low values that extends south over Chicago; this node is associated with 5.79% of temperature heat wave observations. For equivalent temperature heat wave events, observations confined to nodes 5, 14, 15, 19, 20, 24, and 25 where, in the majority of nodes, excess moisture is positioned over Chicago. Although nodes 5 and 14 contain low humidity values they were identified as patterns associated with early heat wave development and dissipation. These results indicate substantial humidity is required for extreme T_E events while extreme temperature events do not necessitate excessive available moisture.

Q3: Are synoptic patterns associated with extreme temperature and extreme equivalent temperature events becoming more prevalent?

Geopotential height and specific humidity nodes containing observations at the 95th percentile for heat wave criteria were analyzed using median of pairwise slopes regression to determine if a significant trend was present. Two nodes responsible for the production of high temperature and high humidity heat waves have been found to be increasing. For geopotential height, node 17 is responsible for 6.82% of equivalent temperature heat wave observations and

was found to be increasing with a significant trend. Specific humidity node 19, the node responsible for 26.14% equivalent temperature and 25.34% of extreme temperature heat wave observations, has been increasing with a significant trend. This node contains available moisture for the Chicago region and is essential for the generation of extreme temperature and equivalent temperature heat wave observations. Increasing frequency of specific humidity node 19 suggests a more frequently occurring synoptic pattern and an increased probability of extreme temperature and equivalent temperature observations occurring. Another indication of increasing heat wave frequency is the elevated pairing frequency between specific humidity node 19 and geopotential height nodes of importance for heat wave generation at the 95th percentile.

Another assessment was the summation of all observations assigned to nodes responsible for heat wave development for both temperature and equivalent temperature. Geopotential height nodes associated with equivalent temperature heat wave formation were found to be increasing with a significant trend. Additionally, specific humidity nodes associated with both temperature and equivalent temperature formation were found to be increasing with significant trends. These findings are similar to Perkins (2015) and Meehl and Tebaldi (2004) who determined heat waves are becoming more frequent, intense and longer lasting with changing global temperatures.

5.2 Study Limitations

While this study successfully analyzes temperature and equivalent temperature in Chicago, there are few limitations. Incorporation of wind values can improve the understanding of moisture advection and wind contributions for heat wave development. For example, moisture advection exacerbated conditions during the Chicago 1999 event. Although areas of high

equivalent temperature were identified, transportation of moisture would increase understanding of surface conditions favorable for extreme equivalent temperature events.

Additionally, self-organizing maps are a robust method of pattern extraction; however random initiation complicates data replication for exact patterns. Because the values are randomly initiated with each implementation of the SOM, exact values are difficult to replicate. However, if all data and methods are properly duplicated, similar results will be obtained.

Furthermore, NCEP/NCAR reanalysis data products of geopotential height and specific humidity were chosen to represent temperature values and available moisture. However, data products can be obtained from alternate sources for several atmospheric variables at various levels. Results gathered from this study reinforce the variable at atmospheric level selections however, numerous additional options are available. Additional analysis can be completed with alternate variables or atmospheric levels to determine the synoptic associations between extreme temperature and equivalent temperature events. Another limitation from data access is the prevalence of missing data values. In the Chicago O'Hare International Airport dataset downloaded from ISD- after processing and conversions- a total of ten values are absent from the data set composed of 28,675 total observations. Most notably, the year 2000 contains 7 omitted observations from a yearly total of 428 observations.

For future expansion of equivalent temperature or synoptic heat wave analysis incorporation of wind patterns into an additional SOM would provide insight on advection of moisture. For example, days identified as exceeding heat wave criteria can be located on a *u* or *v* wind SOM to determine if atmospheric flow is driving moisture into the area of interest or if a strong wind gradient is suppressing potentially cooling lake or oceanic breezes. Another potential future continuation of equivalent temperature synoptic forcings is the inclusion of large-scale flow

patterns such as El Niño Southern Oscillation, Pacific-North American Pattern, or the Northern Annual Mode. For example, Lokith and Broccoli (2013) determined that coupled PNA negative and NAM positive phases resulted in higher than average mean summer temperatures for the northeastern U.S., however the highest possibility for extreme days occurred when neither mode, positive or negative, for PNA or NAM were excessively prominent (Lokith and Broccoli, 2013). This study demonstrates that temperature and humidity are influenced by large-scale circulation. Circulations such as PNA, ENSO, and NAM can impact temperature and precipitation patterns that result in regional climate variability. The characteristics associated with heat wave formation can also be impacted by pattern variability. Additionally, fluctuations in moisture, a necessary component to equivalent temperature, can be attributed to large-scale circulation patterns. Further analysis of these trends and their impacts will improve understanding of extreme equivalent temperature events for the Chicago, IL study region.

5.3 Summary of Results

The following is a summary of major findings from this study:

1. Chicago O'Hare International Airport dataset minimum temperatures are increasing with a significant trend. Increasing minimum temperatures indicates a more compact diurnal temperature range and provides less nighttime relief from extreme temperatures during heat wave events increasing the probability for heat related mortality.
2. Extreme equivalent temperature heat waves require available excess moisture for generation of heat wave observations while extreme temperature observations can occur in the absence of moisture.

3. Geopotential height and specific humidity patterns exceeding the 95th percentile heat wave criteria pair frequently together indicating that the occurrence of a geopotential height or specific humidity node of significance increases the probability of an extreme event.
4. Geopotential height and specific humidity nodes that contain heat wave observations at the 95th percentile possess elevated return frequencies signifying pattern persistence.
5. Geopotential height node 17, responsible for 6.82% of equivalent temperature events, is increasing in frequency with a significant trend.
6. Specific humidity node 19, responsible for 25.34% of 95th percentile temperature heat wave observations and 26.14% of equivalent temperature observations, is increasing in frequency with a significant trend. This signifies an increase in synoptic conditions favorable for extreme temperature and equivalent temperature events.

These five findings are imperative to understanding heat wave development and equivalent temperature extremes in Chicago, IL. Synoptic patterns associated with elevated temperature and equivalent temperatures are increasing with significant trends indicating potential increases extreme events. Additionally, global warming coupled with increasing available moisture signifies more frequent, intense, and longer-lasting heat waves. Identifying synoptic patterns responsible for heat wave generation allows for future prediction of heat wave events. With advanced knowledge, city officials can prepare for extreme conditions and mitigate heat related mortality and morbidity.

REFERENCES

Black, Emily, Mike Blackburn, Giles Harrison, Brian Hoskins, and John Methven. "Factors contributing to the Summer 2003 European Heat wave." *Royal Meteorological Society* 59, no. 8 (2004): 217-23.

Bolton, David. "The Computation of Equivalent Potential Temperature." *Monthly Weather Review* 108 (1980): 1046-053.

Cavazos, Tereza. "Using Self-Organizing Maps to Investigate Extreme Climate Events: An Application to Wintertime Precipitation in the Balkans." *Journal of Climate* 13 (2000): 1718-732.

Ciancarelli, Brittany, Christopher L. Castro, Connie Woodhouse, Francina Dominguez, Hsin-I Chang, Carlos Carrillo, and Daniel Griffin. "Dominant Patterns of US Warm Season Precipitation Variability in a Fine Resolution Observational Record, with Focus on the Southwest." *International Journal of Climatology Int. J. Climatol.*, 2014, 687-707.

Davey, Christopher, Roger Pielkesr, and Kevin Gallo. "Differences Between Near Surface Equivalent Temperature and Temperature Trends for the Eastern United States Equivalent Temperature as an Alternative Measure of Heat Content." *Global and Planetary Change* 54 (2006): 19-32.

Dominguez, Francina, and Praveen Kumar. "Dominant Modes of Moisture Flux Anomalies over North America." *Journal of Hydrometeorology* 6 (2004): 194-209.

Fall, Souleymane, Noah S. Diffenbaugh, Dev Niyogi, Roger A. Pielke, and Gilbert Rochon. "Temperature and Equivalent Temperature over the United States (1979-2005)." *International Journal of Climatology* 30 (2010): 2045-054.

Gaffen, Dian J., and Rebecca J. Ross. "Climatology And Trends Of U.S. Surface Humidity And Temperature." *Journal of Climate* 12 (1999): 811-28.

Gershunov, Alexander, Daniel R. Cayan, and Sam F. Iacobellis. "The Great 2006 Heat wave Over California And Nevada: Signal Of An Increasing Trend." *Journal of Climate* 22 (2009).

Greene, Js, and Ls Kalkstein. "Quantitative Analysis of Summer Air Masses in the Eastern United States and an Application to Human Mortality." *Climate Research*, 1996, 43-53.

Grotjahn, Richard, Robert Black, Ruby Leung, Michael F. Wehner, Mathew Barlow, Mike Bosilovich, Alexander Gershunov, William J. Gutowski, John R. Gyakum, Richard W. Katz, Yun-Young Lee, and Young-Kwon Lim. "North American Extreme Temperature Events and Related Large Scale Meteorological Patterns: A Review of Statistical Methods, Dynamics, Modeling, and Trends." *Clim Dyn Climate Dynamics*, 2015.

Hayhoe, Katharine, Jeff VanDorn, Thomas Croley II, Nicole Schlegal, and Donald Wuebbles. "Regional Climate Projections for Chicago and the US Great Lakes." *Journal of Great Lakes Research* 36 (2010): 7-21.

Hayhoe, Katharine, Scott Sheridan, Laurence Kalkstein, and Scott Greene. "Climate Change, Heat waves, and Mortality Projections for Chicago." *Journal of Great Lakes Research* 36 (2010): 65-73.

Hewitson, B., and R. Crane. "Self-Organizing Maps: Applications to Synoptic Climatology." *Climate Research* 22 (2002): 13-26.

Horton, Daniel E., Nathaniel C. Johnson, Deepti Singh, Daniel L. Swain, Bala Rajaratnam, and Noah S. Diffenbaugh. "Contribution of Changes in Atmospheric Circulation Patterns to Extreme Temperature Trends." *Nature*, 2015, 465-69.

Kalnay, E, M. Kanamitsu, R. Kistler, W. Collins, D. Deaven, L. Gandin, M. Iredell, S. Saha, G. White, J. Woollen, Y. Zhu, A. Leetmaa, R. Reynolds, M. Chelliah, W. Ebisuzaki, W. Higgins, J. Janowiak, K. C. Mo, C. Ropelewski, J. Wang, Roy Jenne, and Dennis Joseph, 1996: The NCEP/NCAR Reanalysis 40-year Project. Bull. Amer. Meteor. Soc., 77, 437 471

Karl, Thomas R., and Richard W. Knight. "The 1995 Chicago Heat Wave: How Likely Is a Recurrence?" *Bull. Amer. Meteor. Soc. Bulletin of the American Meteorological Society*, 1996, 1107-119.

Kohonen, Teuvo. "Essentials of the Self-organizing Map." *Neural Networks* 37 (2013): 52-65.

Kunkle, Kenneth, Stanley Changnon, Beth Reinke, and Raymond Arritt. "The July 1995 Heat Waves in the Midwest: A Climatic Perspective and Critical Weather Factors." *American Meteorological Society* 77, no. 7 (1996): 1507-518.

Lanzante, John R. "Resistant, Robust And Non-Parametric Techniques For The Analysis Of Climate Data: Theory And Examples, Including Applications To Historical Radiosonde Station Data." *International Journal of Climatology Int. J. Climatol.*, 1996, 1197-226.

Liu, Yonggang, and Robert Weisberg. A Review of Self-Organizing Map Applications in Meteorology and Oceanography. INTECH Open Access Publisher, 2011.

Livezey, Robert E., and Richard Tinker. "Some Meteorological, Climatological, and Microclimatological Considerations of the Severe U.S. Heat Wave of Mid-July 1995." *Bull. Amer. Meteor. Soc. Bulletin of the American Meteorological Society*, 1996, 2043 054.

Loikith, Paul, and Anthony Broccoli. "Influence of Recurrent Modes of Climate Variability on the Occurrence of Winter and Summer Extreme Temperatures over North America." *Journal of Climate* 27 (2013): 1600-618.

Lyon, Bradfield. "Southern Africa Summer Drought and Heat Waves: Observations and Coupled Model Behavior." *America Meteorological Society* 22:6033–6046.

Namias, Jerome. "Anatomy Of Great Plains Protracted Heat waves (especially The 1980 U.S. Summer Drought)." *Monthly Weather Review* 110 (1982): 824-38.

Nigro, Melissa, and John Cassano. "Identification of Surface Wind Patterns over the Ross Ice Shelf, Antarctica, Using Self-Organizing Maps." *American Meteorological Society*, 2014.

Palecki, Michael A., Stanley A. Changnon, and Kenneth E. Kunkel. "The Nature and Impacts of the July 1999 Heat Wave in the Midwestern United States: Learning from the Lessons of 1995." *Bull. Amer. Meteor. Soc. Bulletin of the American Meteorological Society*, 2001, 1353-367.

Pan, Zaitao, Raymond Arritt, Eugene Takle, William Gutowski, Chrisotpher Anderson, and Moti Segal. "Altered Hydrologic Feedback in a Warming Climate Introduces a “warming Hole”." *Geophysical Research Letters* 31 (2004).

Pielke, Roger A., Christopher Davey, and Jack Morgan. "Assessing “global Warming” with Surface Heat Content." *Eos Trans. AGU Eos, Transactions American Geophysical Union*, 2004, 210.

Perkins, Sarah. "A Review on the Scientific Understanding of Heat waves- Their Measurement, Driving Mechanisms, and Changes at the Global Scale." *Atmospheric Research* 164:242 67.

Perkins, S. E., and L. V. Alexander. "On the Measurement of Heat Waves." *Journal of Climate J. Climate* 26 (2013): 4500-517.

Pezza, Alexandre Bernardes, Peter Van Rensch, and Wenju Cai. "Severe Heat Waves in Southern Australia: Synoptic Climatology and Large Scale Connections." *Clim Dyn Climate Dynamics*, 2011, 209-24.

Richardson, A.j, C. Risien, and F.a Shillington. "Using Self-Organizing Maps to Identify Patterns in Satellite Imagery." *Progress In Oceanography*, 2003, 223-39.

Robinson, Peter. "On the Definition of a Heat wave." *America Meteorological Society* 40 (2001): 762-75.

Robinson, Peter J. "Temporal Trends in United States Dew Point Temperatures." *International Journal of Climatology* 20 (1999): 985-1002.

Rogers, Jeffrey C., Sheng-Hung Wang, and Jill S. M. Coleman. "Evaluation of a Long Term (1882–2005) Equivalent Temperature Time Series." *Journal of Climate* 20 (2007): 4476 485.

Ross, Rebecca J., and William P. Elliott. "Radiosonde-Based Northern Hemisphere Tropospheric Water Vapor Trends." *Journal of Climate J. Climate*, 2001, 1602-612.

Schoof, Justin, Zach Heern, M.D. Therrell, and J. Remo. “Assessing Trends in Lower Tropospheric Heat Content in the Central United States Using Equivalent Temperature.” *International Journal of Climatology* (2014).

Schuenemann, Keah C., John J. Cassano, and Joel Finnis. "Synoptic Forcing of Precipitation over Greenland: Climatology for 1961–99." *Journal of Hydrometeorology* 10 (2009): 60 78.

Sheridan, Scott, and Cameron Lee. "The Self-Organizing Map in Synoptic Climatological Research." *Progress in Physical Geography* 35, no. 1 (2011):109-19.

Steadman, Robert G. "A Universal Scale of Apparent Temperature." *J. Climate Appl. Meteor. Journal of Climate and Applied Meteorology*, 1984, 1674-687.

Tozuka, Tomoki, Jing-Jia Luo, Sebastien Masson, and Toshio Yamagata. "Tropical Indian Ocean Variability Revealed by Self-organizing Maps." *Climate Dynamics*, 2008, 333-43.

Guthikoda, Shyam. *Khonen Self Organizing Maps*. 2005.

Vavrus, Steve, and Jeff Van Dorn. "Projected Future Temperature and Precipitation Extremes in Chicago." *Journal of Great Lakes Research*, 2009, 22-32.

Vanos, J. K., L. S. Kalkstein, and T. J. Sanford. "Detecting Synoptic Warming Trends across the US Midwest and Implications to Human Health and Heat-related Mortality." *International Journal of Climatology Int. J.Climatol.*, 2014, 85-96.

Wise, Erika K., and Matthew P. Dannenberg. "Persistence of Pressure Patterns over North America and the North Pacific Since AD 1500." *Nature Communications*, 2014.

APPENDIX

APPENDIX A

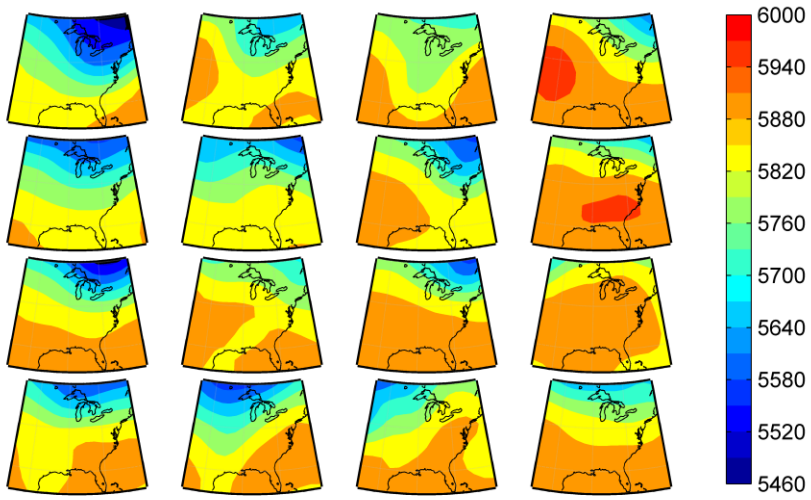

Appendix A: 500 mb Geopotential height SOM using a 4×4 pattern generating 16 nodes.

APPENDIX B

Appendix B: 500 mb Geopotential height SOM frequencies for a 4×4 node array

Geopotential Height 4×4 SOM Frequencies			
Node 1	Node 2	Node 3	Node 4
2.06%	4.66%	5.05%	4.99%
Node 5	Node 6	Node 7	Node 8
5.72%	4.15%	6.66%	8.78%
Node 9	Node 10	Node 11	Node 12
5.71%	9.65%	7.71%	7.32%
Node 13	Node 14	Node 15	Node 16
5.76%	2.73%	4.67%	14.38%

.

APPENDIX C

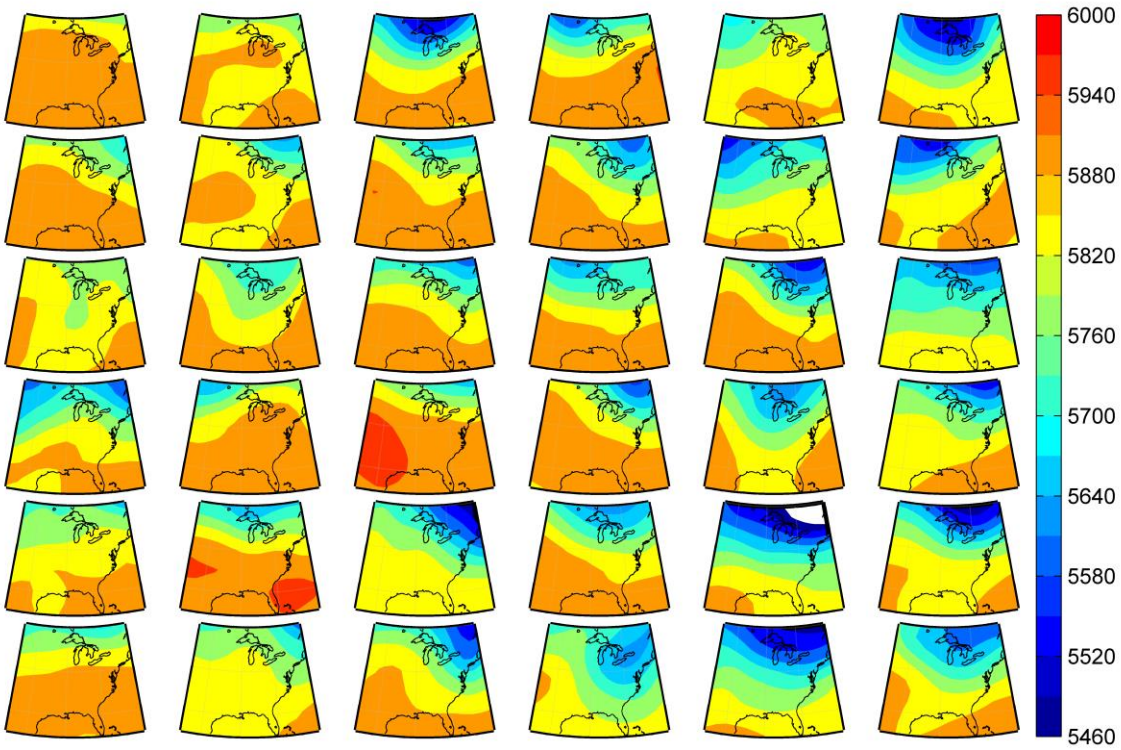

Appendix C: 500 mb Geopotential height SOM using a 6×6 pattern generating 36 nodes.

APPENDIX D

Appendix D: 500 mb Geopotential height SOM frequencies for a 6×6 node array.

Geopotential Height 6×6 SOM Frequencies					
Node 1	Node 2	Node 3	Node 4	Node 5	Node 6
4.22%	2.48%	2.40%	2.76%	2.35%	0.81%
Node 7	Node 8	Node 9	Node 10	Node 11	Node 12
5.72%	2.45%	5.38%	3.50%	1.61%	1.68%
Node 13	Node 14	Node 15	Node 16	Node 17	Node 18
2.21%	3.80%	5.15%	3.71%	3.08%	2.19%
Node 19	Node 20	Node 21	Node 22	Node 23	Node 24
1.57%	2.78%	3.32%	3.14%	1.58%	3.19%
Node 25	Node 26	Node 27	Node 28	Node 29	Node 30
2.86%	3.46%	0.97%	4.98%	0.23%	2.56%
Node 31	Node 32	Node 33	Node 34	Node 35	Node 36
5.29%	2.38%	1.78%	1.02%	1.26%	2.11%

APPENDIX E

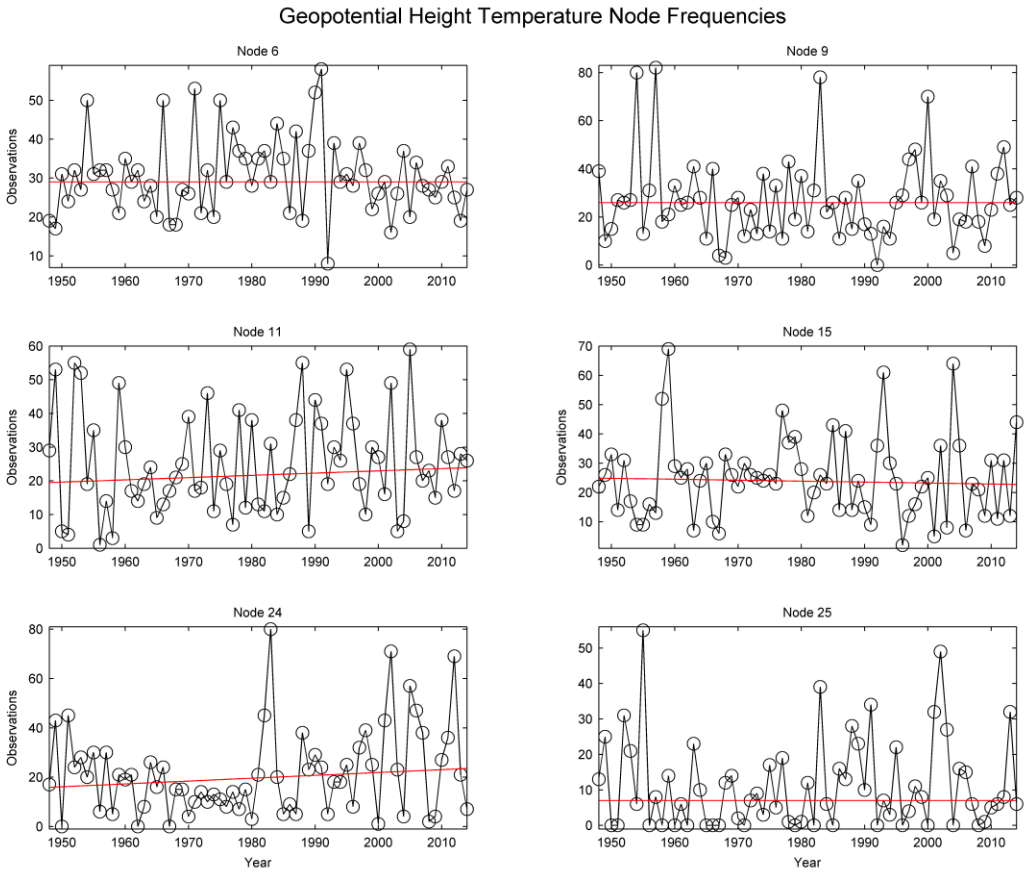

Appendix E: Geopotential height nodes associated with extreme temperature heat wave development. Geopotential height patterns represented are nodes: 6, 9, 11, 15, 24, and 25. Trends were assessed with median pairwise regression with no significant trends identified.

APPENDIX F

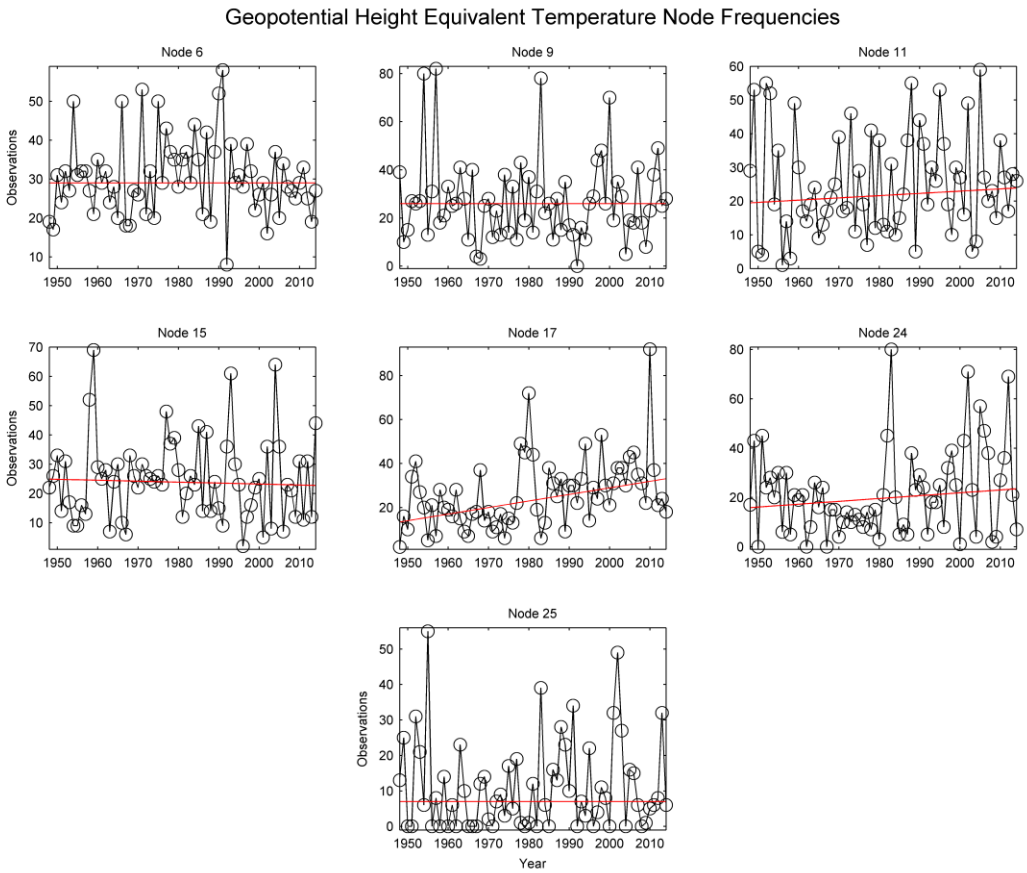

Appendix F: Geopotential height nodes associated with equivalent temperature heat wave development. Geopotential height patterns represented are nodes: 6, 9, 11, 15, 17, 24, and 25. Trends were assessed with median pairwise regression; node 17 was found to be increasing significantly with an associated p-value of 0.00010.

APPENDIX G

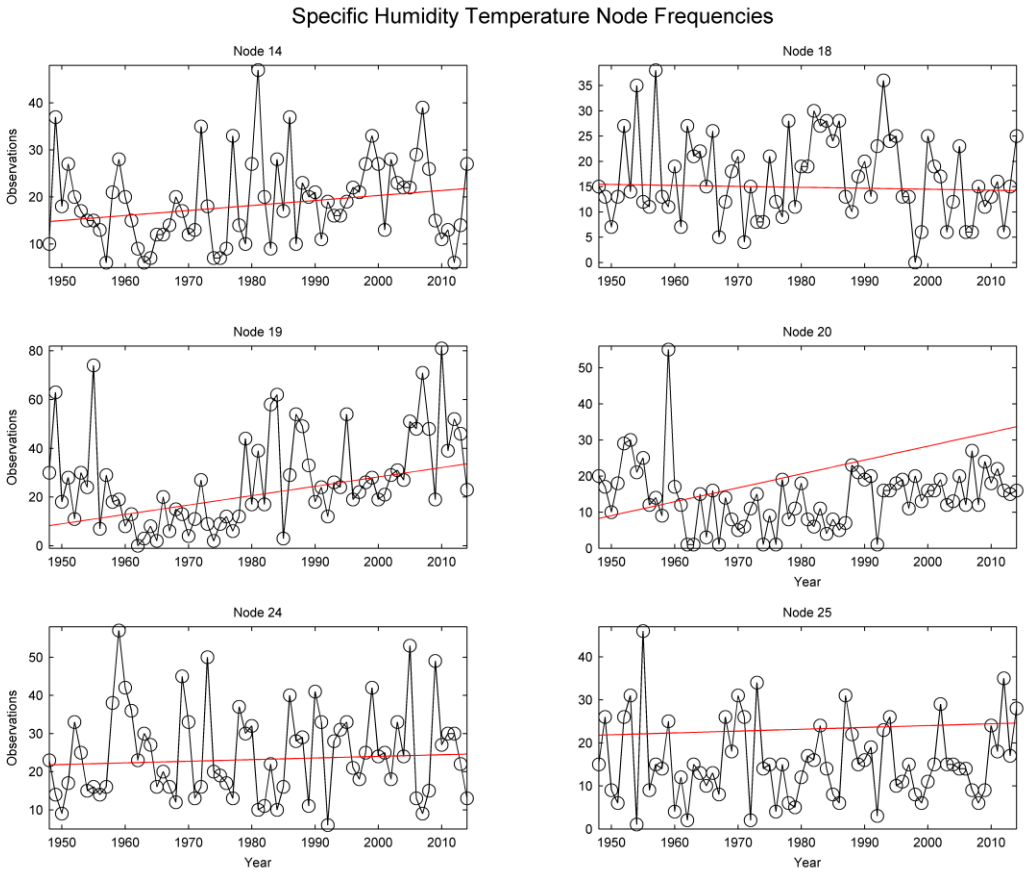

Appendix G: Specific humidity nodes associated with temperature heat wave development. Specific humidity patterns represented are nodes14, 18, 19, 20, 24, and 25. Trends were assessed with median pairwise regression; node 19 was found to be increasing significantly with an associated p-value of 0.0008.

APPENDIX H

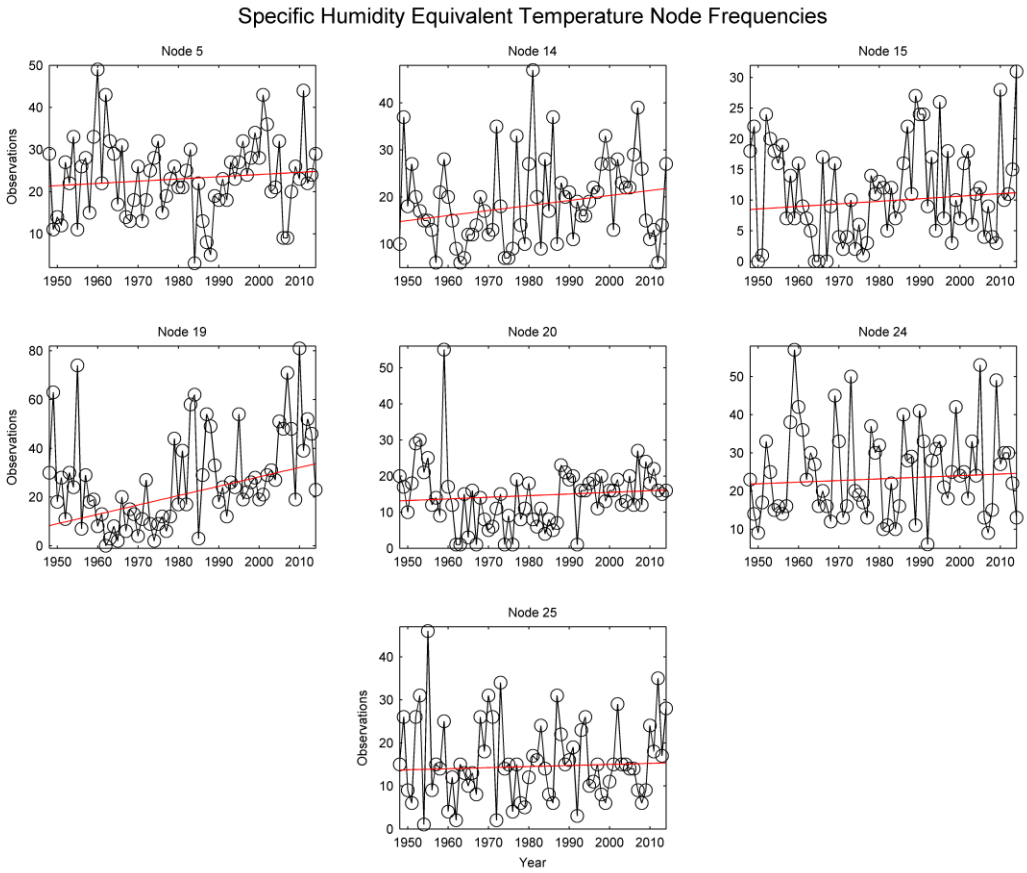

Appendix H: Specific humidity nodes associated with equivalent temperature heat wave development. Specific humidity patterns represented are nodes 5, 14, 15, 19, 20, 24, and 25. Trends were assessed with median pairwise regression; node 19 was found to be increasing significantly with an associated p-value of 0.0008.

APPENDIX I

Appendix I: Trends and associated p-values for 500 mb geopotential height SOM nodes associated with temperature and equivalent temperature heat wave development.

Geopotential Height Node Frequencies for 95th Percentile Observations		
Node	**Trend**	**P-Value**
6	0.00°C	0.9749
9	0.00°C	0.8913
11	0.62°C	0.4126
15	-0.32°C	0.7428
17	2.98°C	0.0001
24	1.15°C	0.2189
25	0.00°C	0.4970

Appendix I: Trends and associated p-values for 850 mb specific humidity SOM nodes associated with temperature and equivalent temperature heat wave development.

Specific Humidity Node Frequencies for 95th Percentile Observations		
Node	**Trend**	**P-Value**
5	0.53°C	0.5544
14	1.06°C	0.0809
15	0.42°C	0.4772
18	-0.19°C	0.5934
19	3.85°C	0.0008
20	0.45°C	0.3230
24	0.43°C	0.5273
25	0.25°C	0.5732

VITA

Graduate School

Southern Illinois University

Brooke L. Haldeman

bhaldeman@siu.edu

Indiana State University

Bachelors of Science, Environmental Science, May 2013

Thesis Title:

Influence of Synoptic Scale Circulation on Equivalent Temperature Extremes in Chicago, IL (1948-2014)

Major Professor: Dr. Justin Schoof